Journal of Chemistry

Catalytic Processes for Water Treatment

Lead Guest Editor: Dr. Rahat Javaid
Guest Editors: Dr. Umair Yaqub Qazi, Dr. Metwally Madkour, and Dr. Amir Ikhlaq

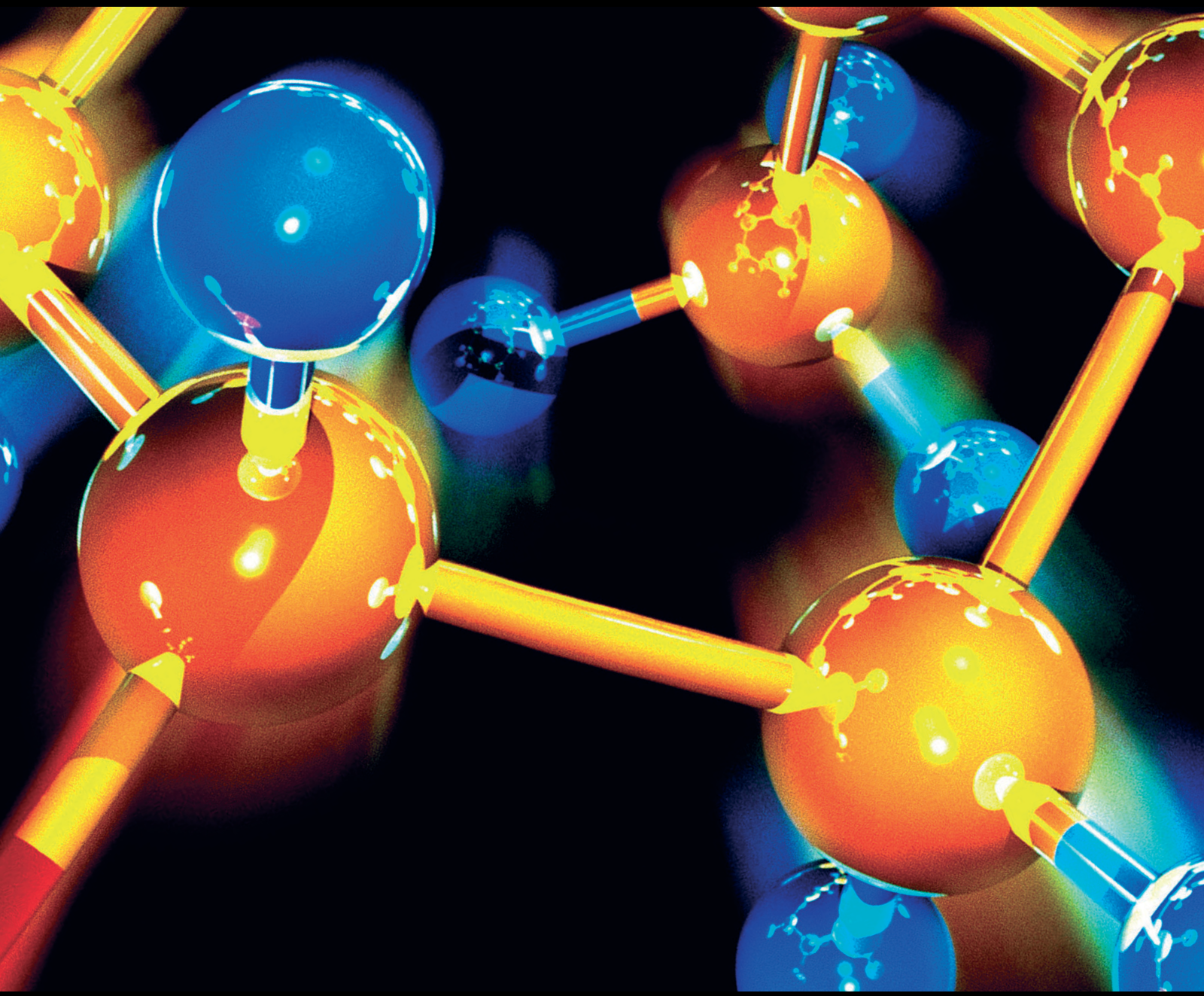

Catalytic Processes for Water Treatment

Journal of Chemistry

Catalytic Processes for Water Treatment

Lead Guest Editor: Dr. Rahat Javaid
Guest Editors: Dr. Umair Yaqub Qazi, Dr. Metwally Madkour, and Dr. Amir Ikhlaq

Chief Editor

Kaustubha Mohanty, India

Associate Editors

Mohammad Al-Ghouti, Qatar
Tingyue Gu, USA
Teodorico C. Ramalho, Brazil
Artur M. S. Silva, Portugal

Academic Editors

Jinwei Duan , China
Luqman C. Abdullah, Malaysia
Dr Abhilash, India
Amitava Adhikary, USA
Amitava Adhikary, USA
Mozhgan Afshari, Iran
Daryoush Afzali, Iran
Mahmood Ahmed, Pakistan
Islam Al-Akraa, Egypt
Juan D. Alché, Spain
Gomaa A. M. Ali, Egypt
Mohd Sajid Ali, Saudi Arabia
Shafaqat Ali, Pakistan
Patricia E. Allegretti, Argentina
Marco Anni, Italy
Alessandro Arcovito, Italy
Hassan Arida, Saudi Arabia
Umair Ashraf, Pakistan
Narcis Avarvari, France
Davut Avci, Turkey
Chandra Azad, USA
Mohamed Azaroual, France
Rasha Azzam, Egypt
Hassan Azzazy, Egypt
Renal Backov, France
Suresh Kannan Balasingam, Republic of Korea
Sukanta Bar, USA
Florent Barbault, France
Maurizio Barbieri, Italy
James Barker, United Kingdom
Salvatore Barreca, Italy
Jorge Barros-Velázquez, Spain
THANGAGIRI Baskaran, India
Haci Baykara, Ecuador
Michele Benedetti, Italy
Laurent Billon, France
Marek Biziuk, Poland
Jean-Luc Blin, France
Tomislav Bolanca, Croatia
Ankur Bordoloi, India
Cato Brede, Norway
Leonid Breydo, USA
Wybren J. Buma, The Netherlands
J. O. Caceres, Spain
Patrizia Calaminici, Mexico
Claudio Cameselle, Spain
Joaquin Campos, Spain
Dapeng Cao, China
Domenica Capasso, Italy
Stefano Caporali, Italy
Zenilda Cardeal, Brazil
Angela Cardinali, Italy
Stefano Carli, Italy
Maria F. Carvalho, Portugal
Susana Casal, Portugal
David E. Chavez, USA
Riccardo Chelli, Italy
Zhongfang Chen, Puerto Rico
Vladislav Chrastny, Czech Republic
Roberto Comparelli, Italy
Filomena Conforti, Italy
Luca Conti, Italy
Christophe Coquelet, France
Filomena Corbo, Italy
Jose Corchado, Spain
Maria N. D.S. Cordeiro, Portugal
Claudia Crestini, Italy
Gerald Culioli, France
Nguyen Duc Cuong, Vietnam
Stefano D'Errico, Italy
Matthias D'hooghe, Belgium
Samuel B. Dampare, Ghana
Umashankar Das, Canada
Victor David, Romania
Annalisa De Girolamo, Italy
Antonio De Lucas-Consuegra, Spain
Marcone A. L. De Oliveira, Brazil
Paula G. De Pinho, Portugal
Damião De Sousa, Brazil
Francisco Javier Deive, Spain
Tianlong Deng, China

Contents

Application of Attapulgite Clay-Based Fe-Zeolite 5A in UV-Assisted Catalytic Ozonation for the Removal of Ciprofloxacin
Amir Ikhlaq, Rahat Javaid, Asia Akram, Umair Yaqub Qazi, Javeria Erfan, Metwally Madkour, Mohamed Elnaiem M. Abdelbagi, Sami M. Ibn Shamsah, and Fei Qi
Research Article (10 pages), Article ID 2846453, Volume 2022 (2022)

Emerging Pollutants in Moroccan Wastewater: Occurrence, Impact, and Removal Technologies
Yassine Jari, Nicolas Roche, Mohamed Chaker Necibi, Souad El Hajjaji, Driss Dhiba, and Abdelghani Chehbouni
Review Article (24 pages), Article ID 9727857, Volume 2022 (2022)

Investigation of Fe-Doped Graphitic Carbon Nitride-Silver Tungstate as a Ternary Visible Light Active Photocatalyst
Eid H. Alosaimi, Nadia Azeem, Noor Tahir, Asim Jilani, Muhammad Zahid, Salman. S. Alharthi, Javed Iqbal, Muhammad Yaseen, Zulfiqar Ahmad Rehan, and Imran Shahid
Research Article (18 pages), Article ID 4660423, Volume 2021 (2021)

Hindawi
Journal of Chemistry
Volume 2022, Article ID 2846453, 10 pages
https://doi.org/10.1155/2022/2846453

Research Article

Application of Attapulgite Clay-Based Fe-Zeolite 5A in UV-Assisted Catalytic Ozonation for the Removal of Ciprofloxacin

Amir Ikhlaq,[1] **Rahat Javaid**,[2] **Asia Akram**,[3] **Umair Yaqub Qazi**,[4] **Javeria Erfan**,[1] **Metwally Madkour**,[5] **Mohamed Elnaiem M. Abdelbagi**,[4] **Sami M. Ibn Shamsah**,[6] **and Fei Qi**[7]

[1]*Institute of Environmental Engineering and Research, University of Engineering and Technology, Lahore, Pakistan*
[2]*Renewable Energy Research Center, Fukushima Renewable Energy Institute, National Institute of Advanced Industrial Science and Technology, AIST, 2-2-9 Machiikedai, Koriyama, Fukushima 963-0298, Japan*
[3]*University of Management and Technology, Johar Town, Lahore, Pakistan*
[4]*Department of Chemistry, College of Science, University of Hafr Al Batin, P.O Box 1803, Hafr Al Batin 39524, Saudi Arabia*
[5]*Chemistry Department, Faculty of Science, Kuwait University, P.O. Box 5969, Safat 13060, Kuwait*
[6]*Department of Mechanical Engineering, College of Engineering, University of Hafr Al Batin, P.O. Box 1803, Hafr Al Batin 31991, Saudi Arabia*
[7]*Beijing Forestry University, No. 35 Qinghua East Road, Haidian District, Beijing 100083, China*

Correspondence should be addressed to Amir Ikhlaq; aamirikhlaq@uet.edu.pk and Umair Yaqub Qazi; umairqazi@uhb.edu.sa

Received 19 July 2021; Accepted 22 April 2022; Published 19 May 2022

Academic Editor: Hassan Arida

For the first time, Fe-zeolite 5A (Fe-Z5A) efficacy in the UV-assisted ozonation process to remove ciprofloxacin (CF) in wastewater is investigated. FTIR, SEM, EDX, BET, and the mass transfer process for point of zero charge are used to characterize the catalyst. Furthermore, the synergic process (UV/O_3/Fe-Z5A) is compared with O_3, O_3/UV, and Fe-Z5A/O_3 processes. The influence of catalyst dose, hydroxyl radical scavenger, and off-gas ozone released is discussed. The removal efficiency of CF in wastewater (for the synergic process) is compared with a single ozonation process. The results indicate that the synergic process was more efficient than others, with about 73% CF being removed (in 60 minutes) in the synergic process. The results also show that synergic processes produce less off-gas ozone than other processes, suggesting more ozone consumption in the synergic process, and confirmed by the radical scavenger effect and hydrogen peroxide decomposition studies. The Fe-Z5A was found to operate through a hydroxyl mechanism in which Fe worked as an active site that promotes the formation of hydroxyl radicals. Finally, the synergic process was more efficient than the ozonation process in the wastewater matrix. Hence, Fe-Z5A/O_3/UV pathway is highly efficient for the degradation of pharmaceuticals in wastewater.

1. Introduction

Photocatalytic ozonation processes are among the best choices for advanced oxidation processes (AOPs) used in wastewater treatment [1–6]. A variety of materials are used as catalysts in these processes, such as activated carbons [7, 8], metal oxides [9–12], and organic-based photocatalysts [13–15]. Due to their stability and selectivity, zeolites were found to be highly significant for practical applications [16–22]. They have already been practically implied as a catalyst, ion-exchanger, and adsorbent in different areas [23–26]. Their unique properties such as silica to alumina ratios, shapes, surface area, and Lewis and Bronsted acid sites make them quite useful option in wastewater treatment [23–25, 27]. Zeolites of different types were successfully studied in the past as catalysts in catalytic ozonation processes, such as ZSM-5, Y-zeolites, MCM-41, zeolite 4A, and natural zeolites [23–25, 27–30].

In recent few years, metal-loaded zeolites were extensively implied as a catalyst in ozone-assisted processes and were found to be highly efficient [31, 32]. Since each type of zeolite may have unique properties and shapes compared

to others, it is indeed important to investigate the ozone-assisted processes in the presence of various types of zeolites. This study is the continuation of the author's previous studies to investigate the applicability and behavior of multiple types and forms of zeolites in ozone-assisted catalytic processes [28, 33]. In this investigation, a comparative study was conducted between UV-assisted and catalytic ozonation processes using iron-coated zeolite 5A (Z5A) as a potential catalyst. To the best of the author's knowledge, this is the first report in which zeolite 5A was tested as a catalyst in the UV-assisted catalytic ozonation process. González-Labrada et al. [34] recently studied the degradation of ciprofloxacin on Fe-MFI zeolites and found significantly higher CF removal than ozonation alone, while the current investigation is based on the UV-irradiated catalytic ozonation process with iron-loaded zeolite and compared with simple catalytic ozonation process. It is significant to mention here that in hydroxyl radical-based catalytic ozonation processes, the hydroxyl radicals in aqueous solutions may combine to form hydrogen peroxide, which may have a negative effect on overall removal efficiency [35]. Therefore, in the current investigation, UV-assisted catalytic ozonation on Fe-Z5A was considered to further decompose hydrogen peroxide (through direct UV irradiation, ozone UV interactions, and Fenton-like decomposition on catalyst surface). Therefore, this study may further help to understand the applicability of a different type of zeolites in natural conditions using a UV-assisted process.

In the current investigation, the antibiotic ciprofloxacin (CF) was selected as the target pollutant. The occurrence of antibiotics was identified even in drinking water across the world [36, 37]. The conventional biological wastewater treatment methods failed to degrade antibiotics and other pharmaceuticals completely, and they were found in their effluents [38]. The continuous exposure of our environment to antibiotics is not only hazardous to human and aquatic organisms but it may result in the evolution of antibiotic-resistant microorganisms in the future [39–42]. These microbes may pose a severe threat to humanity; therefore, it is essential to find novel methods that may be applied in combination with biological processes to eliminate threats to our future generations.

In the current investigation, UV-assisted catalytic ozonation process using iron-loaded zeolite 5A was studied to remove CF. The 5A type of molecular sieves is aluminosilicate Linde type A (LTA) form of zeolites that contain calcium instead of sodium ion having diameter of 5 Å. These types of zeolites are well known for their ability to adsorb pollutants. Therefore, in current investigation, 5A type zeolites loaded with iron were used as catalyst in the ozonation process. Moreover, the catalyst dose effect, hydroxyl radical scavenger (t-butanol), and removal of CF in denoised and wastewater were investigated.

2. Experimental

2.1. Materials and Reagents. The zeolite 5A, ciprofloxacin, and t-butanol (used for hydroxyl radical scavenger effect) were obtained from Sigma-Aldrich (UK). All chemicals were of analytical grade and used without further purification.

2.2. Catalyst Preparation. The Z5A obtained from Sigma-Aldrich (UK) was washed several times with ultrapure deionized water to remove impurities (if any) from Z5A. The iron-loaded Z5A was prepared by using the incipient impregnation method [43–45]. In this method, a weighed amount (6 g) of ferric nitrate nonahydrate ($Fe(NO_3).9H_2O$) was taken in a beaker that contains 20 mL ultrapure deionized water. Then, Z5A (10 g) was placed into the beaker containing iron salt and was continuously stirred at 120 rpm at 100°C till the water evaporated. Then, Fe-Z5A was calcined at 500°C during 4 hrs [43–45]. The Fe-Z5A was dipped into (0.1 M) HNO_3 for 24 hours to remove any unattached iron. Then, it was filtered and washed several times with ultrapure deionized water till the pH of washout water remains constant. Finally, the catalyst was dried in an oven at 103°C overnight [43–45].

2.3. Experimental Procedure. Experiments involving photocatalytic ozonation, catalytic ozonation, and single ozonation were carried out in a semicontinuous reactor (Figure 1). The reactor was installed with UV-light (UV rays (20 W), a wavelength of 254 nm obtained from UV rod (Sylvania Pvt Ltd., Germany). In this study, 2.5 L working solution of ciprofloxacin (initial concentration = 50 ppm) was placed in the reactor. The ozone was introduced (Sky Zone, DA12025B12L, Karachi, Pakistan) continuously into the reactor for 60 minutes. Samples were collected after fixed time intervals and were then quenched with Na_2CO_3 (0.025 M) to remove residual aqueous ozone [33]. Finally, samples were analyzed at 284 nm on HPLC (Hitachi Elite LaChrom L-2130) equipped with C18 column (4.6 × 250 mm, Poroshell 120). All the samples were also scanned on a UV-Vis spectrophotometer (PerkinElmer Lambda 35 double beam) between 200 nm and 700 nm to observe any byproducts formed. The removal efficiencies of CF were determined by using the following equation.

$$\text{Ciprofloxacin removal}\,(\%) = \frac{A_o - A_t}{A_O} \times 100, \qquad (1)$$

where A_t is the peak area time t, and A_o is the peak area at t = o.

2.4. Analytical Procedures

2.4.1. Ozone Dose. The ozone dose was determined by using the iodometric method described elsewhere [46]. Such ozone was bubbled into two sets of flasks (Figure 1) containing 2% KI solution (100 mL). After the entire process, 5 mL H_2SO_4 (2 N) was added to each flask to liberate iodine. Then, the solution was titrated against 0.005 N $Na_2S_2O_3$ using a starch indicator [27] [46]. Ozone dose was calculated using the following formula:

$$\text{Ozone dose}\left(\frac{\text{mg}}{\text{min}}\right) = \frac{\text{Volume of titrant} * \text{normality of titrant} * 24}{\text{Time}}. \qquad (2)$$

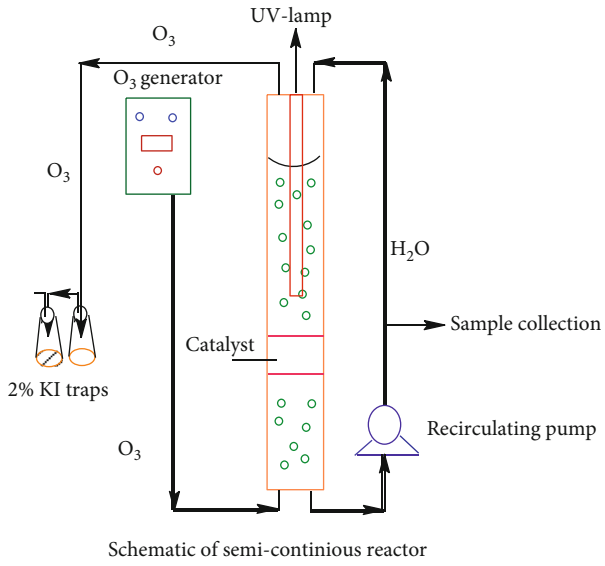

Figure 1: Schematic of semicontinuous reactor for the treatment of ciprofloxacin by the catalytic ozonation process.

2.4.2. Analysis of Ciprofloxacin. Ciprofloxacin concentration was quantified by determining the peak areas before and after treatment using the HPLC system (Hitachi Elite LaChrom L-2130) containing C18 column (4.6 × 250 mm, Poroshell 120). The method was developed before analysis, and the mobile phase composition was 50 : 50 acetonitrile-phosphate buffer (0.2 M KH_2PO_4 and 0.2 M NaOH). The samples were analyzed by injecting a 10 μL solution at a mobile phase flow rate of 1 mL/min.

2.4.3. Analysis of Hydrogen Peroxide. The amount of hydrogen peroxide was monitored by observing the resorufin fluorescence spectrum using a fluorescence spectrometer (F-4500 Japan) having 5 nm slits. Fluorescence was monitored at 587 nm (a calibration curve was drawn by reacting H_2O_2 and Amplex Red reagent [35]).

3. Results and Discussion

3.1. Catalyst Characteristics. The zeolite 5A is a calcium zeolite having the composition Ca4,5 $[(AlO_2)12(SiO_2)12]$ nH_2O. The catalyst was loaded with Fe^{+3} by the impregnation method [47], and the presence of iron on the catalyst was confirmed by FTIR analysis, using PerkinElmer (USA) spectrum 400 analyzer. The results presented in Figure 2 clearly show the iron loading on Z5A. The spectra indicate that a sharp peak at about 970 cm^{-1} reflects stretching vibrations of Si–O and Al–OH [45]. A comparative study shows that a new peak at about 1,442 cm^{-1} is due to iron loading and corresponds to Fe–OH stretching vibrations [45]. The Fe-Z5A surface morphology (Figure 3) and elemental analysis were investigated by SEM–EDX using Tescan, (UK), Vega LMU. The iron was found to be 5%. The SEM image (Figure 2) shows that the surface of the catalyst was smooth and porous. The surface area and pore size were quantified by the BET method. The nitrogen adsorption at 77 K was

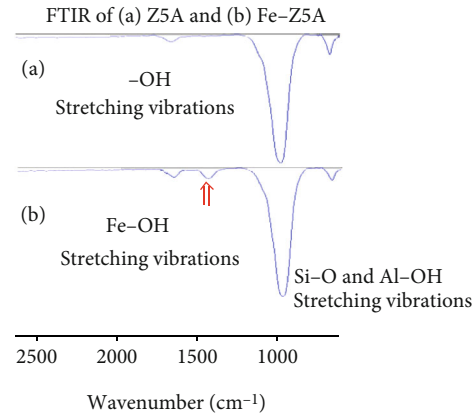

Figure 2: FTIR spectra of Z5A and Fe-Z5A.

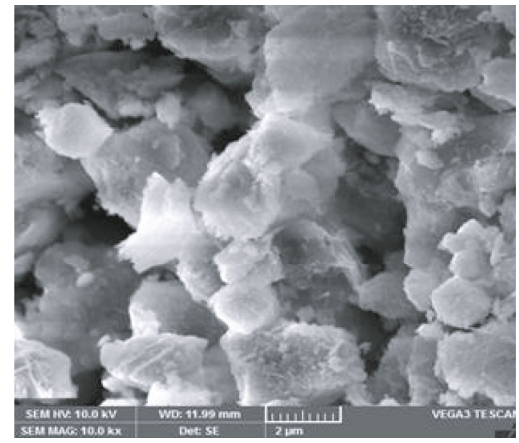

Figure 3: SEM image of Fe-Z5A.

determined by using adsorption isotherms (Figure 4). The Kelvin equation and BJH method were adopted for the determination of porosities [28]. The surface area of Fe-Z5A was 93.25 m^2/g, and the pore size was 5 Å. The mass titration method was used to determine the point of zero charge of Fe-Z5A [48] and was found to be 6.6.

3.2. Comparison of Studied AOPs. The results presented in Figure 5 indicate the comparison between various advanced oxidation processes under similar conditions. The highest removal efficiency was observed for the synergic (O_3/Fe-Z5A/UV) process. For example, the removal efficiencies (in 60 minutes) were 73.4%, 65.6%, 57.1%, and 49.3% for O_3/Fe-Z5A/UV, O_3/Fe-Z5A, O_3/UV, and O_3, respectively (Figure 4). The synergic process (catalytic ozonation with UV irradiation) involves various reactions leading to the production of hydroxyl radicals (equations (3)–(7)). These reactions involves the interaction of ozone with the active sites of catalyst (Fe) leading to the production of hydroxyl radicals (equations (3)–(7)) [35, 49, 50]. In addition, the catalyst may be activated by UV irradiation resulting in the formation of hydroxyl radicals (equation (8)) [51]. The interactions of molecular ozone with UV radiations may also facilitate the production of hydroxyl radicals (equations (9)

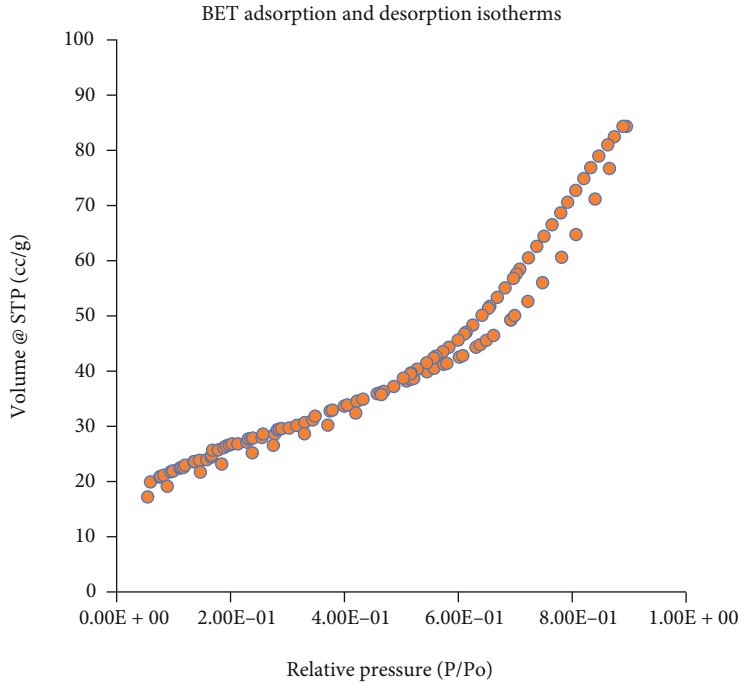

Figure 4: BET isotherm of Fe-zeolite A.

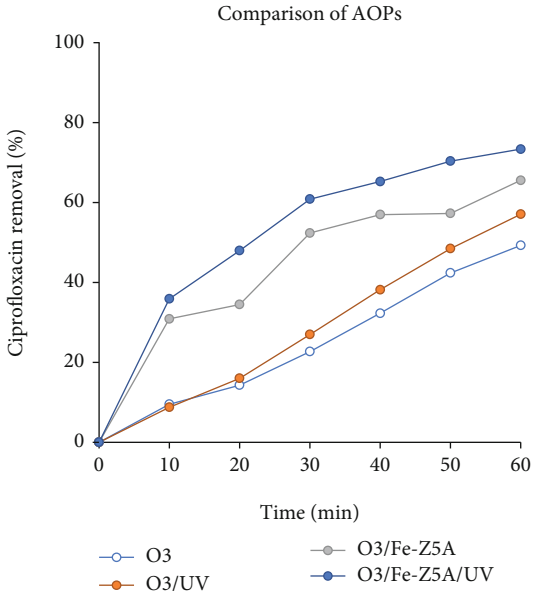

Figure 5: Comparison of AOPs for the removal of ciprofloxacin ($C_{o\,(\text{cipro})}$ = 50 mg/L; pH = 6.5 ± 0.2; O_3 = 0.9 mg/L; volume = 2.5 L; catalyst dose = 25 g: T = 60 min).

and (10)) [52] that reacts with CP leading to its degradation (equation (11)).

$$\text{Z5A} - \text{Fe} - \text{OH} + \text{O}_3 \longrightarrow \text{O}_2 + \text{Z5A} - \text{Fe} - \text{HO}_2{}^{\circ}, \quad (3)$$

$$\text{Z5A} - \text{Fe} - \text{HO}_2{}^{\circ} \longrightarrow \text{Z5A} - \text{Fe} + {}^{\circ}\text{O}_2{}^{-} + \text{H}^{+}, \quad (4)$$

$$\text{Z5A} - \text{Fe} - \text{HO}_2{}^{\circ} + \text{O}_3 \longrightarrow \text{Z5A} - \text{Fe} - \text{HO}_3{}^{\circ} + \text{O}_2, \quad (5)$$

$$\text{Z5A} - \text{Fe} - \text{HO}_3{}^{\circ} \longrightarrow \text{Z5A} - \text{Fe} + {}^{\circ}\text{O}_3{}^{-} + \text{H}^{+}, \quad (6)$$

$${}^{\circ}\text{O}_3{}^{-} + \text{H}_2\text{O} \longrightarrow {}^{\circ}\text{OH} + \text{OH}^{-} + \text{O}_2, \quad (7)$$

$$\text{Fe}^{3+} + \text{H}_2\text{O} + \text{h}\upsilon \longrightarrow \text{Fe}^{2+} + {}^{\circ}\text{OH} + \text{H}^{+}, \quad (8)$$

$$\text{h}\upsilon + \text{O}_3 + \text{H}_2\text{O} \longrightarrow \text{H}_2\text{O}_2 + \text{O}, \quad (9)$$

$$\text{H}_2\text{O}_2 + \text{h}\upsilon \longrightarrow 2{}^{\circ}\text{OH}, \quad (10)$$

$$\text{CF} + {}^{\circ}\text{OH} \longrightarrow \text{CO}_2 + \text{H}_2\text{O}. \quad (11)$$

Additionally, the significantly higher removal efficiency of the O_3/UV process compared to O_3 alone (Figure 5) suggested that UV-rays were involved in the decomposition of ozone, resulting in the production of active oxygen species, and enhance the removal [52].

The adsorption of pollutants on the catalyst surface may also play an important role in the overall removal efficiency of pollutants in water. Therefore, the charge on the pollutant and catalyst may be important in such studies. The point of zero charge of catalyst and pKa values of pollutants may help to identify charges on them while comparing with the initial pH of water [50, 53, 54]. Therefore, in catalytic processes, the point of zero charge of catalyst and pKa values of CF plays an important role [55]. Since the pKa_1 (6.0) of CF is near the point of zero charge ($pH = pH_{pZc}$) of Fe-Z5A, pKa_2 (8.8) is more than the pH of the CP solution (CP solution: pH = 6.5 ± 0.2). Thus, at the analyzed pH, the CF may acquire a positive charge (PKa_2 is more than solution pH, while the zeolite surface may have a slight negative charge (as pH_{pzc} of zeolite is slightly above CP solution pH)); this further aids in the adsorption of CF on the catalyst surface

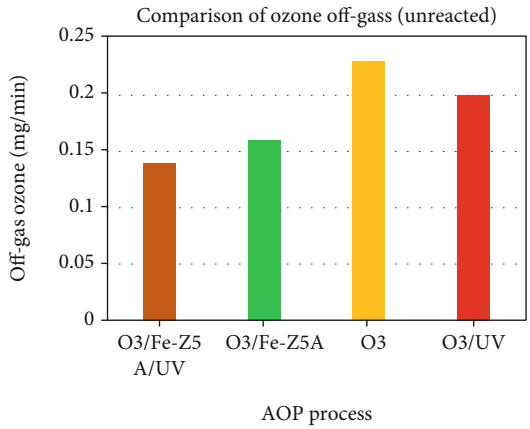

Figure 6: Comparison of AOPs for off-gas measured from KI traps during the removal of ciprofloxacin ($C_{o\,(cipro)}$ = 50 mg/L; pH = 6.5 ± 0.2; O_3 = 0.9 mg/L; volume = 2.5 L; catalyst dose = 25 g: T = 60 min).

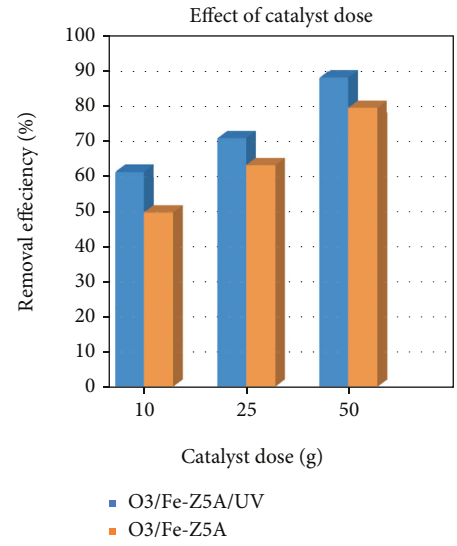

Figure 7: Catalyst dose effect on ciprofloxacin removal ($C_{o\,(cipro)}$ = 50 mg/L; pH = 6.5 ± 0.2; O_3 = 0.9 mg/L; volume = 2.5 L; catalyst dose = 10 g, 25 g, and 50 g: T = 60 min).

and has a positive impact on the removal performance as compared to processes without catalyst [50, 53, 54].

It is worth mentioning that gaseous ozone (unreacted) released from the reactor was measured (Figure 6). It was also observed that the synergic process produced the least amount of ozone (mg/min). For example, 0.14 mg/min, 0.16 mg/min, 0.2 mg/min, and 0.23 mg/min were quantified for O_3/Fe-Z5A/UV, O_3/Fe-Z5A, O_3UV, and O_3 processes, respectively (Figure 6). The results exhibit an important correlation between the CF removed and off-gas ozone released in various processes. The off-gas ozone resealed in above-mentioned processes was in the opposite order to the removal efficiency of CF in the various processes (Figures 5 and 6). The synergic process was found to have the least off-gas ozone release. It is hypothesized that more ozone decomposition may result in the production of active oxygen species compared to others in the synergic process.

3.3. Catalyst (Fe-Z5A) Dose Effect. It is essential to investigate the role of the proposed catalyst in UV and O_3; therefore, the catalyst dose effect is studied. The results presented in Figure 7 indicate that with an increase in catalyst dose, the removal efficiency of CF improved for both UV/O_3/Fe-Z5A and O_3/Fe-Z5A processes. Hence, it is suggested that a higher catalyst dose increases the number of active sites, leading to more decomposition of aqueous ozone and the generation of hydroxyl radicals.

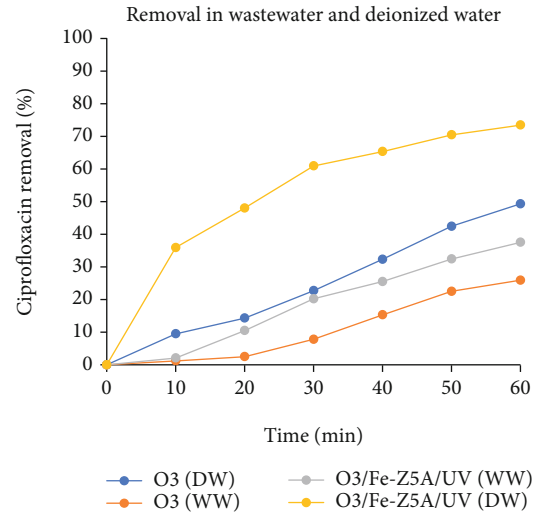

Figure 8: Comparison of ciprofloxacin removal in municipal wastewater and deionized water using O_3 and UV/O_3/FeZ5A ($C_{o\,(cipro)}$ = 50 mg/L; COD = 104 mg/L; pH_{DW} = 6.5 ± 0.2; pH_{ww} = 7.2 ± 0.2; O_3 = 0.9 mg/L; volume = 2.5 L; catalyst dose = 25 g: T = 60 min).

3.4. Ciprofloxacin Removal in Municipal Wastewater. In this study, the CF was spiked in municipal wastewater samples to investigate the removal efficiency of the synergic process in a real wastewater matrix. In most of the previous findings, aqueous solutions of pharmaceuticals were prepared to investigate the processes. However, it is indeed essential to test a catalytic process in real conditions since the wastewater matrix is more complex and contains inhibitors such as turbidity, radical scavengers, bacteria etc.

The results presented in Figure 8 show that the removal efficiency of the synergic process was decreased significantly in wastewater. This may be due to the presence of inhibitors in wastewater [56]. Furthermore, the COD in wastewater due to organic pollutants may also compete with the removal of CF. Interestingly, when the results were compared with single ozonation, it was observed that the efficiency of CF removal was significantly higher in catalytic ozonation process as compared with ozonation alone in both the deionized water and wastewater (Figure 8). For example, the removal efficiency (in 60 minutes) of CF was 49.3%, 37.5%, and 25.9% for synergic process in wastewater, single ozonation in wastewater, and single ozonation in deionized

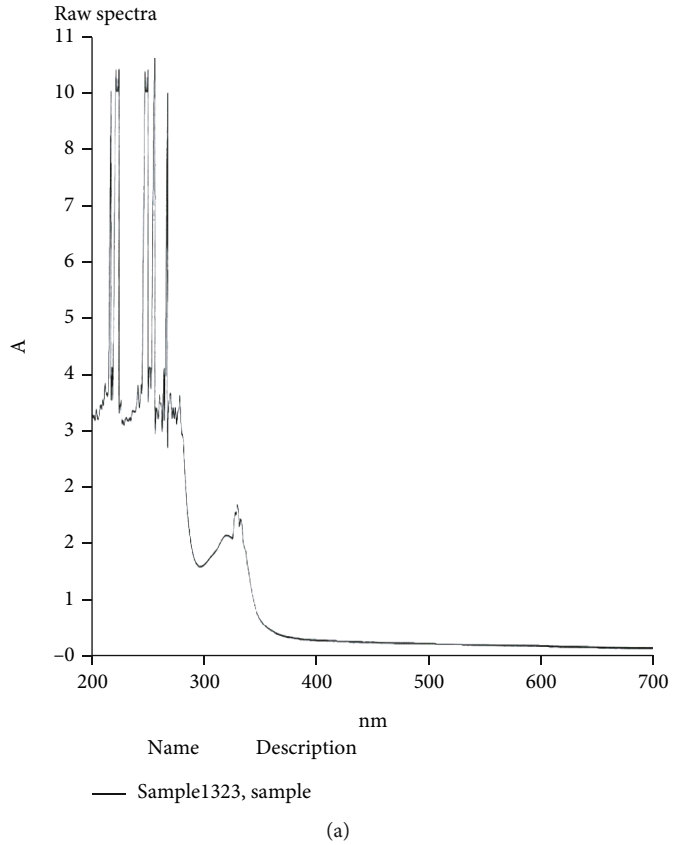

(a)

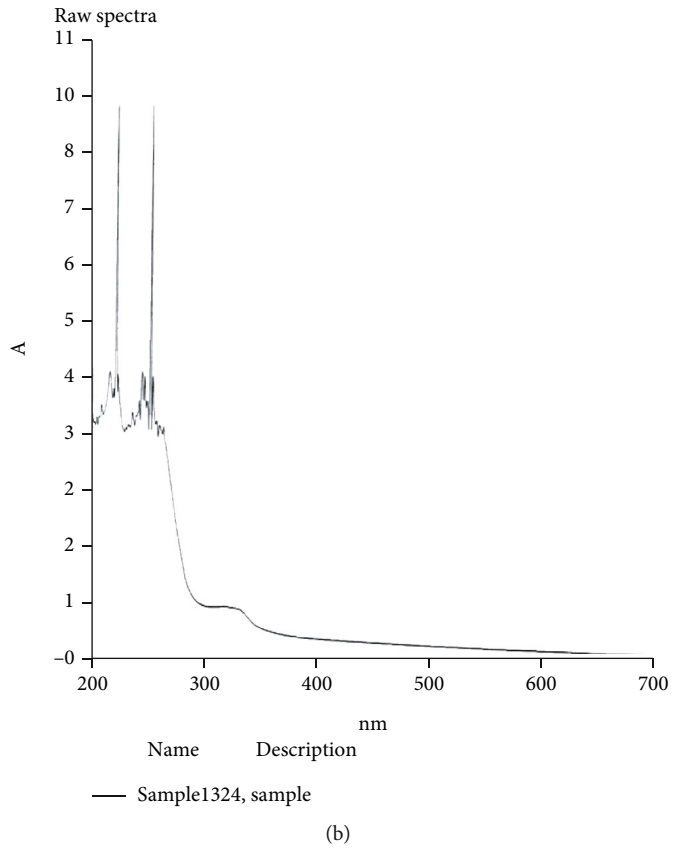

(b)

Figure 9: Spectrophotometer analysis of wastewater before (a) and after treatment (b) with the UV/Fe-Z5A/O3 process (spiked $C_{o\,(\text{cipro})}$ = 50 mg/L; COD = 104 mg/L; pH = 7.2 ± 0.2; O_3 = 0.9 mg/L; volume = 2.5 L; catalyst dose = 25 g: T = 60 min).

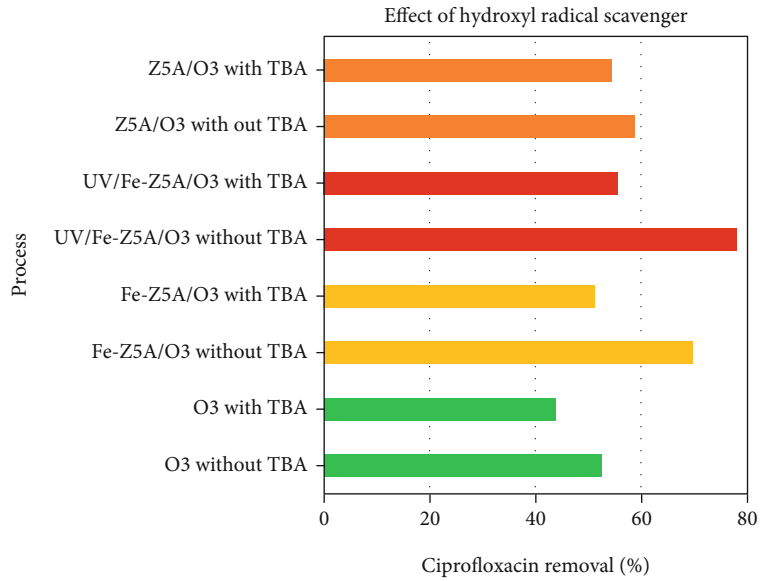

Figure 10: TBA effect on ciprofloxacin removal for O_3, O_3/Z5A, O_3/Fe-Z5A, and UV/O_3/FeZ5A processes ($C_{o\,(\text{cipro})}$ = 50 mg/L; TBA = 50 ppm; pH = 6.5 ± 0.2; O_3 = 0.9 mg/L; volume = 2.5 L; catalyst dose = 25: T = 60 min).

water, respectively (Figure 7). Therefore, the results suggest that the synergic process (UV/O_3/Fe-Z5A) is even effective in real conditions for the removal of pharmaceuticals in wastewater. The UV scan of CF spiked wastewater before and after treatment with a synergic process (Figure 9) also clearly indicates the removal of organic pollutants in the presence of the synergic process.

3.5. Mechanism of Synergic Process

3.5.1. Radical Scavenger Effect. The t-butanol, due to its high rate of reaction with hydroxyl radicals, was found to be effective in investigating the production of hydroxyl radicals in AOPs [57]. The current investigation results (Figure 10) suggested that the synergic process involves the radical-based mechanism. Moreover, in the synergic process, more decrease in removal efficiency was observed with TBA than other studied processes. This further supports our hypothesis that the synergic process is highly effective compared to others because it leads to the more decomposition of aqueous ozone, leading to hydroxyl radicals (Figure 10). Interestingly, the findings presented in Figure 10 agree with the results of off-gas ozone shown in Figure 5.

When the results were compared to single ozonation, the results indicate that in the Z5A/O_3 process, no significant decrease in CP efficiency was observed in the presence of TBA. This suggested that Z5A/O_3 removes CF through a nonradical mechanism [28, 33]. In contrast, iron-loaded zeolites follow a radical mechanism (Figure 10). Therefore, the current investigation also helps further to understand the importance of iron loading on zeolites. Since wastewater is a complex media in which various kinds of radical scavengers such as phosphates and sulfates may be present in significant amounts, it is critical to select such catalysts that may follow radical and selectively nonradical mechanisms.

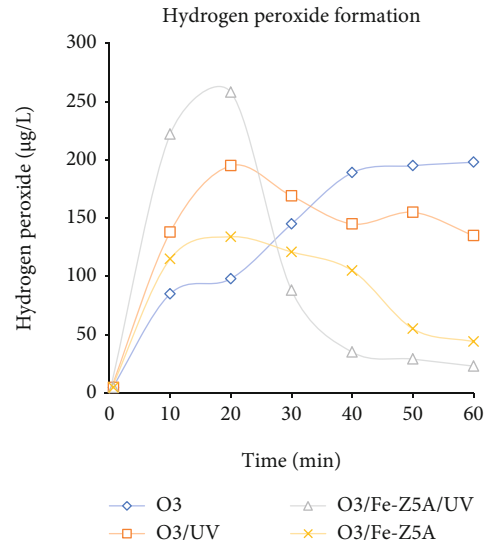

Figure 11: Formation of hydrogen peroxide in synergic process, catalytic ozonation, single ozonation, and ozone UV process (C_o Amplex Red = 15 mg/L; pH = 6.5 ± 0.2; O_3 = 0.9 mg/L; volume = 2.5 L; catalyst dose = 25: T = 60 min).

Therefore, zeolites are among the unique catalysts that may follow both mechanisms, and metal loadings on them may be significant in the generation of hydroxyl radicals [32, 49].

3.5.2. Formation of Hydrogen Peroxide. Understanding the mechanism of the synergic pathway and verifying its effectiveness, the production of H_2O_2 in various processes was investigated. The hydrogen peroxide may form either by the combination of two hydroxyl radicals in bulk or by UV irradiation of ozone in the presence of water molecules

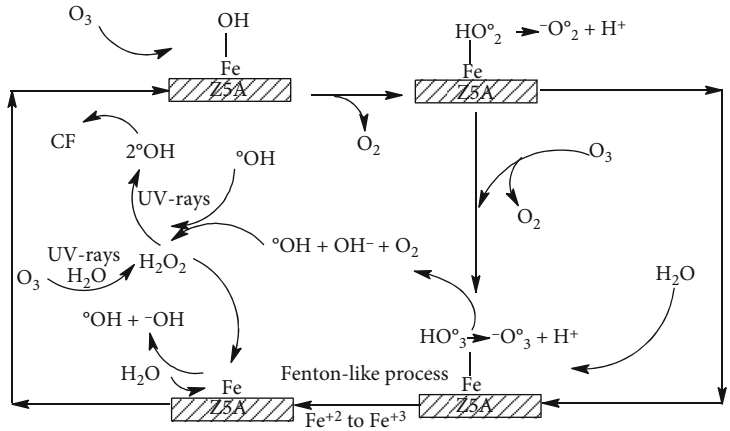

Figure 12: Mechanism of UV-assisted catalytic ozonation on Fe-Z5A.

[52] as shown in the following equations.

$$h\upsilon + O_3 + H_2O \longrightarrow H_2O_2 + O, \quad (12)$$

$$^{o}OH + {}^{o}OH \longrightarrow H_2O_2. \quad (13)$$

Therefore, in the catalytic ozonation process (without UV) and single ozonation process, many hydroxyl radicals may combine to form stable H_2O_2 with low reactivity with organic pollutants. Hence, in the current investigation, UV-based catalytic ozonation process may decompose the formed H_2O_2 by either a Fenton-like mechanism [58] or by UV irradiation (Figures 11 and 12).

Figure 11 indicates that H_2O_2 production was the highest in the synergic process in the first 20 minutes. On the other hand, its decomposition was also the highest in the case of the synergic process. A higher H_2O_2 was formed in the synergic process and the generation of more ^{o}OH radicals (Figure 11). Experiments further confirmed this in the presence of hydroxyl radical scavengers (Figure 9).

Interestingly, Figure 11 also shows that the formation of H_2O_2 markedly decreased after 20 minutes when the synergic process was used. This is attributed to Fenton-like decomposition on catalyst surface (Figure 11) and H_2O_2 due to UV-rays in bulk (equation (4)), leading to the generation of reactive oxygen species. Consequently, it elaborates that the effectiveness of the synergic process was due to the decomposition of H_2O_2 causing the formation of hydroxyl radicals that further leads to degradation of CF. Mechanism of UV-assisted catalytic ozonation on Fe-Z5A is fully described in Figure 12.

4. Conclusions

Based on the results, it is concluded that the synergic process (UV/O_3/Fe-Z5A) was the most efficient process as compared to other studied processes (O_3, O_3/UV, and O_3/Fe-Z5A processes). The TBA effect suggested that the Fe-Z5A/O_3 process degrades ciprofloxacin via hydroxyl radical-based mechanism. The synergic process was also influential in real wastewater in removing ciprofloxacin as compared with single ozonation process. The synergic process effectively decomposes hydrogen peroxide leading to the production of fewer hydroxyl radicals than other studied processes.

Data Availability

The data used to support the findings of this study are included within the article additional information/data that will be available upon request.

Conflicts of Interest

The authors have no conflicts of interest to declare that are relevant to the content of this article.

Acknowledgments

Dr. Amir Ikhlaq and Fei Qi highly acknowledge the Pakistan Science Foundation (PSF) for their funding and support under PSF/CRP 18th Protocol (12). We highly appreciate the support of theInstitute of Environmental Engineering, UET Lahore, Pakistan. In addition, the authors extend their appreciation to the Deanship of Scientific Research, University of Hafr Al Batin for financial support through the research group project No. S-0048-1443.

References

[1] F. J. Beltrán, A. Aguinaco, J. F. García-Araya, and A. Oropesa, "Ozone and photocatalytic processes to remove the antibiotic sulfamethoxazole from water," *Water Research*, vol. 42, no. 14, pp. 3799–3808, 2008.

[2] M. Mehrjouei, S. Müller, and D. Möller, "A review on photocatalytic ozonation used for the treatment of water and wastewater," *Chemical Engineering Journal*, vol. 263, pp. 209–219, 2015.

[3] R. Javaid, H. Kawanami, M. Chatterjee, T. Ishizaka, A. Suzuki, and T. M. Suzuki, "Fabrication of microtubular reactors coated with thin catalytic layer (M=Pd, Pd–Cu, Pt, Rh, Au)," *Catalysis Communications*, vol. 11, no. 14, pp. 1160–1164, 2010.

[4] R. Javaid, U. Y. Qazi, and S. I. Kawasaki, "Highly efficient decomposition of Remazol Brilliant Blue R using tubular

reactor coated with thin layer of PdO," *Journal of Environmental Management*, vol. 180, pp. 551–556, 2016.

[5] R. Javaid, H. Kawanami, M. Chatterjee, T. Ishizaka, A. Suzuki, and T. M. Suzuki, "Sonogashira C-C coupling reaction in water using tubular reactors with catalytic metal inner surface," *Chemical Engineering Journal*, vol. 167, no. 2-3, pp. 431–435, 2011.

[6] U. Y. Qazi, Z. Shervani, and R. Javaid, "Green synthesis of silver nanoparticles by pulsed laser irradiation: effect of hydrophilicity of dispersing agents on size of particles," *Frontiers in Nanoscience and Nanotechnology*, vol. 4, pp. 61–69, 2015.

[7] I. Velo-Gala, J. J. López-Peñalver, M. Sánchez-Polo, and J. Rivera-Utrilla, "Activated carbon as photocatalyst of reactions in aqueous phase," *Applied Catalysis B: Environmental*, vol. 142-143, pp. 694–704, 2013.

[8] N. M. Mahmoodi, "Photocatalytic ozonation of dyes using multiwalled carbon nanotube," *Journal of Molecular Catalysis A: Chemical*, vol. 366, pp. 254–260, 2013.

[9] S. Anandan, G. J. Lee, P. K. Chen, C. Fan, and J. J. Wu, "Removal of Orange II dye in water by visible light assisted photocatalytic ozonation using Bi2O3and Au/Bi2O3nanorods," *Industrial and Engineering Chemistry Research*, vol. 49, no. 20, pp. 9729–9737, 2010.

[10] J. Xiao, Y. Xie, and H. Cao, "Organic pollutants removal in wastewater by heterogeneous photocatalytic ozonation," *Chemosphere*, vol. 121, pp. 1–17, 2015.

[11] A. Tabasum, M. Alghuthaymi, U. Y. Qazi et al., "Uv-accelerated photocatalytic degradation of pesticide over magnetite and cobalt ferrite decorated graphene oxide composite," *Plants*, vol. 10, no. 1, pp. 1–18, 2020.

[12] U. Y. Qazi, R. Javaid, N. Tahir, A. Jamil, and A. Adeel, "Design of advanced self-supported electrode by surface modification of copper foam with transition metals for efficient hydrogen evolution reaction," *International Journal of Hydrogen Energy*, vol. 45, no. 58, pp. 33396–33406, 2020.

[13] Y. Wang, Y. Xie, H. Sun, J. Xiao, H. Cao, and S. Wang, "Efficient catalytic ozonation over reduced graphene oxide for p-hydroxylbenzoic acid (PHBA) destruction: active site and mechanism," *ACS Applied Materials & Interfaces*, vol. 8, no. 15, pp. 9710–9720, 2016.

[14] A. Ikhlaq, R. Fatima, U. Y. Qazi et al., "Combined iron-loaded zeolites and ozone-based process for the purification of drinking water in a novel hybrid reactor: removal of faecal coliforms and arsenic," *Catalysts*, vol. 11, no. 3, p. 373, 2021.

[15] U. Y. Qazi, C. Z. Yuan, N. Ullah et al., "One-step growth of iron-nickel bimetallic nanoparticles on FeNi alloy foils: highly efficient advanced electrodes for the oxygen evolution reaction," *ACS Applied Materials & Interfaces*, vol. 9, no. 34, pp. 28627–28634, 2017.

[16] M. U. Rahman, U. Y. Qazi, T. Hussain et al., "Solar driven photocatalytic degradation potential of novel graphitic carbon nitride based nano zero-valent iron doped bismuth ferrite ternary composite," *Optical Materials*, vol. 120, article 111408, 2021.

[17] R. Javaid, U. Y. Qazi, A. Ikhlaq, M. Zahid, and A. Alazmi, "Subcritical and supercritical water oxidation for dye decomposition," *Journal of Environmental Management*, vol. 290, article 112605, 2021.

[18] A. Ikhlaq, F. Javed, A. Akram et al., "Treatment of leachate through constructed wetlands using Typha angustifolia in combination with catalytic ozonation on Fe-zeolite A," *International Journal of Phytoremediation*, vol. 23, pp. 809–817, 2021.

[19] N. Tahir, M. Zahid, H. N. Bhatti et al., "Silver-doped ternary compounds for wastewater remediation," in *Silver Nanomaterials for Agri-Food Applications*, pp. 623–653, Elsevier, 2021.

[20] M. Madkour, Y. Abdelmonem, U. Y. Qazi, R. Javaid, and S. Vadivel, "Efficient Cr(vi) photoreduction under natural solar irradiation using a novel step-scheme ZnS/Snin4S8nano-heterostructured photocatalysts," *RSC Advances*, vol. 11, no. 47, pp. 29433–29440, 2021.

[21] N. Fatima, U. Y. Qazi, A. Mansha et al., "Recent developments for antimicrobial applications of graphene-based polymeric composites: a review," *Journal of Industrial and Engineering Chemistry*, vol. 100, pp. 40–58, 2021.

[22] U. Y. Qazi, R. Javaid, M. Zahid, N. Tahir, A. Afzal, and X. M. Lin, "Bimetallic NiCo–NiCoO2 nano-heterostructures embedded on copper foam as a self-supported bifunctional electrode for water oxidation and hydrogen production in alkaline media," *International Journal of Hydrogen Energy*, vol. 46, no. 36, pp. 18936–18948, 2021.

[23] N. M. Mahmoodi and M. H. Saffar-Dastgerdi, "Zeolite nanoparticle as a superior adsorbent with high capacity: synthesis, surface modification and pollutant adsorption ability from wastewater," *Microchemical Journal*, vol. 145, pp. 74–83, 2019.

[24] Y. Xu, Q. Wang, B. A. Yoza et al., "Catalytic ozonation of recalcitrant organic chemicals in water using vanadium oxides loaded ZSM-5 zeolites," *Frontiers in Chemistry*, vol. 7, p. 384, 2019.

[25] H. Einaga and S. Futamura, "Catalytic oxidation of benzene with ozone over Mn ion-exchanged zeolites," *Catalysis Communications*, vol. 8, no. 3, pp. 557–560, 2007.

[26] J. A. Medrano, A. Garofalo, L. Donato et al., "CO selective oxidation using catalytic zeolite membranes," *Chemical Engineering Journal*, vol. 351, pp. 40–47, 2018.

[27] H. Valdés, V. J. Farfán, J. A. Manoli, and C. A. Zaror, "Catalytic ozone aqueous decomposition promoted by natural zeolite and volcanic sand," *Journal of Hazardous Materials*, vol. 165, no. 1-3, pp. 915–922, 2009.

[28] A. Ikhlaq, S. Waheed, K. S. Joya, and M. Kazmi, "Catalytic ozonation of paracetamol on zeolite a: non-radical mechanism," *Catalysis Communications*, vol. 112, pp. 15–20, 2018.

[29] C. W. Kwong, C. Y. H. Chao, K. S. Hui, and M. P. Wan, "Catalytic ozonation of toluene using zeolite and MCM-41 materials," *Environmental Science & Technology*, vol. 42, no. 22, pp. 8504–8509, 2008.

[30] Y. Kitada, H. Kawahata, A. Suzuki, and T. Oomori, "Catalytic activity and stability of Y zeolite for phenol degradation in the presence of ozone," *Applied Catalysis B: Environmental*, vol. 82, no. 3-4, pp. 163–168, 2008.

[31] N. A. S. Amin, J. Akhtar, and H. K. Rai, "Catalytic ozonation of aqueous phenol over metal-loaded HZSM-5," *Water Science and Technology*, vol. 63, no. 8, pp. 1651–1656, 2011.

[32] C. Chen, X. Yan, B. A. Yoza et al., "Efficiencies and mechanisms of ZSM5 zeolites loaded with cerium, iron, or manganese oxides for catalytic ozonation of nitrobenzene in water," *Science of the Total Environment*, vol. 612, pp. 1424–1432, 2018.

[33] A. Ikhlaq and B. Kasprzyk-Hordern, "Catalytic ozonation of chlorinated VOCs on ZSM-5 zeolites and alumina: formation of chlorides," *Applied Catalysis B: Environmental*, vol. 200, pp. 274–282, 2017.

[34] K. González-Labrada, R. Richard, C. Andriantsiferana, H. Valdés, U. J. Jáuregui-Haza, and M. H. Manero, "Enhancement of ciprofloxacin degradation in aqueous system by heterogeneous catalytic ozonation," *Environmental Science and Pollution Research*, vol. 27, no. 2, pp. 1246–1255, 2020.

[35] A. Ikhlaq, D. R. Brown, and B. Kasprzyk-Hordern, "Mechanisms of catalytic ozonation: an investigation into superoxide ion radical and hydrogen peroxide formation during catalytic ozonation on alumina and zeolites in water," *Applied Catalysis B: Environmental*, vol. 129, pp. 437–449, 2013.

[36] A. J. Watkinson, E. J. Murby, D. W. Kolpin, and S. D. Costanzo, "The occurrence of antibiotics in an urban watershed: from wastewater to drinking water," *Science of the Total Environment*, vol. 407, no. 8, pp. 2711–2723, 2009.

[37] W. Li, Y. Shi, L. Gao, J. Liu, and Y. Cai, "Occurrence of antibiotics in water, sediments, aquatic plants, and animals from Baiyangdian Lake in North China," *Chemosphere*, vol. 89, no. 11, pp. 1307–1315, 2012.

[38] J. Xu, Y. Xu, H. Wang et al., "Occurrence of antibiotics and antibiotic resistance genes in a sewage treatment plant and its effluent-receiving river," *Chemosphere*, vol. 119, pp. 1379–1385, 2015.

[39] R. Javaid and U. Y. Qazi, "Catalytic oxidation process for the degradation of synthetic dyes: an overview," *International Journal of Environmental Research and Public Health*, vol. 16, no. 11, article 2066, 2019.

[40] L. Hu, G. X. Hao, H. D. Luo et al., "Bifunctional 2D cd(II)-based metal-organic framework as efficient heterogeneous catalyst for the formation of C-C bond," *Crystal Growth & Design*, vol. 18, no. 5, pp. 2883–2889, 2018.

[41] A. Zeb, S. Sahar, U. Y. Qazi et al., "Intrinsic peroxidase-like activity and enhanced photo-Fenton reactivity of iron-substituted polyoxometallate nanostructures," *Dalton Transactions*, vol. 47, no. 21, pp. 7344–7352, 2018.

[42] H. H. Zou, C. Z. Yuan, H. Y. Zou et al., "Bimetallic phosphide hollow nanocubes derived from a prussian-blue-analog used as high-performance catalysts for the oxygen evolution reaction," *Science and Technology*, vol. 7, no. 7, pp. 1549–1555, 2017.

[43] A. Ikhlaq, M. Anis, F. Javed et al., "Catalytic ozonation for the treatment of municipal wastewater by iron loaded zeolite A," *Desalin Water Treat*, vol. 152, pp. 108–115, 2019.

[44] Y. Flores, R. Flores, and A. A. Gallegos, "Heterogeneous catalysis in the Fenton-type system reactive black 5/H2O2," *Journal of Molecular Catalysis A: Chemical*, vol. 281, no. 1-2, pp. 184–191, 2008.

[45] F. Adam, T. S. Chew, and J. Andas, "A simple template-free sol-gel synthesis of spherical nanosilica from agricultural biomass," *Journal of Sol-Gel Science and Technology*, vol. 59, no. 3, pp. 580–583, 2011.

[46] A. D. Eaton, M. A. H. Franson, L. S. Clesceri, E. W. Rice, and A. E. Greenberg, *Standard methods for the examination of water & wastewater*, American Public Health Association (APHA), Washington, DC, USA, 2005.

[47] M. Tekbaş, H. C. Yatmaz, and N. Bektaş, "Heterogeneous photo-Fenton oxidation of reactive azo dye solutions using iron exchanged zeolite as a catalyst," *Microporous and Mesoporous Materials*, vol. 115, no. 3, pp. 594–602, 2008.

[48] J. P. Reymond and F. Kolenda, "Estimation of the point of zero charge of simple and mixed oxides by mass titration," in *Powder Technol.*, pp. 30–36, Elsevier Sequoia SA, 1999.

[49] D. Gümüş and F. Akbal, "A comparative study of ozonation, iron coated zeolite catalyzed ozonation and granular activated carbon catalyzed ozonation of humic acid," *Chemosphere*, vol. 174, pp. 218–231, 2017.

[50] A. Ikhlaq, D. R. Brown, and B. Kasprzyk-Hordern, "Catalytic ozonation for the removal of organic contaminants in water on alumina," *Applied Catalysis B: Environmental*, vol. 165, pp. 408–418, 2015.

[51] S. Gomez, L. Lerici, C. Saux et al., "Fe/ZSM-11 as a novel and efficient photocatalyst to degrade Dichlorvos on water solutions," *Applied Catalysis B: Environmental*, vol. 202, pp. 580–586, 2017.

[52] A. Latifoglu and M. D. Gurol, "The effect of humic acids on nitrobenzene oxidation by ozonation and O3/UV processes," *Water Research*, vol. 37, no. 8, pp. 1879–1889, 2003.

[53] J. Choina, H. Kosslick, C. Fischer, G. U. Flechsig, L. Frunza, and A. Schulz, "Photocatalytic decomposition of pharmaceutical ibuprofen pollutions in water over titania catalyst," *Applied Catalysis B: Environmental*, vol. 129, pp. 589–598, 2013.

[54] D. Shan, S. Deng, C. Jiang et al., "Hydrophilic and strengthened 3D reduced graphene oxide/nano-Fe3O4hybrid hydrogel for enhanced adsorption and catalytic oxidation of typical pharmaceuticals," *Nano*, vol. 5, no. 7, pp. 1650–1660, 2018.

[55] Y. Sun, H. Li, G. Li, B. Gao, Q. Yue, and X. Li, "Characterization and ciprofloxacin adsorption properties of activated carbons prepared from biomass wastes by H3PO4 activation," *Bioresource Technology*, vol. 217, pp. 239–244, 2016.

[56] N. Kishimoto, Y. Yasuda, H. Mizutani, and Y. Ono, "Applicability of ozonation combined with electrolysis to 1,4-Dioxane removal from wastewater containing radical scavengers," *Ozone Science and Engineering*, vol. 29, no. 1, pp. 13–22, 2007.

[57] A. Ikhlaq, D. R. Brown, and B. Kasprzyk-Hordern, "Mechanisms of catalytic ozonation on alumina and zeolites in water: formation of hydroxyl radicals," *Applied Catalysis B: Environmental*, vol. 123-124, pp. 94–106, 2012.

[58] R. Gonzalez-Olmos, U. Roland, H. Toufar, F. D. Kopinke, and A. Georgi, "Fe-zeolites as catalysts for chemical oxidation of MTBE in water with H2O2," *Applied Catalysis B: Environmental*, vol. 89, no. 3-4, pp. 356–364, 2009.

Hindawi
Journal of Chemistry
Volume 2022, Article ID 9727857, 24 pages
https://doi.org/10.1155/2022/9727857

Review Article

Emerging Pollutants in Moroccan Wastewater: Occurrence, Impact, and Removal Technologies

Yassine Jari,[1] **Nicolas Roche**,[1,2] **Mohamed Chaker Necibi**,[1] **Souad El Hajjaji**,[1,3] **Driss Dhiba**,[1] **and Abdelghani Chehbouni**[1,4]

[1]*International Water Research Institute (IWRI), Mohammed VI Polytechnic University, Ben Guerir 43150, Morocco*
[2]*Aix-Marseille University, CNRS, IRD, INRAE, Coll France, CEREGE, CEDEX, Aix-en-Provence 13454, France*
[3]*Laboratory of Spectroscopy Molecular Modelling Materials Nanomaterials Water and Environment (LS3MN2E-CERNE2D), Faculty of Sciences, Mohammed V University in Rabat, Rabat, Morocco*
[4]*Centre D'études Spatiales de la Biosphère (Cesbio), Institut de Recherche Pour le Développement (IRD), Unité Mixte de Recherche (UMR), Toulouse 31401, France*

Correspondence should be addressed to Yassine Jari; yassine.jari@um6p.ma

Received 11 October 2021; Revised 7 December 2021; Accepted 27 December 2021; Published 25 January 2022

Academic Editor: Umair Yaqub Qazi

The rapid growth of anthropogenic activities in recent decades has resulted in the appearance of numerous new chemical compounds in the environment, known as "emerging pollutants" (EPs) or "contaminants of emerging concern" (CECs). Although partially or not yet regulated or monitored, there is growing research interest in these EPs among the scientific community because of their bioaccumulation, persistence, and adverse effects. Among these, endocrine disruptors, pesticides, and pharmaceuticals can have harmful impacts on human health and the ecosystem. Conventional wastewater treatment technologies are not effective in removing these contaminants, allowing them to be released into the receiving environment. In order to improve the understanding of emerging pollutants, this review discusses the source, occurrence, and impacts of bisphenol A, atrazine, amoxicillin, and paracetamol as model molecules of emerging environmental pollutants, an issue that remains underrepresented in Morocco. Then, treatment methods for EPs are reviewed, including adsorption, advanced oxidation processes, biodegradation, and hybrid treatment. It is proposed that adsorption and photocatalysis can be used as simple, effective, and environmentally friendly technologies for their removal. Thus, we summarize some of the adsorbent and photocatalyst materials applied in recent work to control these pollutants. Towards the end of this paper, the development of inexpensive and locally available (Morocco) materials to remove these compounds from wastewater is considered.

1. Introduction

Studies on wastewater quality have generally focused on priority pollutants, nutrients, microbial contaminants, heavy metals, and dyes. Recently, a wide range of pollutants (emerging pollutants) have attracted researchers' attention and pose a risk to the environment and human health, namely, compounds generated by applying new technological processes [1, 2]. Emerging pollutants (EPs), also known as emerging contaminants (ECs) or contaminants of emerging concern (CECs), are a set of newly identified natural or synthetic chemical compounds that are not monitored but may enter the environment and harm aquatic life and humans [3–5]. The Journal *Emerging Contaminants* has defined these compounds as "*. . .chemicals that are not currently (or have been only recently) regulated and about which there exist concerns regarding their impact on human or ecological health.*" [6].

Emerging pollutants (EPs), such as endocrine disruptors, pesticides, pharmaceuticals, and their degradation products, are of growing and global concern. They can have negative impacts on human and ecosystem health. However, their presence in the environment is generally in the low concentration range (from $\mu g\ L^{-1}$ to $ng\ L^{-1}$) [3, 7]. Therefore,

numerous studies have been conducted worldwide on the pollution of the aquatic environment by EPs and have confirmed their presence in almost all aqueous media, such as surface water, groundwater, seawater, drinking water, and wastewater [1, 5, 7, 8].

To date, studies on the identification of these pollutants are extremely limited in a number of developing countries, particularly in Africa as well as in other parts of the world, and are relatively new in some of them, due to a variety of factors, including the lack of analytical methods for detecting pollutants in wastewater. Indeed, scientists in these countries need to accelerate research on the presence and fate of emerging contaminants as recalcitrant water-borne pollutants, from their emission to their discharge into the environment, in order to address threats to human health and environment [3].

Numerous treatment technologies for emerging pollutants have been adopted to reduce their impacts. Current treatment processes fall into three categories: physical, chemical, and biological. Techniques such as adsorption, advanced oxidation processes (AOPs), and biological treatment have been explored to counteract the adverse effects of these contaminants [9]. In particular, adsorption treatment is an effective way to remove emerging contaminants that tend to spread in the environment. In addition, photocatalytic degradation is considered a promising technique for mineralizing a large proportion of trace micropollutants using sunlight [10]. However, new treatment technologies are needed to provide high-quality water for human and environmental needs [11].

Morocco is one of the developing countries that has started to address this type of issues. This review aims to present an overview of the state of the art in the Moroccan context concerning emerging contaminants such as endocrine disruptors, pesticides, and pharmaceuticals. The focus is on a general description of the source of four typical EPs (bisphenol A, atrazine, amoxicillin, and paracetamol), their occurrence in the aquatic environment, and their environmental impacts. Then, treatment methods for these compounds, including adsorption, advanced chemical oxidation, biodegradation, and hybrid processes, are reviewed.

The ultimate purpose of this review is to present the core of emerging pollutant treatment via adsorption and photocatalytic degradation, as well as their combination. The research directions in this field should focus on the valorization of natural resources and waste in order to develop highly efficient adsorbents and photocatalysts from locally sourced materials. In addition, solar energy systems should be given special attention in Morocco in order to make more efficient use of these renewable energy sources. Towards the end of the paper, the application of coupled adsorption and photocatalysis for the treatment of emerging pollutants in Moroccan wastewater is considered.

2. Emerging Pollutants (EPs)

Emerging contaminants are typically substances with a newly identified source/alternative route to humans [9]. They can enter the environment from various sources, such as industrial effluents, agricultural runoff, and leaking domestic wastewater and municipal wastewater treatment plants [9, 10]. Figure 1 depicts the pathways of EPs into the aquatic environment. According to previous studies, existing conventional wastewater treatment plants are ineffective in removing/degrading many of these contaminants, allowing them to be released into the environment and threaten living organisms and human health [3, 11].

2.1. Endocrine Disruptors (EDs). Endocrine disruptors are defined as chemical substances of natural or synthetic origin that can interfere with the hormonal system (in which hormones work as chemical messengers to control and coordinate body functions) [7, 12] by altering processes such as the synthesis, storage, release, metabolism, and transport of the body's natural hormones [10]. These are compounds that can accumulate in the environment and have harmful effects on the ecosystem and on human health.

EDs are classically grouped into families according to their use, including pesticides, flame retardants, natural and synthetic hormones, plasticizers, personal care products, detergents, and some pharmaceuticals [13, 14]. They are present in almost all aqueous media at various levels, such as surface water, groundwater, seawater, wastewater from wastewater treatment plants, and drinking water [15]. These components are of great concern because of their negative impact on the ecosystem.

2.2. Pesticides. Pesticides encompass all compounds intended to prevent, destroy, repel, or mitigate pests [16]. Their use can be diverse, being applied on agricultural land, private gardens, and other public spaces [17]. They are widely used in different parts of the world, according to the literature review.

Pesticides are generally classified into four broad categories according to their intended targets: herbicides, insecticides, fungicides, and bactericides [16]. Although applied to the soil, these substances can be transported offfield into water bodies by surface runoff and percolation through the soil, thereby affecting water quality by posing a risk to aquatic compartments and human health [18, 19].

2.3. Pharmaceuticals. Pharmaceuticals are organic compounds used in medicines to prevent and treat disease and protect public health [20]. Medicines for human or veterinary use are increasingly part of everyday life. They can be classified according to their therapeutic category, such as analgesics, antibiotics, anti-inflammatories, antidepressants, lipid-lowering drugs, and beta-blockers [21].

Pharmaceuticals have been found in wastewater effluents, surface water, groundwater, and sea water at different concentrations [22]. They reach water bodies from various sources, such as excretion by the human body (which introduces them into the sewage system), drainage water, or industrial effluents [23, 24]. Some substances are highly soluble in water, and conventional wastewater treatment processes are not designed to remove these pollutants,

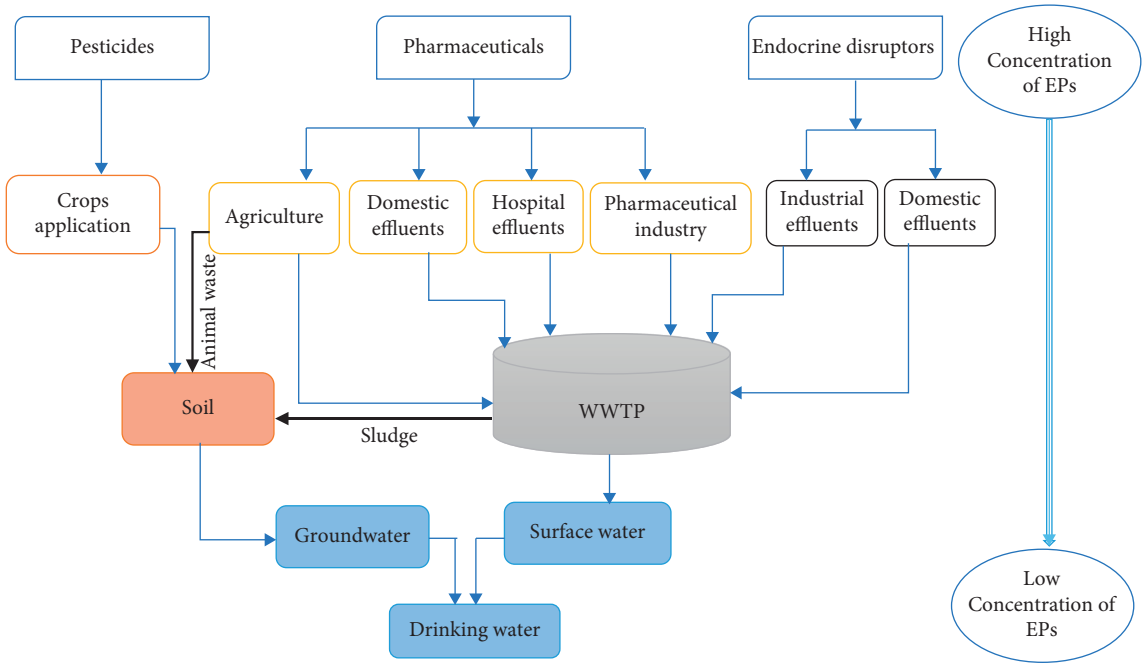

Figure 1: Pathways of EPs from the source to the aquatic environment.

allowing them to enter surface water [20]. The widespread presence of these contaminants in the environment has attracted worldwide interest and attention.

3. Representatives of EPs

Among the various emerging pollutants in the environment, bisphenol A (an endocrine disruptor), atrazine (herbicide), amoxicillin (an antibiotic), and paracetamol (an analgesic) were chosen as model molecules for discussion and critical review because of their widespread presence, bioaccumulation, and adverse effects on the aquatic environment and humans. A general description of the applications of these compounds in human life is given below.

3.1. Bisphenol A (BPA). Bisphenol A (BPA, 4, 4′-dihydroxy-2, 2′-diphenylpropane) is a widely used chemical in industry, synthesised by the Russian chemist Aleksandr P. Dianin in 1891 [25]. It is used as an intermediate in the production of polymeric materials such as polycarbonates and epoxy resins. It is present in many products, such as baby bottles, paper, toys, packaging, food containers, paints, medical equipment, and electronics [26, 27]. Bisphenol A is a white crystalline solid with the chemical formula $C_{15}H_{16}O_2$, a molecular weight of 228.29 g mol^{-1}, a low solubility in water (120 mg L^{-1} at 20°C), a log K_{OW} partition coefficient of 3.6, and an acidity constant of 10.3 [28].

BPA is one of the most manufactured and used chemicals in the world. Between 2013 and 2019, global BPA production was found to increase at an annual rate of 4.6% [29]. Studies in several countries have shown the presence of BPA in surface water, groundwater, wastewater, and sludge [29, 30]. It is introduced into the environment from various sources, such as sewage plant effluents, landfill leachate, and industrial discharges [31, 32]. Due to its endocrine-disrupting properties, BPA is considered an environmental contaminant of concern. Its use has been restricted in many countries, such as the European Union, North America, Norway, and China [29, 33].

3.2. Atrazine (ATZ). Atrazine (2-chloro-4-ethylamino-6-isopropylamino-1, 3, 5 triazine) is the active substance of a plant protection product belonging to the triazine chemical family which has a herbicidal effect. It is widely used in agriculture to control weeds in various crops, such as maize, sorghum, and sugarcane [34, 35]. Atrazine is a weak base with the chemical formula $C_8H_{14}ClN_5$, a molecular weight of 215.68 g mol^{-1}, and a low solubility in water (35 mg L^{-1} at 25°C) but a high solubility in organic solvents, with a log K_{OW} partition coefficient of 2.61. It exists as colourless crystals [36].

Although produced to control weeds, atrazine can migrate from soils into the aquatic environment, eventually affecting water quality [37]. Atrazine is frequently detected in soil, surface water, and groundwater, and its routes of entry into the environment mainly include runoff, leaching, and precipitation [36, 37]. Atrazine has endocrine-disrupting properties, and it is a carcinogen that can interfere with ecosystems and cause severe risks to humans, animals, and aquatic life [35, 38]. The European Union banned the compound in 2004, and its use is declining in Canada, while it is still used in other countries, including the United States, China, India, and Brazil [39].

3.3. Amoxicillin (AMX). Amoxicillin is a beta-lactam antibiotic belonging to the penicillin class, used to treat microbial infections by inhibiting the growth of protozoa,

bacteria, and fungi [39, 40]. Amoxicillin is one of Morocco's most commonly sold and used drugs [41]. Amoxicillin is a white powder with the chemical formula $C_{16}H_{19}N_3O_5S$, a molecular weight of 365.4 g mol^{-1}, a water solubility of 3430 mg L^{-1} at 20°C, and a log K_{OW} partition coefficient of 0.87. Amoxicillin is extremely unstable and degrades rapidly into a variety of degradation products [42].

Antibiotics, including AMX, are among the many emerging pollutants that have been detected in various environmental matrices, including rivers, groundwater, drinking water, and wastewater treatment plants [41, 43]. They are released into the environment from the pharmaceutical industry, hospital effluents, livestock waste, and sewage effluents [42, 44]. AMX can cause the selection of antibiotic-resistant bacteria and toxicological problems in the aquatic environment, impacting aquatic life and other organisms [45–47]. The widespread use of antibiotics has attracted scientific attention in recent years because of their subsequent release into the environment.

3.4. Paracetamol (PCM). Paracetamol (N-(4-hydroxyphenyl) acetamide), also known as acetaminophen, is a chemical compound used as an analgesic (painkiller) and antipyretic (fever reducer) and is one of the most commonly used and prescribed medicines in the world [48]. In Morocco, it is ranked as the most sold drug [41]. It is recommended as a first-line treatment to reduce fever caused by COVID-19 [49]. Paracetamol is a weak acid with the chemical formula $C_8H_9NO_2$, a molecular weight of 151.16 g mol^{-1}, a high solubility in water (14000 mg L^{-1} at 20°C), and a log K_{OW} partition coefficient of 0.46. It is a white crystallized powder [42]. Paracetamol is capable of being converted into a toxic substance.

Due to its extensive use, its presence has been detected in various environmental matrices, namely, wastewater, surface water, groundwater, sludge, and sediments [38]. The presence of medicines (including paracetamol) in the environment is due to different sources: humans (excretion of drugs or their metabolites that are not absorbed by the human body), industry (manufacturing residues of pharmaceuticals), and agriculture (animal husbandry) [50].

Although the concentration of these substances in aquatic environments is in the range of ng L^{-1} to μg L^{-1}, the continued consumption of these low concentrations can have adverse effects on human health and aquatic organisms [51]. Indeed, the significant presence of traces of these pollutants and, in particular, their metabolites in the environment has become a significant concern, requiring the development of specific innovative treatment techniques to reduce their harmful effects. Table 1 briefly summarizes the physicochemical properties of bisphenol A, atrazine, amoxicillin, and paracetamol.

4. Occurrence in the Environment

Several studies have investigated the presence and effects of emerging pollutants in the aquatic environment, such as the toxicity of bisphenol A and atrazine and the accumulation of certain pharmaceuticals (e.g., amoxicillin and paracetamol), as their concentrations at a certain location and over time differ considerably.

The occurrence of bisphenol A, atrazine, amoxicillin, and paracetamol in surface water, groundwater, wastewater, and seawater from 11 countries was examined in this study, and the results are summarised in Table 2. For instance, Chaib et al. [52] determined the presence of seven antibiotics in the Sebou River (surface water) of the city of Fez (Morocco), in which amoxicillin had the highest concentration (C_{Max} = 4107 ng L^{-1}). In contrast, Radwan et al. [53] found phenolic EDs in surface and groundwater in Egypt and bisphenol A was most frequently detected in surface water with the maximum (C_{Max}) and average (C_{Avg}) concentrations (85,500 and 1085.3 ng L^{-1}, respectively), followed by methylparaben in groundwater with a C_{Max} of 680 ng L^{-1} and a C_{Avg} of 71.1 ng L^{-1}; these results show that bisphenol A is present at high concentrations in water resources in Egypt.

The herbicide atrazine and its metabolites desethylatrazine and hydroxyatrazine were detected in shallow groundwater in the Chesapeake Bay catchment at different concentrations (13.5, 6.5, and 8.5 ng L^{-1}, respectively) [59]. ATZ was also present in all samples and is the predominant pesticide, with detection frequencies of 100%, in the Liaodong Peninsula (China) [54]. As for surface water and groundwater, seawater pollution is the highest in the Eastern Mediterranean Sea (Saronikos Gulf and Elefsis Bay in Central Aegean). Alygizakis et al. [63] investigated the presence of 158 pharmaceuticals and drugs in seawater, in which amoxicillin was the compound detected at the highest levels (up to 127.8 ng L^{-1}). The source of these pollutants is treated wastewater from the greater Athens region, as this area is affected by various anthropogenic pressures.

Indeed, wastewater treatment plants (WWTPs) are considered the main pathway for the transfer of micropollutants to the aquatic environment. The finding of Palli et al. [56] stated nine pharmaceuticals belonging to different therapeutic groups in a campaign conducted in 2017; in the influents of WWTPs in Tuscany (Italy), paracetamol and amoxicillin were frequently detected at higher concentrations (3914 and 2002 ng L^{-1}, respectively). Furthermore, Xue and Kannan [57] studied the presence of eight bisphenols in the final effluent of the Albany Area WWTP (USA). BPA was the most detected compound, at an average concentration of 90.0 ng L^{-1}, and incomplete removal of these compounds was observed, with the highest removal rate (52%) being after secondary treatment. Currently, conventional wastewater treatment processes have proven to be less effective in removing emerging micropollutants. Therefore, they are the main supplier of these pollutants to the environment.

The monitoring and determination of emerging pollutants in aqueous samples involves different analytical techniques. In general, an analytical procedure consists of four main steps: sample preparation, extraction, separation, detection, and quantification (Figure 2) [7]. Most samples require preparation so that they can be easily processed. Liquid samples are often concentrated first with solid adsorbents and then eluted with a suitable organic solvent or

Table 1: Physicochemical properties of bisphenol A, atrazine, amoxicillin, and paracetamol.

Compounds	Chemical formula	Chemical structure	CAS number	Molecular weight (g/mol)	Water solubility (mg/L)	Log K_{ow}	Pk_a	References
Bisphenol A	$C_{15}H_{16}O_2$	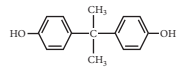	80-05-7	228.29	120 (at 20°C)	3.60	10.30	[28]
Atrazine	$C_8H_{14}ClN_5$	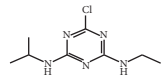	1912-24-9	215.68	35 (at 25°C)	2.61	—	[36]
Amoxicillin	$C_{16}H_{19}N_3O_5S$	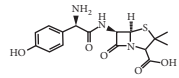	26787-78-0	365.4	3430 (at 20°C)	0.87	3.20	[42]
Paracetamol	$C_8H_9NO_2$	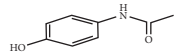	103-90-2	151.16	14000 (at 20°C)	0.46	9.38	[42]

CAS = chemical abstracts service; log K_{ow} = octanol-water partition coefficient; pK_a = acid dissociation constant.

Table 2: Occurrence of emerging pollutants in the aquatic environment.

Type of water	Sample (country)	Pollutants	Concentration (ng L^{-1})	Extraction and detection methods	LODs/LOQs* (ng L^{-1})	References
Surface water	Sebou River, Morocco	Amoxicillin	<158.3–4107	SPE-LC-MS/MS	n. a	[52]
	Nile River, Egypt	Bisphenol A	1085.3	UPLC-MS/MS	n. a	[53]
	Liaodong Peninsula, China	Atrazine	8.7–64.8	SPE-TQMS	(0.1–1.5)*	[54]
	Al-Asfar and Al-Hubail lakes, Saudi Arabia	Paracetamol and bisphenol A	PCM = 105–3069 BPA = 484.9	SPE-UHPLC/MS/MS	(0.3–2.5)*	[55]
Wastewater	WWTP of Tuscany, Italy	Paracetamol and amoxicillin	PCM = 3914 AMX = 2002	SPE-LC/MS	n. a	[56]
	Albany area of New York State (final effluent), USA	Bisphenol A	49.9	SPE-HPLC/MS/MS	n. a	[57]
	Grahamstown wastewater, South Africa	Bisphenol A	1468.3	SPE-UHPLC/MS/MS	1.0	[58]
Ground water	Groundwater of Chesapeake, USA	Atrazine, deethylatrazine (DEA), and hydroxyatrazine (HA)	ATZ = 13.5 DEA = 6.5 HA = 8.3	LC/MS/MS	n. a	[59]
	Shallow Nile aquifers, Egypt	Bisphenol A	71.1	UPLC-MS/MS	n. a	[53]
	Groundwater of Lagos, Nigeria	Amoxicillin and paracetamol	44–6490 1–188	UPLC-HRMS	n. a	[60]
Sea water	Marine waters, Turkey	Bisphenol A	4160–16920	SPE-HPLC/FLD	n. a	[61]
	Marine waters, Portugal	Paracetamol	53.2–269.7	SPE-UHPLC/MS/MS	0.26/0.80*	[62]
	Eastern Mediterranean Sea, Greece	Amoxicillin	<5.0–127.8	UHPLC/MS	8.2	[63]

LODs: limit of detections, LOQs: limit of quantifications, SPE: solid phase extraction, LC: liquid chromatography, MS: mass spectrometry, HPLC: high-performance liquid chromatography, UPLC: ultraperformance liquid chromatography, UHPLC: ultra-high-performance liquid chromatography, FLD: fluorescence detector, TQMS: triple quadrupole mass spectrometer, HRMS: high-resolution mass spectrometry, n. a: not available.

solvent mixture [64]. For extraction, there are many techniques such as solid phase extraction (SPE), liquid-liquid extraction (LLE), and accelerated solvent extraction (ASE). The choice of a specific extraction technique depends largely on the types of samples, the analyte, and the desired turnaround time [64]. In addition, separation, detection, and quantification are usually performed by liquid or gas chromatography in most cases, coupled with mass spectrometry (MS), due to the high selectivity and sensitivity they offer [65]. Further details on analytical techniques for emerging pollutants in water can be found in the following publications [66, 67].

5. Environmental Impact of EPs

5.1. On the Worldwide Level. The continuous entry of emerging pollutants into the environment is increasingly affecting the quality of water resources, fauna, and flora.

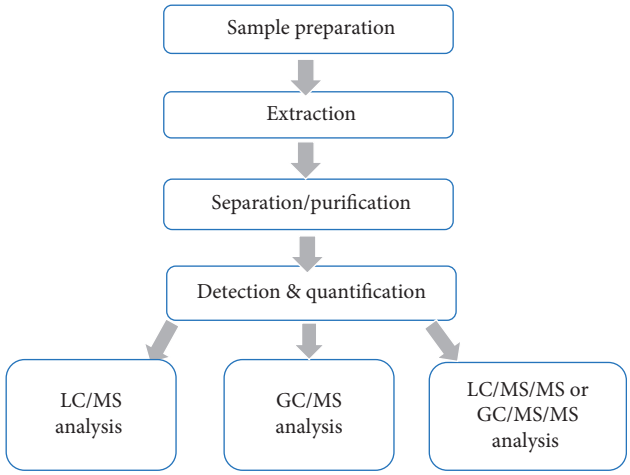

Figure 2: Typical analytical procedure for the measurement of emerging pollutants in aqueous samples.

Several studies conducted worldwide have focused on these pollutants to better understand their toxicity, environmental impact, and behaviour in different aquatic environments. Contaminants from industrial additives, pesticides, and pharmaceuticals, which are persistent compounds, enter water bodies from a variety of sources and can exceed acceptable levels and accumulate, resulting in adverse effects on the environment and human communities [3, 8, 11].

As illustrated in Figure 3, emerging pollutants have a significant effect on humans and animals. One of the consequences of endocrine disruption is that it affects on the endocrine system by mimicking, suppressing, or altering the function of hormones [68]. Exposure to EDs has been shown to reduce male sperm count and increase testicular, prostate, ovarian, and breast cancer, as well as reproductive malfunctions [15, 68]. Moreover, some of the most noticeable effects of EDs on animals are the changes in reproductive anatomy, fertility, eggshell thinning, and hormonal activity [70]. Pharmaceuticals and pesticides can also have an effect on the growth, reproduction, and evolution of species in the environment.

For instance, bisphenol A, a chemical widely used in the manufacture of plastics, has been confirmed to act as an endocrine disruptor, affecting organs such as the thyroid, thymus, and pancreas, due to its ability to bind to various receptors associated with the endocrine system, thereby disrupting their functions [56, 63]. BPA has adverse effects on plants, animals, and humans. Some studies have indicated that exposure to BPA causes numerous endocrine, reproductive, and metabolic diseases in humans, including breast, endometrial, prostate, ovarian, and testicular cancers, diabetes, obesity, hypertension, and heart disease [57, 64]. Several countries have banned its use in consumer products in response to these concerns, including baby bottles [30].

The effects of BPA on animals revealed a decrease in the number of elongated spermatids in the seminiferous tubules of pubertal ICR mice and a decrease in sperm count in Holtzman rats [71]. Additionally, the effects on fish have been investigated, including transcriptional activation of estrogen receptor-responsive genes, increased brain aromatase activity, induction of VTG in males, disruption of gametogenesis in males and females, altered development (neuronal, cardiac, germ cell, and sexual differentiation), and changes in sex ratios following embryonic exposure [72].

On the other hand, atrazine is a herbicide applied in various crops to control weeds. However, this compound can also directly or indirectly affect other organisms [37]. In aquatic ecosystems, atrazine can have harmful effects on aquatic animals and plants. Many organs, such as the kidneys, liver, gills, and other organs of fish, are affected after exposure [35]. Atrazine is an endocrine-disrupting compound that can also alter male reproductive tissue when animals are exposed to it during development [73]. Moreover, it was discovered that ATZ induced DNA methylation in the carp brain and induced autophagy in the liver, and it can also affect human health through the skin and respiratory contact, causing ovarian and breast cancer and affecting the human vascular system [74].

Pharmaceuticals are a specific class of compounds used worldwide to treat disease and restore the health of the body [75]. Still, they can also have harmful effects and contribute to pollution. In the aquatic environment, amoxicillin (an antibiotic) creates an ecological imbalance by producing toxic effects on aquatic organisms, altering plant growth, causing abnormalities in the anatomy of many organisms [41, 43], and leading to the development of multidrug-resistant bacteria [76]. Amoxicillin is a potential mutagen, carcinogen, and teratogen at higher doses; it is toxic to the fish *Oryzias latipes* and has a 96 h LC50 of 1000 mg L^{-1} [77].

Paracetamol has adverse effects when overdosed, inducing the proliferation of breast cancer cells. This toxicity is typically attributed to reactive oxygen species, which cause a variety of effects ranging from protein denaturation to lipid peroxidation and DNA damage [78]. PCM was also evaluated for its toxicity against a variety of aquatic species, including bivalve species (*C. fluminea*) and crustaceans (*Daphnia magna*). Exposure to increasing concentrations significantly altered the redox status of *C. fluminea*. Likewise, it caused death in a chronic toxicity experiment with *Daphnia magna* at higher concentrations (1.2–1.7 mg L^{-1}) [79].

5.2. At the National Level (Morocco). Due to population growth and the increase in agricultural and industrial activities, Morocco's water resources are subject to increasing and continuous pressure that affects their quality. The aquatic environment remains the most affected due to wastewater discharge containing industrial products, pharmaceuticals, and others, which are incompletely eliminated by treatment plants and seriously pollute the water bodies.

The 3rd report entitled "The state of the environment in Morocco, 2015" [80], from the Ministry of Energy, Mines, Water, and the Environment, in charge of the environment, provides information on the main activities causing pollution of the aquatic environment: the industrial sector accounts for a considerable proportion of polluting emissions.

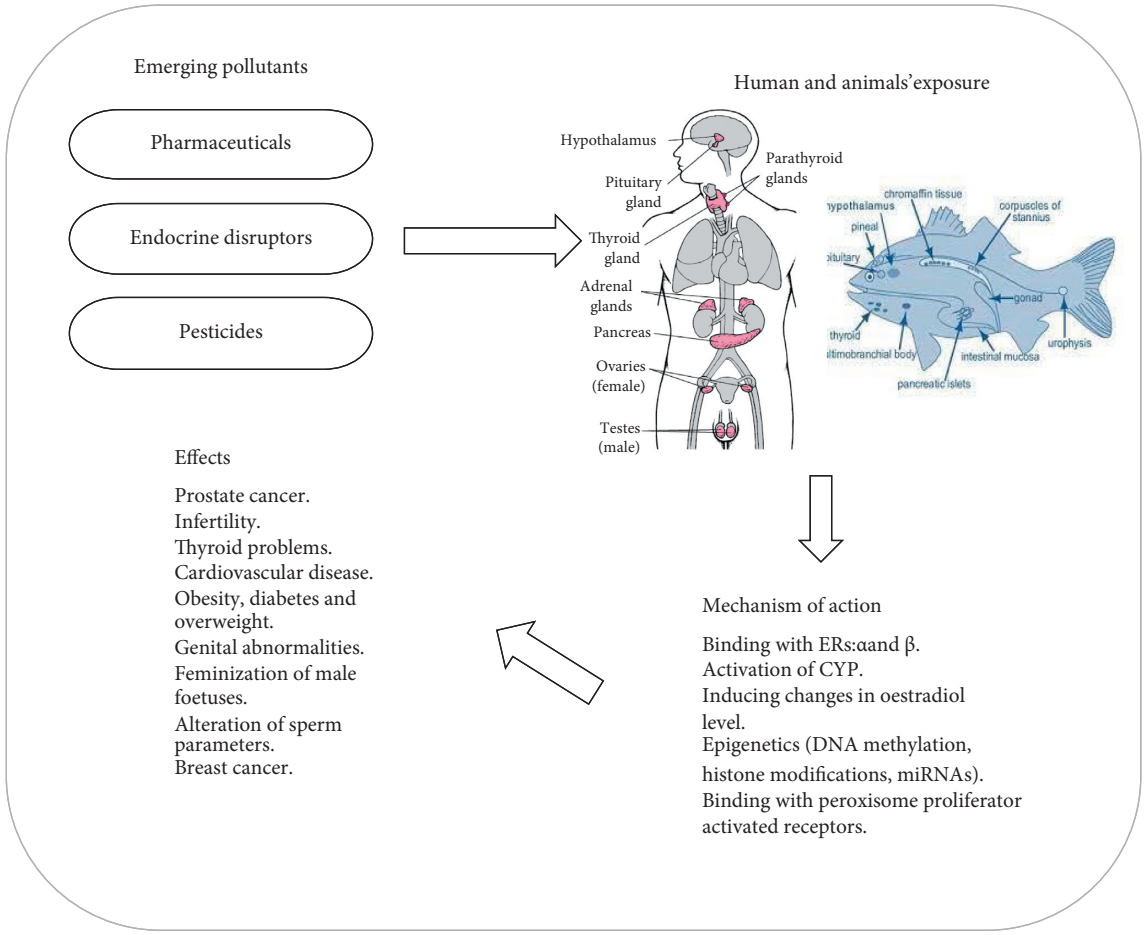

Figure 3: Schematic representation of emerging pollutant exposures, mode of action, and their health effects (based on [25, 68, 69]). Abbreviations: ERs, estrogen receptors; CYP, cytochrome P450 genes; and DNA, deoxyribonucleic acid.

The production of industrial wastewater in Morocco is around 964 million m^3 per year, i.e., 92% of the water initially taken from the sea and freshwater resources. The chemical and parachemical industries are the main sources of wastewater discharge, with an annual volume of 931 million m^3, while the other sources with an impact on the volume of wastewater are the agroindustry, the textile and leather sectors, and, to a lesser extent, the mechanical and metallurgical industries.

Furthermore, urban wastewater discharge is also a major source of pollution, with the annual volume of wastewater discharged into the natural environment (sea, rivers, sewers, etc.) without prior treatment estimated at 870 million m^3 in 2020 and predicted to be 1039 million m^3 in 2030. For example, the two main rivers of Morocco, the Sebou and the Oum Er Rbia, regularly experience critical pollution situations lasting several years. Additionally, the agricultural sector consumes an excessive amount of water (85–90% of resources absorbed by agriculture). Therefore, the leaching of phytosanitary products used in agriculture may also lead to water contamination by pesticides [81].

These different and large quantities of effluents released into the environment may contain varying concentrations of emerging pollutants, including pesticides, industrial products, and pharmaceutical products. For instance, an integrated study by Azzouz et al. [82] showed the presence of six types of endocrine disruptor (including BPA) in fish and seafood samples from Europe and North Africa. This study shows the consumption of these pollutants by aquatic organisms.

The finding of Chafi et al. [83] indicated that 27 endocrine disruptors and pharmaceuticals are present in Moroccan surface waters (Bouregreg River), in which bisphenol A and paracetamol are presented with maximum concentrations (302 and 120 ng L^{-1}). On the other hand, Chaib et al. [52] studied the occurrence of amoxicillin and other antibiotics in the surface water of the city of Fez (Morocco), where amoxicillin concentration reached 4107 ng L^{-1}. Indeed, few research studies have been conducted in Morocco on the effects of these contaminants on human health and the environment. Therefore, further research on this aspect is needed.

6. Treatment Processes for EP Removal

Varying levels of emerging pollutants in water matrices have attracted the interest of scientists around the world. There is, therefore, a need to protect humans and the environment from these contaminants and their impact. Emerging pollutants can be removed from water by chemical, physical,

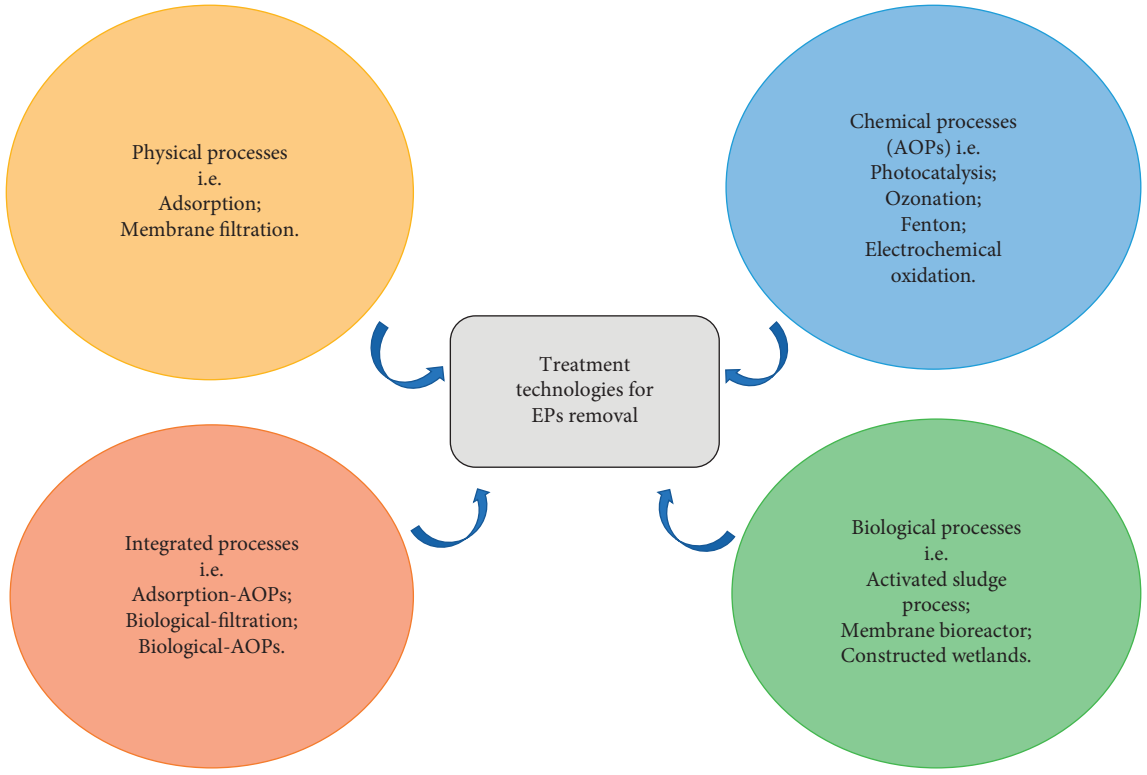

Figure 4: Common treatment technologies for EP removal.

biological, and hybrid processes. The most common technologies for their removal are shown in Figure 4.

Chemical treatment generally means the use of chemicals in a series of reactions to facilitate the process of disinfecting wastewater, and the chemical oxidation method has been employed to convert pollutants into a harmless form [68]. Thus, physical treatment techniques are frequently used due to their simplicity and adaptability. Commonly used physical processes include adsorption and membrane technologies, such as microfiltration, ultrafiltration, nanofiltration, and reverse osmosis. In addition, biological treatment uses a variety of micro-organisms to remove contaminants by biodegradation. The main non-conventional biological processes are activated sludge processes, constructed wetlands, and membrane bioreactors (MBRs).

Hybrid wastewater treatment is a system that integrates two or more treatment processes, in which all chemical, physical, and/or biological treatment techniques are integrated to facilitate the removal of contaminants from wastewater. The following sections of the document provide a more detailed overview of treatment techniques that have been applied to reduce the effects of these contaminants in wastewater. These methods are adsorption, advanced oxidation processes, biological processes, and hybrid (integrated) processes.

6.1. Adsorption. Adsorption is a mass transfer process that involves the mass movement of the adsorbate from the liquid or gas phase to the surface of the adsorbent [84]. Adsorption mechanisms generally include physical adsorption related to van der Waals force and ion exchange and chemical adsorption corresponding to the formation of chemical bonds [85]. Adsorption is a widely applied technology for the removal of various contaminants from water and wastewater because it is simple, effective, cheap, and environmentally friendly [80, 81]. This process can be influenced by many conditions, such as the nature and concentration of the adsorbate and the adsorbent, the presence of other pollutants, and temperature and experimental parameters such as contact time, pH, and adsorbent surface [15].

Many researchers have explored the removal of emerging pollutants by adsorption. Activated carbon is the best and most widely used adsorbent globally due to its high efficiency in removing different types of contaminants. However, it is expensive and difficult to regenerate, which requires the search for other materials with similar efficiency [81]. Other materials have been studied as alternatives to activated carbon, such as activated biochar, clay, zeolites, silica gel, chitosan, metal-organic frameworks, polymers, agricultural waste and by-products, biosorbents, and composite materials. Table 3 shows some adsorbent materials that have recently been applied to remove the studied pollutants from aqueous solutions.

Many studies have been conducted on the adsorption of emerging pollutants by different materials. Some studies have used carbon-based adsorbents to remove several types of pollutants. Zbair et al. [86] studied the adsorption of bisphenol A in water by activated carbon prepared from argan nut shells and activated by phosphoric acid, removing 1250 mg/g BPA. The optimized variables were 0.01 g, 60 mg L^{-1} and 6.5 as adsorbent dosage, initial BPA concentration,

Table 3: Removal efficiency, isotherms, and kinetic parameters for the removal of the studied emerging pollutants by different adsorbents.

Adsorbate	Adsorbent	Surface area (m^2/g)	Removal (%)	Q_m (mg/g)	Adsorption isotherm	Operating conditions	Additional information	References
Bisphenol A	Activated carbon from argan waste	1372	95	1250	Langmuir	200 mL of BPA (60 mg/L); $m = 0.01$ g of adsorbent; PH = 6.5; $T = 293$ K; $t = 3$ h; SS = 200 rpm; pseudo-second-order	Activated carbon prepared from the shell of the argan nut and activated by phosphoric acid	[86]
	Activated biochar from kraft lignin	1053		220	Dual-site Langmuir	[BPA] = 100 mg/L; [adsorbent] = 0.36 g/L; $T = 25^{\circ}C$; $t = 24$ h; SS = 250 rpm; Elovich model	Activated carbon from kraft lignin showed a high BPA uptake value in a batch experiment with synthetic wastewater	[87]
	Clay	15.74		109.89	Langmuir and Freundlich	[BPA] = 50 mg/L; PH = 7; $T = 25^{\circ}C$ $t = 4$ h; pseudo-second-order	Batch experiment was carried out to determine the adsorption characteristics of calcium-modified montmorillonite clay towards BPA	[88]
	Graphene oxide (GO)	—	96.2	3293.9	Sips	30 mL of BPA (1 mg/L); $m = 2.5$ mg of adsorbent; PH = 7; $T = 25^{\circ}C$; $t = 120$ min; pseudo-second-order; $K_2 = 25.2$ g mg^{-1} min^{-1}	The hybrid of GO with Fe_2O_3 nanoparticles (Fe_2O_3-GO) had a higher adsorption at a lower initial BPA concentration, batch experiment with synthetic wastewater	[89]
	Polymer	—		65.3	Langmuir	20 mL of BPA (100 mg/L); $m = 5$ mg of adsorbent; PH = 7; $T = 25^{\circ}C$; SS = 200 rpm; pseudo-second-order	Synthesis of a water-insoluble polymer (b-PEI-PEG-β-CD) that could easily remove BPA from synthetic wastewater	[90]
	Sulfonated tea leaves	—		236.8	Langmuir	20 mL of BPA (100 ppm); $m = 10$ mg of adsorbent; $T = 25^{\circ}C$; PH = 8; SS = 700 rpm; pseudo-second-order; $K_2 = 0.000356$ g/mg min	Sulfonation of tea leaves generates the sulfonated carbonaceous product TW-SO_3H with high adsorption capacity towards BPA	[91]

Table 3: Continued.

Adsorbate	Adsorbent	Surface area (m^2/g)	Removal (%)	Q_m (mg/g)	Adsorption isotherm	Operating conditions	Additional information	References
Atrazine	Metal-organic frameworks (MOFs)	2210	98	36	Langmuir	10 mL of ATZ (10 ppm); $m = 3.5$ mg of adsorbent; $T = 25^{\circ}C$; $t = 1$ min	Adsorption of atrazine in Zr_6-based metal-organic structures showed a high adsorption capacity (98%) in 1 minute	[92]
	Polyaniline-derived carbon	—		943.0	Langmuir	100 mL of ATZ (50 mg/L); $m = 3$ mg of adsorbent; $T = 25^{\circ}C$; PH = 7; $t = 12$ h	Preparation and use of polyaniline carbons for the adsorptive removal of ATZ from synthetic wastewater	[93]
	Biosorbent from eucalyptus bark	—	87.95	936.1	Freundlich	10 mL of ATZ (1 mg/L); $m = 30$ mg of adsorbent; $T = 25^{\circ}C$; $t = 24$ h; SS = 225; pseudo-second-order	*Eucalyptus tereticornis* L. bark, a waste product, is used to remove atrazine in a batch adsorption experiment	[94]
	Biochar	—	96	79.6	Freundlich	10 mL of ATZ (2 mg/L); $m = 50$ mg of adsorbent; $T = 25^{\circ}C$; $t = 20$ min; pseudo-second-order	P-doped biochar from corn straw, prepared and activated with H_3PO_4, was able to remove 96% of atrazine	[95]
Amoxicillin	Activated carbon from date pits	1325		424.3	Langmuir	10 mL of AMX (100 mg/L); $m = 10$ mg of adsorbent; $T = 22^{\circ}C$; PH = 4; $t = 300$ min; pseudo-second-order	Activated carbon is derived from date pits and prepared by thermal activation with carbon dioxide, used for the removal of amoxicillin in a batch adsorption experiment	[96]
	Natural phosphate	20		3.2	—	100 mL of AMX (20 mg/L); $m = 200$ mg of adsorbent; $T = 25^{\circ}C$; PH = [5–6]; $t = 120$ min	Natural phosphate from the sedimentary phosphate rocks of Morocco	[97]
	Multiwall carbon nanotubes	—		159.4	Langmuir	100 mL of AMX (50 mg/L); $m = 0.1$ g of adsorbent; $T = 60^{\circ}C$; PH = 7; $t = 75$ min; pseudo-second-order	Multiwalled carbon nanotubes are used as an adsorbent for the removal of amoxicillin from an aqueous solution in a batch experiment	[98]
	Activated carbon	807	76		Langmuir	2000 mL of AMX (40 mg/L); $m = 2$ g of adsorbent; $T = 25^{\circ}C$; PH = 6.9; $t = 30$ min; SS = 300 rpm; pseudo-second-order	Activated carbon modified with zinc acetate and activated with phosphoric acid was used in a batch adsorption experiment	[99]
	Modified clay	242.36		647.7	Langmuir	20 mL of AMX (50 mg/L); $m = 2$ mg of adsorbent; $T = 30^{\circ}C$; PH = 7.5; $t = 60$ min; SS = 120 rpm; pseudo-second-order	Montmorillonite clay modified with L-methionine amino acid was used for amoxicillin adsorption	[100]

Table 3: Continued.

Adsorbate	Adsorbent	Surface area (m^2/g)	Removal (%)	Q_m (mg/g)	Adsorption isotherm	Operating conditions	Additional information	References
Paracetamol	Commercial activated carbon	983		560	Langmuir	[PCM] = 50 mg/L; [adsorbent] = 167 mg/L; T = 25°C; PH = 3; t = 24; SS = 250 rpm; pseudo-second-order	Commercial activated carbon was used for the adsorptive removal of paracetamol in a batch adsorption experiment	[48]
	Modified clay	216		22.08	Redlich–Peterson	50 mL of PCM (100 mg/L); m = 5 mg of adsorbent; T = 25°C; PH = 7; t = 180 min; pseudo-second order	Natural montmorillonite clay pillared with titanium oxide	[101]
	Coffee-based biomaterial	888.1	98	50	Freundlich	[PCM] = 200 mg/L; [adsorbent] = 4 g/L; PH = 6.5; t = 60 min; pseudo-second-order	The raw biomaterial treated chemically by phosphoric acid	[102]
	Silica gel	264		95	Langmuir	[PCM] = 100 mg/L; [adsorbent] = 167 mg/L; T = 25°C; PH = 3; t = 24 h; SS = 250 rpm; pseudo-second-order	Removal of paracetamol by silica gel in a batch adsorption experiment	[48]

and pH. Adsorption experiments revealed that the adsorbent was more efficient due its large specific surface area (1372 m^2/g). The obtained adsorption data were highly correlated with the pseudo-second-order model and the Langmuir isotherm.

Meanwhile, Suo et al. [95] found that P-doped biochar from maize straw was able to remove 96% of atrazine within 20 min and at a temperature of 25°C. The experimental data were best fitted by a pseudo-second-order kinetic model and the Freundlich isotherm. Additionally, the prepared adsorbent can be reused up to five cycles. There are other studies on the adsorption of these pollutants by mineral adsorbents; Chauhan et al. [101] investigated the removal of paracetamol by natural montmorillonite clay coated with titanium oxide and found a lower adsorption capacity of 22.08 mg/g at a fixed adsorbent dose (0.1 g L^{-1}). Pseudo-first-order and pseudo-second-order models were used to determine the adsorption kinetics.

Rock phosphate from sedimentary phosphate rocks in Morocco was used to remove amoxicillin and other organic micropollutants. The optimized parameters for contact time, adsorbent concentration, pH, and initial AMX concentration were 120.0 min, 2.0 g L^{-1}, 6.0, and 20 ppm, respectively. The mechanism of adsorption was related to the nature of van der Waals interactions [97]. Atrazine adsorption in Zr6-based metal-organic frameworks (MOFs) showed a high adsorption capacity (98%) within 1 minute, owing to the framework's large pores that facilitate diffusion and the abundance of potential π–π interaction sites at the pyrene-based linkers. Additionally, the adsorbent was easily regenerated following atrazine adsorption using acetone washing while retaining 99% of its initial atrazine uptake [92].

Other researchers have used waste materials as low-cost adsorbents. Mandal and Singh [94] studied the removal of atrazine by eucalyptus bark in a batch adsorption experiment. The removal efficiency showed that 30 g L^{-1} of adsorbent was capable of removing up to 87.95% of atrazine at a concentration of 1 mg L^{-1}. Kinetic analysis of the equilibrium data indicated that atrazine sorption was best explained by a pseudo-second-order kinetic model. Moreover, sulfonation of tea leaves generates the sulfonated carbon product TW-SO_3H, which has a high adsorption capacity for BPA (236.80 mg g^{-1} at 25°C). The adsorbent exhibited electrostatic interaction and π–π stacking properties that enabled efficient BPA adsorption. The Langmuir and Temkin isotherm models best fit the experimental data for the BPA adsorption processes [91].

Numerous factors can affect the adsorption process, including adsorbent dosage, pollutant concentration, solution pH, contact time, temperature, the nature of the adsorbent and adsorbate, and the presence of other pollutants [84]. The transfer of pollutants in aqueous media can be understood by considering the adsorption isotherm, kinetic, and thermodynamic studies. Adsorption isotherms can be used to determine the mass of adsorbate that is taken onto the surface or interface of an adsorbent at a given temperature and equilibrium. Numerous adsorption isotherm models (Langmuir, Freundlich, Koble–Corrigan, and others) have been proposed to account for the adsorption capacity of pollutants on the adsorbent [81, 84].

Furthermore, adsorption kinetic study provides detail on the rate and mechanism that governs the adsorption phenomenon. The main models used in the literature are the pseudo-first-order kinetic, the pseudo-second-order kinetic, the Elovich model, and the intraparticle diffusion kinetic model [103]. Besides, thermodynamic study elucidates the nature of the adsorption process whether it is of physical/chemical or endothermic/exothermic or spontaneous. The obtained values of entropy change (ΔS^0), Gibbs function change (ΔG^0), enthalpy change (ΔH^0), and activation energy (Ea) can be used to infer the spontaneity of the adsorption

process and the adsorption interaction's exothermic/endothermic behavior [84]. Due to its multiple advantages, the adsorption technique is one of the most effective and widely applicable low-cost methods for the treatment of emerging pollutants. Therefore, additional effective and low-cost materials (adsorbents) for wastewater treatment are required.

6.2. Advanced Oxidation Processes (AOPs). AOPs are a family of technologies based on the production of hydroxyl radicals (OH^*), which are stronger oxidants (oxidation potential of 2.8 V) and capable of reacting rapidly with most organic compounds present in water and wastewater [104, 105]. The generation of these reactive radicals can be achieved by several processes, including homogeneous and/or heterogeneous phase photocatalytic processes (H_2O_2/UV, O_3/UV, Fe^{2+}/H_2O_2/UV, and TiO_3/UV), homogeneous phase chemical oxidation processes (H_2O_2/Fe^{2+} and H_2O_2/O_3), electrochemical oxidation processes, and sonochemical oxidation processes [106]. AOPs, including Fenton reactions, photocatalytic oxidation, ozonation, and electrochemical oxidation reactions, are effective in removing emerging pollutants that are difficult to treat by means of conventional physicochemical and biological techniques. The efficiencies of some common advanced oxidation processes are presented in Table 4.

In Fenton and Fenton-type reactions, hydroxyl radicals are usually generated by the decomposition of hydrogen peroxide under the action of an iron-rich catalyst ($BaFe_{12}O_{19}$, α-FeOOH, Fe_3O_4, etc.) [104, 105, 107]. The hydrogen peroxide used in the catalytic reaction usually comes from external addition and in situ generation [121]. However, when mixed with an iron (II) (Fe^{2+}) catalyst to form the Fenton reagent, the oxidation potential of (H_2O_2) increases. A mixture of (H_2O_2) and (Fe^{2+}) salts is added directly to the wastewater [122], according to the following reaction:

$$Fe^{2+} + H_2O_2 \longrightarrow Fe^{3+} + OH^- + OH^*. \quad (1)$$

Fenton-based processes have been successfully applied to the treatment of various types of Moroccan wastewater, including textile wastewater [123], landfill leachates [124, 125], and emerging pollutants in aqueous solutions. For instance, the electro-Fenton process has been applied to remove moxifloxacin in acidic media at pH 3.0. The mineralization of moxifloxacin was achieved by multiple OH^* attacks with several intermediates formed during the treatment process [126]. Likewise, Rachidi et al. [127] investigated the same process for the removal of the antidepressant sertraline hydrochloride. The maximum degradation occurred at 400 mA with an optimal Fe^{2+} concentration of 0.1 mM.

Photocatalysis is a sustainable technology for treating organic pollutants in wastewater that involves the use of photocatalysts, having the ability of being activated under light irradiation [128]. The photocatalysis technique is based on the reaction between organic pollutants and powerful oxidizing and reducing agents (h^+ and e^-) generated by a light source on the surface of photocatalysts [129]. The typical photocatalytic mechanism involved in the removal of aqueous phase contaminants is depicted in Figure 5.

Titanium dioxide (TiO_2) is the most widely used photocatalyst due to its numerous advantages in the degradation of contaminants. TiO_2 is less efficient in absorbing solar light. Therefore, most of studies focus on its modification through doping with metals (such as Ag^+, Fe^{3+}, and Co^{3+}) and nonmetals (including N, S, F, C, B, and P) to enhance its visible light-absorbing capacity [130]. Moreover, researchers have been attracted to investigate other photocatalytic materials for wastewater treatment applications, including oxides and perovskites (e.g., ZnO, WO_3, V_2O_5, $BiVO_4$, Ag_3VO_4, and $SrTiO_3$), bismuth oxyhalides (e.g., BiOCl, BiOBr, and BiOI), and sulfides (e.g., CdS, ZnS, and MoS_2), as well as various composite materials [131].

Numerous photocatalytic materials have been employed for the treatment of hazardous contaminants in wastewater [132, 133]. Tabasum et al. [134] studied the photocatalytic potentials of graphene oxide-doped metal ferrites (GO-Fe_3O_4 and GO-$CoFe_2O_4$) for acetamiprid degradation. During the first hour of exposure to UV radiation, degradation efficiencies of 90% and 97%, respectively, were achieved. Additionally, the performance of graphene-oxide-based metal ferrites for pesticide pollutant removal was investigated [135]. The composites were found to be highly biodegradable (90%) within 60 minutes of UV degradation. Qureshi et al. [136] synthesized graphene oxide decorated $ZnWO_4$ (GO-$ZnWO_4$) nanocomposites by a hydrothermal process and used for the degradation of a pharmaceutical product (cetirizine hydrochloride) under UV irradiation. The photocatalyst was able to degrade up to 89% of the contaminant in water.

Another semiconducting photocatalyst has been developed and is being applied to the treatment of emerging pollutants, such as zinc oxide-hydroxyapatite (HAp). El Bekkali et al. [137] explored the use of ZnO-HAp for antibiotic removal from contaminated water under UV irradiations. The photodegradation efficiency of the nanocomposites was significantly higher than that of the photocatalytic particles alone. In addition, activated carbon-based coloured titania nanoparticles showed an excellent performance in removing emerging drugs from wastewater, such as amoxicillin and paracetamol, when exposed to visible light [138]. Furthermore, Bougdour et al. [139] used the $S_2O_8^{2-}$/Fe^{2+}/UV process to investigate the treatment and mineralization of real wastewater from the Moroccan textile industry. The results indicated that the rate of pollutant mineralization is 87%.

Ozonation processes are based on the use of ozone, which is a powerful oxidizing agent. After reacting with the pollutants, ozone is transformed into oxygen [140]. This process has shown relative efficiency in treating emerging pollutants; 100% removal was achieved for bisphenol A in real secondary wastewater effluents [113]. Similarly, total degradation and 94% mineralization of paracetamol were achieved for reaction times of 15 minutes [116]. Likewise, microbubble ozonation improved the degradation of atrazine (90%) at different pH levels in a semibatch experiment [114]. Electrochemical oxidation is mainly based on electron

Table 4: Advanced oxidation processes for the degradation of emerging pollutants present in water.

Process	Target compound	Materials	Degradation (%)	Conditions	Additional information	References
Fenton/Fenton-like processes	Bisphenol A	$BaFe_{12}O_{19}$-Ag_3PO_4	79.9	[BPA] = 20 mg/L; [catalyst] = 1 g/L 300 W; Xe arc lamp ($\lambda > 420$ nm); $T = 30^{\circ}C$; $t = 30$ min	The reactive oxygen species are produced by the timely decomposition of H_2O_2 generated on the surface of Ag_3PO_4 via the $BaFe_{12}O_{19}$	[107]
	Atrazine	α-FeOOH	100	[ATZ] = 20 mg L^{-1}; [α-FeOOH] = 0.1 g L^{-1}; [H_2O_2] = 1.0 mM; [hydroxylamine] = 0.5 mM; $T = 25^{\circ}C$; PH = 5; $t = 60$ min	Surface Fenton system constructed with hydroxylamine (NH_2OH), goethite (α-FeOOH), and H_2O_2 (α-FeOOH-HA/H_2O_2) to degrade atrazine	[104]
	Amoxicillin	TiO_2-GO-Fe_3O_4	90	[AMX] = 10 mg/L; [catalyst] = 0.5 g L^{-1}; $t = 120$ min; PH = 3; $T = 25^{\circ}C$	The combination of TiO_2 and Fe_3O_4 nanoparticles on graphene oxide (GO) nanoplatelets (TiO_2-GO-18wt% Fe_3O_4) shows excellent AMX degradation under visible irradiation and 90% TOC removal	[105]
	Paracetamol	Fe_3O_4-SiO_2-Cu	100	[PCM] = 2.0 mg L^{-1}; [catalyst] = 0.2 g L^{-1}; [H_2O_2] = 15 mM; $t = 20$ min PH = 5.0; $T = 25^{\circ}C$	The catalytic tests were carried out in a four-vial collared reactor equipped with a temperature-controlled heating mantle; paracetamol was almost completely degraded within 20 minutes	[108]
Photocatalysis	Bisphenol A	B-TiO_2-graphene oxide	47.66	[Catalyst] = 1000 mg L^{-1}; [BPA] = 10 mg L^{-1}; $t = 240$ min; PH = 5; $T = 25^{\circ}C$; $K_1 = 0.0023$ min^{-1}	Hydrothermal preparation of the photocatalyst, 300 W xenon lamp (1000 W/m^2 light intensity) with solar irradiation	[109]
	Atrazine	Bi_2MoO_6/PMS	99	[Bi_2MoO_6] = 0.6 g/L; [PMS] = 0.8 mM; [ATZ] = 2.5 mg/L; $t = 60$ min; $T = 25^{\circ}C$; visible light irradiation	Bismuth molybdate (Bi_2MoO_6) prepared via the hydrothermal method and applied to activate peroxymonosulfate (PMS)	[110]
	Amoxicillin	Ag/TiO_2/mesoporous g-C_3N_4	71	[Catalyst] = 1000 mg L^{-1}; [AMX] = 5 mg L^{-1}; $t = 60$ min	Hospital wastewater, 300 W xenon lamp ($\lambda > 420$ nm) with visible light irradiation	[111]
	Paracetamol	Fe_2O_3-TiO_2	95.85	[Catalyst] = 1.25 g L^{-1}; [PCM] = 30 mg L^{-1}; PH = 11; solar irradiation	Fe_2O_3-TiO_2 is synthesised by the sol-gel method for the degradation of paracetamol in synthetic wastewater	[112]

Table 4: Continued.

Process	Target compound	Materials	Degradation (%)	Conditions	Additional information	References
Ozonation	Bisphenol A	Ni-Fe LDHs/O_3	100	[BPA] = 10 mg L^{-1}; [catalyst] = 0.3 g L^{-1}; [ozone] = 9.0 mg L^{-1}; [TOC] = 9 mg L^{-1}; [COD] = 32 mg L^{-1}; t = 120 min	Ni-Fe LDH showed effective catalytic performance in the catalytic ozonation of BPA in real secondary effluent wastewater. BPA could be completely removed, and the final removal of TOC and COD was 56% and 68%	[113]
	Atrazine	O_3 (microbubble)	95.3	[ATZ] = 1.16 umol L^{-1}; [ozone] = 1 mg L^{-1}; gas flow: 0.5 L min^{-1}; t = 120 min; T = 20°C	Microbubble ozonation enhanced the degradation of atrazine at different pH levels in a semibatch experiment	[114]
	Amoxicillin	O_3	70	[AMX] = 20 uM; [ozone] = 75 mg L^{-1}; gas flow: 1 L min^{-1}; T = 23°C; PH = 6.8	The degradation of amoxicillin by ozonation resulted in 70% removal with an ozone dose of 75 mg L^{-1}	[115]
	Paracetamol	MgO/O_3	100	Ozone dose: 1.8 mg/min; [MgO] = 0.1 g L^{-1}; [PCM] = 50 mg L^{-1}; t = 15 min; PH = 5.4	MgO powder was used as a catalyst for the ozonation of paracetamol; total degradation and 94% mineralisation were achieved at reaction times of 15 min	[116]
Electrochemical	Bisphenol A	Nb/BDD	90	[BPA] = 5.0 mM; flow rate = 384 mL min^{-1}; j = 42.7 mA cm^{-2}; t = 4 h; PH = [7–10]; T = [6–20°C]	The application of electrochemical oxidation has shown high removal efficiency of BPA	[117]
	Atrazine	Nb/BDD	99	1.5 L of 100 ug L^{-1} atrazine 0.03 M Na_2SO_4; j = 2 mA cm^{-2}; PH = 3; T = 23°C; t = 45 min; batch mode with undivided cylindrical cell	More than 99% of ATZ was removed by anodic oxidation; the atrazine-desethyl-desisopropyl (DEDIA) was the most important by-product recorded	[118]
	Amoxicillin	Ti/Cu-PbO_2	99.4	250 mL of 100 mg L^{-1} amoxicillin; 0.1 M Na_2SO_4; j = 30 mA cm^{-2}; PH 3.5; room temperature; t = 150 min; pseudo-first-order reaction	Copper-doped PbO_2 electrode was prepared and used as an anode to degrade amoxicillin in a laboratory-scale experiment. The optimum removal of AMX and COD was 99.4% and 46.3% after 150 minutes of electrolysis	[119]
	Paracetamol	Pt/Ag-Agcl	90	250 mL of 20 mg L^{-1} paracetamol; 0.1 M Na_2SO_4; j = 5.1 mA cm^{-2}; PH = 4; t = 240 min	The maximum removal of PCM, COD, and TOC reached 90%, 82%, and 65% after 240 min, with the formation of by-products (hydroquinone, benzoquinone, and carboxylic acid) during the electrolysis process	[120]

transfer. Insoluble electrodes (Nb/BDD; Ti/Cu-PbO_2; and Pt/Ag-Agcl) are commonly used [117, 119, 120] to promote the generation of hydroxyl radicals and allow the complete oxidation of a large number of organic molecules contained in wastewater.

AOPs can be used to treat aqueous solutions loaded with organic matter, either as a pretreatment to transform the refractory compounds into biodegradable products or as a final treatment to completely mineralize the organic compounds [106]. They have several advantages in terms of high oxidation efficiency, their ability to treat almost all organic matter, faster reaction rates, and absence of secondary pollution, and they have no negative impact on the environment [141]. The main disadvantage of these processes is

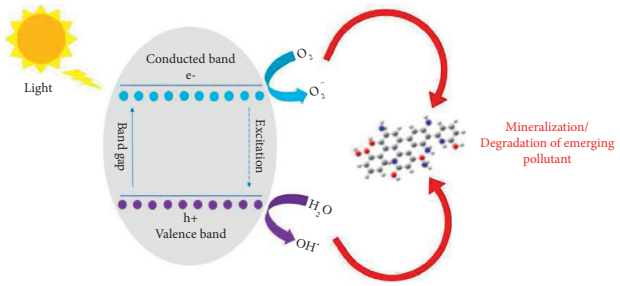

Figure 5: Mechanism of photocatalytic degradation of EPs.

the associated capital and operating costs. Therefore, environment-friendly energy-saving techniques should be used, such as solar energy, for oxidation [140].

6.3. Biological Processes. Biological treatment is a widely used technology for treating wastewater and is also frequently applied for the treatment of emerging pollutants [74]. Many researchers have studied the biodegradation of these substances in various systems, including conventional activated sludge [142], which is the main bioprocess for organic matter removal in wastewater treatment plants [143], sequential batch reactors (SBRs) [144], constructed wetlands (CWs) [145], membrane bioreactors, etc.

In general, the biodegradation of micropollutants in biological processes depends on several factors: the nature of the micropollutants, the characteristics of the organisms, the type of water matrix, and the operating conditions [15, 117]. Table 5 presents biological processes used for the degradation of the studied emerging pollutants. It also summarizes the degradation conditions and removal efficiency. Biodegradation is considered to be one of the current methods for treating a wide range of contaminants. It has many advantages in terms of economy, environment friendliness, and low cost [119,151]. In addition, some persistent substances are able to pass through biological wastewater treatment processes [152] and, therefore, have negative effects on the environment. Under these conditions, adsorption and advanced oxidation processes are possible complementary routes for removing these contaminants.

6.4. Hybrid Processes. The limited effectiveness of conventional treatment processes for the removal of many emerging pollutants is encouraging the development of hybrid technologies using the different removal potential of different processes to overcome the limitations of the removal of these compounds [153]. The hybrid process is based on combining two or more treatment techniques for the effective removal of recalcitrant micropollutants [152].

Advanced oxidation techniques have been used to improve the efficiency of the different physical and biological treatment processes (Table 6). For instance, Jiang et al. [154] studied adsorption treatment in combination with photocatalysis to treat bisphenol A. BPA molecules are rapidly adsorbed onto boron- and nitrogen-codoped graphene aerogels and eventually mineralize after exposure to visible light. Moreover, Taylor et al. [156] suggested a pretreatment in the Fenton process to disintegrate amoxicillin and, thus, facilitate its removal by biodegradation. On the other hand, Iborra-clar et al. [157] investigated the biodegradation of paracetamol in the activated sludge process in combination with activated carbon (AC), and the system was able to degrade paracetamol in wastewater completely.

7. Challenges and Perspectives

Different treatment processes have been developed to limit the release of emerging contaminants into the environment, and each has shown its advantages and disadvantages. Adsorption is a simple and low-energy process, but it requires a large amount of adsorbent. The complete mineralization of pollutants characterizes AOPs under low operating conditions. For instance, photocatalytic water treatment uses sunlight as a nonpolluting energy source, making it one of the most promising methods for the degradation of pollutants. However, photocatalysis has the disadvantage of low light transmittance and slow reaction kinetics [158], limiting its large-scale application. Biological treatment is a widely used method for wastewater treatment, but it is less effective in removing some emerging micropollutants, allowing them to be released into the aquatic environment.

As there is no perfect treatment method, researchers have attempted to provide integrated solutions, such as the coupling of adsorption and photocatalysis, which are simple and environment-friendly processes that appear to be effective in removing micropollutants. This hybrid technology integrates both techniques' advantages through the removal of pollutants from the aqueous phase by adsorption and the degradation of trace organic pollutants by photocatalysis. The main hybrid technologies to be considered are simultaneous combination (one step) and separate coupling (two steps). Figure 6 shows the operation schemes of these technologies.

7.1. Simultaneous Coupling of Adsorption and Photocatalysis. Many studies focus on the treatment of different pollutants in water by the combination of adsorption and photocatalysis, as the catalytic reaction is related to surface adsorption. For example, Luo et al. [159] synthesised TiO_2-wood charcoal composites for the removal of bisphenol A and found that synergistic adsorption and photocatalytic degradation were effective in removing hydrophobic bisphenol A. Wang et al. [160] prepared iodine-doped biochar as a photocatalyst adsorbent for the removal of phenol and tetracycline and observed that iodine doping enhances adsorption by creating additional pores and leads to strong photoinduced excitation, which increases the photocatalytic activity of the iodine-doped biochar for the degradation of organic pollutants. Bouyarmane et al. [161] prepared TiO_2-hydroxyapatite nanocomposites for the degradation of drugs in solution under UV light, and the results revealed that the pharmaceuticals were preferentially adsorbed onto the apatite-rich composites, while their photodegradation was more efficient in the TiO_2-rich phases.

Table 5: Biological processes used for the degradation of emerging pollutants.

Pollutant	Process	Type of effluent and operating conditions	Degradation	Additional information	References
Bisphenol A	Aerobic granular sludge	Synthetic municipal wastewater with the following concentrations: COD = 445 mg/L; BPA = 2 mg/L; pH = 7.5–8.0; $T = 20^{\circ}C$; $t = 16$ h	39%	Mixed community of microorganisms in aerobic granular media was used, BPA degraders were active at the beginning of the reactor cycle, and no BPA degradation by-products were detected	[146]
	Sequencing batch biofilm reactor	Synthetic wastewater with the following concentrations: BPA = 10 mg/L; 10 mL of activated sludge; 57.5 g/L of waste iron; PH = 8; $T = 21^{\circ}C$; $t = 100$ min	92%	Acclimatisation of activated sludge with BPA and waste zero-valent iron had a positive effect on BPA removal in a sequential batch biofilm reactor	[144]
Atrazine	Anaerobic moving bed biofilm reactor	Pilot-scale study with synthetic wastewater, ATZ = 0.1 mg/L; COD = 500 mg/L; HRT = 24 h; $T = 32^{\circ}C$; PH = 7.5	ATZ = 60.5% COD = 97.4%	The biofilm moving bed anaerobic reactor showed excellent efficiency in the removal of organic matter and atrazine	[147]
	Denitrifying bioreactors	Laboratory experiments with synthetic wastewater, [ATZ] = 20 ug/L; (NO_3-N) = 1.5 mg/L; $T = 21^{\circ}C$; HRT= (4-8-24–72 h)	ATZ = 53% NO3-N = 100%	NO3-N and atrazine removal increased with increasing HRT. At 4 h, the wood chip bioreactor removed 65% of the NO_3-N and 25% of the atrazine, but at 72 h, the bioreactor removed all NO3-N and 53% of the atrazine	[148]
Amoxicillin	Anaerobic degradation systems	Laboratory experiments with synthetic wastewater; [AMX] = 2500 ug/L; $T = 37^{\circ}C$; PH = 7.2	AMX is completely eliminated	Amoxicillin was completely eliminated under anaerobic conditions. However, analysis identified amoxicillin penicilloic acid, amoxilloic acid, amoxicillin diketopiperazine, and phenol hydroxypyrazine as by-products	[149]
	Anaerobic digestion and aerobic-sequencing batch reactor	Lab-scale combined anaerobic and aerobic processes for swine wastewater treatment containing 19 antibiotics; HRT = 3.3 days; total antibiotic concentrations 99.2 to 339.3 μg/L; COD = 5683 mg/L; [AMX] = 60 ng/L	Antibiotics = 92% COD = 95%	Biodegradation of antibiotics was favoured in the SBR, while the degradation of COD was favoured in the anaerobic reactor	[150]
Paracetamol	Activated sludge	Laboratory experiments with synthetic wastewater; activated sludge comes from an aerobic tank in a wastewater treatment plant. [PCM] = 100 mg/L; $t = 72$ h	99%	The pseudomonas population could eliminate PCM at levels up to 590 mg/L and could also metabolize the PCM-derived metabolites 4-aminophenol, hydroquinone, and 1, 4-benzoquinone at varying levels	[142]
	Constructed wetlands (CWs)	Pilot-scale vertical flow constructed wetland with hospital wastewater; [PCM] = 10 mg/L; HRT = 5 d; media bed: sand and gravel	>99%	*S. validus* peroxidase enzymes are planted in the CW to control PCM. The vertical flow CW was effective in removing PCM (>99%) in hospital wastewater treatment	[145]

Table 6: Removal of emerging pollutants by hybrid processes.

Pollutant	Processes	Operating conditions	Removal efficiency	Additional information	References
Bisphenol A	Adsorption - photocatalysis	[BPA] = 20 mg/L; [Photocatalyst] = 1 g/L; t = 1 h; T = 25°C; batch photoreactor with visible light irradiation	BPA = 96% TOC = 88%	BPA molecules are rapidly adsorbed onto boron and nitrogen codoped graphene aerogels and eventually mineralised upon exposure to visible light	[154]
Atrazine	Adsorption-ozonation	[ATZ] = 0.7 mg/L; [Adsorbent] = 16 mg/L; [O_3] = 19.7 mg/L; t = 17 min; T = 25°C; batch experiments with synthetic wastewater	ATZ = 90%	A better reduction of atrazine (90%) is obtained when the treatment starts with powdered activated carbon followed by ozone, with a contact time of 17minutes	[155]
Amoxicillin	Fenton-activated sludge	1 mg/L of AMX; 6 mL of H_2O_2 (30% w/w), 4 mL heptahydrated ferrous sulphate ($FeSO_4{\cdot}7H_2O$) solution T = 40°C; t = 70 min	AMX = 85.13%	The pretreatment in the Fenton process disintegrated the AMX, thus reducing these toxic effects in the subsequent treatment, as the activated sludge can easily degrade the antibiotic	[156]
Paracetamol	Biological-adsorption	2 mg/L of PCM; 1.5 g/L of granular activated carbon	PCM = 100%	The hybrid sequential batch reactor- (SBR-) activated carbon system was able to completely degrade paracetamol in wastewater	[157]

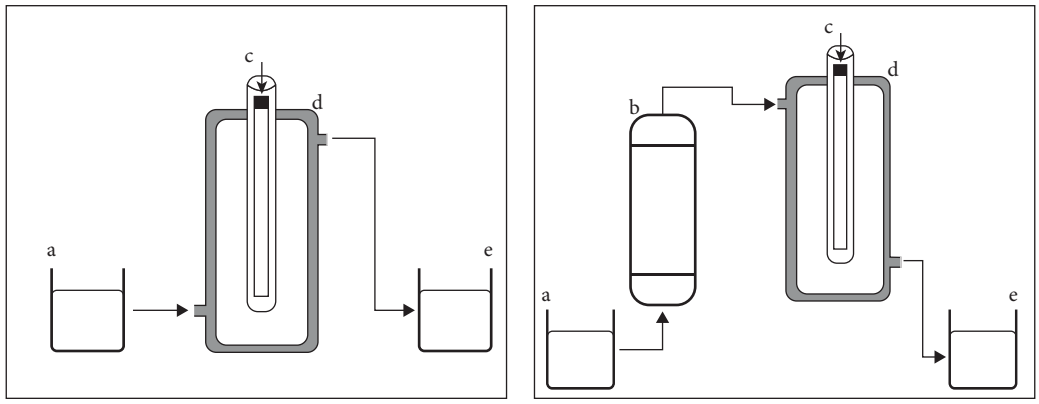

Figure 6: Operation schemes of (a) simultaneous combination (one step) and (b) separate coupling (two steps) of adsorption and photocatalysis (a, wastewater influent; b, adsorption column; c, lamp; d, photocatalytic reactor; and e, wastewater effluent).

7.2. Separate Coupling of Adsorption and Photocatalysis. The literature review shows that several researchers have been interested in the simultaneous combination of adsorption and photocatalysis. However, although this coupling can be carried out simultaneously to obtain the advantages of both techniques in a single step, if problems such as the low use of light and the need for agitation cannot be solved appropriately, the large-scale technical application of photocatalysis appears uncertain. Zhang et al. [158] developed an adsorptive photocatalyst (Zn-doped B_iOI) for the removal of antibiotics from water with a parallel coupling of adsorptive separation followed by photodegradation. The results show that the Zn-doped B_iOI has a removal rate of more than 95% after 5 min of adsorption for the six antibiotics tested. Subsequently, trace contaminants were effectively degraded during the subsequent visible light irradiation process.

Many adsorbent materials have been reported in the literature for their ability to remove different types of emerging pollutants, including carbonaceous materials, agricultural solid waste, and nanomaterials, clays. Some adsorbents are more widely studied than others, such as activated carbon, which is the most frequently used adsorbent for removing EPs. Indeed, much attention should be given to local (Moroccan) materials such as phosphate waste rock, which is generated in large volumes and occupies large areas in mining sites, Moroccan clays, and agricultural waste, by improving their properties to develop effective materials, can be used instead of expensive commercial adsorbents for the removal of micropollutants.

In addition, many photocatalysts (TiO_2, Z_nO, WO_3, etc.) have been studied and found to be suitable for the degradation of emerging pollutants. Among the different photocatalytic semiconductors, titanium dioxide (TiO_2) seems

to be the most often applied in water treatment, as it presents better photocatalytic performances. Still, its photoexcitation requires the use of ultraviolet irradiation, which limits the use of solar irradiation. Indeed, the development of new photocatalysts based on low-cost materials and allowing photodegradation under natural irradiation (solar radiation) is a challenge for future work.

8. Conclusions

The widespread presence of emerging pollutants in the environment has attracted worldwide attention because of their severe impacts on the environment and human health. Previous studies have shown that conventional wastewater treatment plants are not effective in treating these contaminants. The data presented in this review summarize the current knowledge on the occurrence, impact, and treatment of bisphenol A, atrazine, amoxicillin, and paracetamol in the environment. These compounds are frequently detected in various aqueous matrices and are among the most common emerging pollutants that can adversely affect humans and the environment. Different treatment methods have been developed to reduce the impacts of these contaminants. Likewise, the adsorption method has the following advantages: reduced energy consumption, simple operating conditions, reduced sludge production, and better adaptation to the removal of environmental pollution from water. Studies have shown that activated carbon is the most widely used adsorbent for the removal of different types of pollutants. In addition, the degradation of contaminants by photocatalysis is a promising method that allows for complete mineralization, without the production of sludge and with scalable applications using sunlight as a renewable and nonpolluting energy source. Titanium dioxide is the most widely applied photocatalyst in water treatment. On this basis, the search for other and more efficient materials is needed. Therefore, the challenge is to develop a treatment process by coupling adsorption and photocatalysis using inexpensive and locally available (Morocco) materials capable of removing/degrading EPs in a wide range of environments rather than being limited to one type of emerging pollutant.

Conflicts of Interest

The authors declare no conflicts of interest.

Acknowledgments

The authors are grateful to the Mohammed VI Polytechnic University of Benguerir and the OCP foundation for supporting this research work.

References

[1] K. Vargas-Berrones, L. Bernal-Jácome, L. Díaz de León-Martínez, and R. Flores-Ramírez, "Emerging pollutants (EPs) in latin América: a critical review of under-studied EPs, case of study-nonylphenol-," *Science of the Total Environment*, vol. 726, Article ID 138493, 2020.

[2] I. Anastopoulos, I. Pashalidis, A. G. Orfanos et al., "Removal of caffeine, nicotine and amoxicillin from (waste)waters by various adsorbents. A review," *Journal of Environmental Management*, vol. 261, Article ID 110236, 2020.

[3] M. C. Necibi, D. Dhiba, and S. El Hajjaji, "Contaminants of emerging concern in African wastewater effluents: occurrence, impact and removal technologies," *Sustainability*, vol. 13, no. 3, p. 1125, 2021.

[4] M. Ouda, D. Kadadou, B. Swaidan et al., "Emerging contaminants in the water bodies of the middle east and North Africa (MENA): a critical review," *Science of the Total Environment*, vol. 754, Article ID 142177, 2021.

[5] C. Egbuna, C. N. Amadi, K. C. Patrick-Iwuanyanwu et al., "Emerging pollutants in Nigeria: a systematic review," *Environmental Toxicology and Pharmacology*, vol. 85, Article ID 103638, 2021.

[6] T. Salthammer, "Emerging indoor pollutants," *International Journal of Hygiene and Environmental Health*, vol. 224, Article ID 113423, 2020.

[7] J.-Q. Jiang, Z. Zhou, and V. K. Sharma, "Occurrence, transportation, monitoring and treatment of emerging micro-pollutants in waste water-a review from global views," *Microchemical Journal*, vol. 110, pp. 292–300, 2013.

[8] K. M. Gani, N. Hlongwa, T. Abunama, S. Kumari, and F. Bux, "Emerging contaminants in South African water environment-a critical review of their occurrence, sources and ecotoxicological risks," *Chemosphere*, vol. 269, Article ID 128737, 2021.

[9] O. C. Olatunde, A. T. Kuvarega, and D. C. Onwudiwe, "Photo enhanced degradation of contaminants of emerging concern in waste water," *Emerging Contaminants*, vol. 6, pp. 283–302, 2020.

[10] X. Gao, S. Kang, R. Xiong, and M. Chen, "Environment-friendly removal methods for endocrine disrupting chemicals," *Sustainability (Switzerland)*, vol. 12, p. 7615, 2020.

[11] L. Zhao, J. Deng, P. Sun et al., "Nanomaterials for treating emerging contaminants in water by adsorption and photocatalysis: systematic review and bibliometric analysis," *Science of the Total Environment*, vol. 627, pp. 1253–1263, 2018.

[12] P. D. Darbre, "What are endocrine disrupters and where are they found?" *Endocrine Disruption and Human Health*, vol. 24, pp. 3–26, 2015.

[13] F. A. Caliman and M. Gavrilescu, "Pharmaceuticals, personal care products and endocrine disrupting agents in the environment-a review," *CLEAN-Soil, Air, Water*, vol. 37, no. 4-5, pp. 277–303, 2009.

[14] J. P. Laurenson, R. A. Bloom, S. Page, and N. Sadrieh, "Ethinyl estradiol and other human pharmaceutical estrogens in the aquatic environment: a review of recent risk assessment data," *The AAPS Journal*, vol. 16, no. 2, pp. 299–310, 2014.

[15] W. T. Vieira, M. B. De Farias, M. P. Spaolonzi, M. G. C. Da Silva, and M. G. Adeodato Vieira, "Endocrine-disrupting compounds: occurrence, detection methods, effects and promising treatment pathways-a critical review," *Journal of Environmental Chemical Engineering*, vol. 9, no. 1, Article ID 104558, 2021.

[16] A. Jurado, E. Vàzquez-Suñé, J. Carrera, M. López de Alda, E. Pujades, and D. Barceló, "Emerging organic contaminants in groundwater in Spain: a review of sources, recent occurrence and fate in a European context," *Science of the Total Environment*, vol. 440, pp. 82–94, 2012.

[17] M. A. Hassaan and A. El Nemr, "Pesticides pollution: classifications, human health impact, extraction and

treatment techniques," *The Egyptian Journal of Aquatic Research*, vol. 46, no. 3, pp. 207–220, 2020.

[18] R. M. de Souza, D. Seibert, H. B. Quesada, F. de Jesus Bassetti, M. R. Fagundes-Klen, and R. Bergamasco, "Occurrence, impacts and general aspects of pesticides in surface water: a review," *Process Safety and Environmental Protection*, vol. 135, pp. 22–37, 2020.

[19] K. Y. Foo and B. H. Hameed, "Detoxification of pesticide waste via activated carbon adsorption process," *Journal of Hazardous Materials*, vol. 175, pp. 1–11, 2010.

[20] L. M. Madikizela, S. Ncube, and L. Chimuka, "Analysis, occurrence and removal of pharmaceuticals in African water resources: a current status," *Journal of Environmental Management*, vol. 253, Article ID 109741, 2020.

[21] J. Rivera-Utrilla, M. Sánchez-Polo, M. Á. Ferro-García, G. Prados-Joya, and R. Ocampo-Pérez, "Pharmaceuticals as emerging contaminants and their removal from water. A review," *Chemosphere*, vol. 93, no. 7, pp. 1268–1287, 2013.

[22] M. de Oliveira, B. E. F. Frihling, J. Velasques, F. J. C. M. Filho, P. S. Cavalheri, and L. Migliolo, "Pharmaceuticals residues and xenobiotics contaminants: occurrence, analytical techniques and sustainable alternatives for wastewater treatment," *Science of the Total Environment*, vol. 705, Article ID 135568, 2020.

[23] C. F. Couto, L. C. Lange, and M. C. S. Amaral, "Occurrence, fate and removal of pharmaceutically active compounds (PhACs) in water and wastewater treatment plants—a review," *Journal of Water Process Engineering*, vol. 32, Article ID 100927, 2019.

[24] A. Barra Caracciolo, E. Topp, and P. Grenni, "Pharmaceuticals in the environment: biodegradation and effects on natural microbial communities. A review," *Journal of Pharmaceutical and Biomedical Analysis*, vol. 106, pp. 25–36, 2015.

[25] O. E. Ohore and S. Zhang, "Endocrine disrupting effects of bisphenol A exposure and recent advances on its removal by water treatment systems. A review," *Scientific African*, vol. 5, Article ID e00135, 2019.

[26] K. Aschberger, S. Munn, H. Olsson et al., "European union risk assessment report-BPA (4,4′–isopropylidenediphenol (Bisphenol–A))," *Engineering*, vol. 221, 2010.

[27] Z. Sheng, C. Wang, F. Ren, Y. Liu, and B. Zhu, "Molecular mechanism of endocrine-disruptive effects induced by Bisphenol A: the role of transmembrane G-protein estrogen receptor 1 and integrin $\alpha v\beta 3$," *Journal of Environmental Sciences*, vol. 75, pp. 1–13, 2019.

[28] Z.-H. Deng, N. Li, H.-L. Jiang, J.-M. Lin, and R.-S. Zhao, "Pretreatment techniques and analytical methods for phenolic endocrine disrupting chemicals in food and environmental samples," *TrAC Trends in Analytical Chemistry*, vol. 119, Article ID 115592, 2019.

[29] C. Xiao, L. Wang, Q. Zhou, and X. Huang, "Hazards of bisphenol A (BPA) exposure: a systematic review of plant toxicology studies," *Journal of Hazardous Materials*, vol. 384, Article ID 121488, 2020.

[30] C. J. Catenza, A. Farooq, N. S. Shubear, and K. K. Donkor, "A targeted review on fate, occurrence, risk and health implications of bisphenol analogues," *Chemosphere*, vol. 268, Article ID 129273, 2021.

[31] M. Noszczyńska and Z. Piotrowska-Seget, "Bisphenols: application, occurrence, safety, and biodegradation mediated by bacterial communities in wastewater treatment plants and rivers," *Chemosphere*, vol. 201, pp. 214–223, 2018.

[32] A. Bhatnagar and I. Anastopoulos, "Adsorptive removal of bisphenol A (BPA) from aqueous solution: a review," *Chemosphere*, vol. 168, pp. 885–902, 2017.

[33] Y. Hu, Q. Zhu, X. Yan, C. Liao, and G. Jiang, "Occurrence, fate and risk assessment of BPA and its substituents in wastewater treatment plant: a review," *Environmental Research*, vol. 178, Article ID 108732, 2019.

[34] N. Zhou, Y. Liu, S. Cao, R. Guo, Y. Ma, and J. Chen, "Biodegradation of bisphenol compounds in the surface water of Taihu lake and the effect of humic acids," *Science of the Total Environment*, vol. 723, Article ID 138164, 2020.

[35] N. Akhtar, M. Fiaz Khan, S. Tabassum, and E. Zahran, "Adverse effects of atrazine on blood parameters, biochemical profile and genotoxicity of snow trout (schizothorax plagiostomus)," *Saudi Journal of Biological Sciences*, vol. 28, no. 3, pp. 1999–2003, 2021.

[36] B. Mathon, M. Ferreol, M. Coquery, J.-M. Choubert, J.-M. Chovelon, and C. Miège, "Direct photodegradation of 36 organic micropollutants under simulated solar radiation: comparison with free-water surface constructed wetland and influence of chemical structure," *Journal of Hazardous Materials*, vol. 407, Article ID 124801, 2021.

[37] L. A. J. Vieira, R. D. F. B. Alves, P. E. Menezes-Silva et al., "Water contamination with atrazine: is nitric oxide able to improve pistia stratiotes phytoremediation capacity?" *Environmental Pollution*, vol. 272, Article ID 115971, 2021.

[38] K. O. K'oreje, M. Okoth, H. Van Langenhove, and K. Demeestere, "Occurrence and treatment of contaminants of emerging concern in the African aquatic environment: literature review and a look ahead," *Journal of Environmental Management*, vol. 254, Article ID 109752, 2020.

[39] F. P. de Albuquerque, J. L. de Oliveira, V. Moschini-Carlos, and L. F. Fraceto, "An overview of the potential impacts of atrazine in aquatic environments: perspectives for tailored solutions based on nanotechnology," *Science of the Total Environment*, vol. 700, Article ID 134868, 2020.

[40] P. Vanraes, G. Willems, A. Nikiforov et al., "Removal of atrazine in water by combination of activated carbon and dielectric barrier discharge," *Journal of Hazardous Materials*, vol. 299, pp. 647–655, 2015.

[41] "Association Marocaine de l'Industrie Pharmaceutique (AMIP), Le Secteur Pharmaceutique Marocain: Réalités sur le Prix des Médicaments et Intérêt du Secteur. Synthése," AMIP, Casablanca, Morocco, 15 pages, 2010, http://www.amip.ma.

[42] A. Rempel, J. P. Gutkoski, M. T. Nazari et al., "Current advances in microalgae-based bioremediation and other technologies for emerging contaminants treatment," *Science of the Total Environment*, vol. 772, Article ID 144918, 2021.

[43] M. A. E. de Franco, C. B. de Carvalho, M. M. Bonetto, R. d. P. Soares, and L. A. Féris, "Removal of amoxicillin from water by adsorption onto activated carbon in batch process and fixed bed column: kinetics, isotherms, experimental design and breakthrough curves modelling," *Journal of Cleaner Production*, vol. 161, pp. 947–956, 2017.

[44] E. Felis, J. Kalka, A. Sochacki et al., "Antimicrobial pharmaceuticals in the aquatic environment-occurrence and environmental implications," *European Journal of Pharmacology*, vol. 866, Article ID 172813, 2020.

[45] J. M. Chaba and P. N. Nomngongo, "Effective adsorptive removal of amoxicillin from aqueous solutions and wastewater samples using zinc oxide coated carbon nanofiber composite," *Emerging Contaminants*, vol. 5, pp. 143–149, 2019.

[46] M. E. Matsubara, K. Helwig, C. Hunter, J. Roberts, E. L. Subtil, and L. H. G. Coelho, "Amoxicillin removal by pre-denitrification membrane bioreactor (A/O-MBR): performance evaluation, degradation by-products, and antibiotic resistant bacteria," *Ecotoxicology and Environmental Safety*, vol. 192, Article ID 110258, 2020.

[47] C.-W. Yang, C. Liu, and B.-V. Chang, "Biodegradation of amoxicillin, tetracyclines and sulfonamides in wastewater sludge," *Water*, vol. 12, no. 8, p. 2147, 2020.

[48] A. Spaltro, M. N. Pila, D. D. Colasurdo et al., "Removal of paracetamol from aqueous solution by activated carbon and silica. Experimental and computational study," *Journal of Contaminant Hydrology*, vol. 236, Article ID 103739, 2021.

[49] J. Goscianska, A. Olejnik, A. Ejsmont, A. Galarda, and S. Wuttke, "Overcoming the paracetamol dose challenge with wrinkled mesoporous carbon spheres," *Journal of Colloid and Interface Science*, vol. 586, pp. 673–682, 2021.

[50] I. Villaescusa, N. Fiol, J. Poch, A. Bianchi, and C. Bazzicalupi, "Mechanism of paracetamol removal by vegetable wastes: the contribution of π-π interactions, hydrogen bonding and hydrophobic effect," *Desalination*, vol. 270, no. 1-3, pp. 135–142, 2011.

[51] J. Żur, D. Wojcieszyńska, K. Hupert-Kocurek, A. Marchlewicz, and U. Guzik, "Paracetamol-toxicity and microbial utilization. Pseudomonas moorei KB4 as a case study for exploring degradation pathway," *Chemosphere*, vol. 206, pp. 192–202, 2018.

[52] O. Chaib, B. Arhoune, S. Achour et al., "Occurrence and seasonal variation of antibiotics in Fez-Morocco surface water," *American Journal of Environmental Sciences*, vol. 15, no. 4, pp. 127–136, 2019.

[53] E. K. Radwan, M. B. M. Ibrahim, A. Adel, and M. Farouk, "The occurrence and risk assessment of phenolic endocrine-disrupting chemicals in Egypt's drinking and source water," *Environmental Science and Pollution Research*, vol. 27, no. 2, pp. 1776–1788, 2020.

[54] H. Xie, X. Wang, J. Chen et al., "Occurrence, distribution and ecological risks of antibiotics and pesticides in coastal waters around Liaodong Peninsula, China," *Science of the Total Environment*, vol. 656, pp. 946–951, 2019.

[55] Y. Picó, R. Alvarez-Ruiz, A. H. Alfarhan, M. A. El-Sheikh, H. O. Alshahrani, and D. Barceló, "Pharmaceuticals, pesticides, personal care products and microplastics contamination assessment of Al-Hassa irrigation network (Saudi Arabia) and its shallow lakes," *Science of the Total Environment*, vol. 701, Article ID 135021, 2020.

[56] L. Palli, F. Spina, G. C. Varese et al., "Occurrence of selected pharmaceuticals in wastewater treatment plants of tuscany: an effect-based approach to evaluate the potential environmental impact," *International Journal of Hygiene and Environmental Health*, vol. 222, no. 4, pp. 717–725, 2019.

[57] J. Xue and K. Kannan, "Mass flows and removal of eight bisphenol analogs, bisphenol A diglycidyl ether and its derivatives in two wastewater treatment plants in New York State, USA," *Science of the Total Environment*, vol. 648, pp. 442–449, 2019.

[58] A. I. Farounbi and N. P. Ngqwala, "Occurrence of selected endocrine disrupting compounds in the eastern cape province of South Africa," *Environmental Science and Pollution Research*, vol. 27, no. 14, pp. 17268–17279, 2020.

[59] T. J. Thompson, M. A. Briggs, P. J. Phillips et al., "Groundwater discharges as a source of phytoestrogens and other agriculturally derived contaminants to streams," *Science of the Total Environment*, vol. 755, Article ID 142873, 2021.

[60] A. J. Ebele, T. Oluseyi, D. S. Drage, S. Harrad, and M. Abou-Elwafa Abdallah, "Occurrence, seasonal variation and human exposure to pharmaceuticals and personal care products in surface water, groundwater and drinking water in Lagos state, Nigeria," *Emerging Contaminants*, vol. 6, pp. 124–132, 2020.

[61] K. Ozhan and E. Kocaman, "Temporal and spatial distributions of bisphenol A in marine and freshwaters in Turkey," *Archives of Environmental Contamination and Toxicology*, vol. 76, no. 2, pp. 246–254, 2019.

[62] P. Paíga, L. H. M. L. M. Santos, and C. Delerue-Matos, "Development of a multi-residue method for the determination of human and veterinary pharmaceuticals and some of their metabolites in aqueous environmental matrices by SPE-UHPLC-MS/MS," *Journal of Pharmaceutical and Biomedical Analysis*, vol. 135, pp. 75–86, 2017.

[63] N. A. Alygizakis, P. Gago-Ferrero, V. L. Borova, A. Pavlidou, I. Hatzianestis, and N. S. Thomaidis, "Occurrence and spatial distribution of 158 pharmaceuticals, drugs of abuse and related metabolites in offshore seawater," *Science of the Total Environment*, vol. 541, pp. 1097–1105, 2016.

[64] H.-G. Ni, H. Zeng, and E. Y. Zeng, "Sampling and analytical framework for routine environmental monitoring of organic pollutants," *TrAC Trends in Analytical Chemistry*, vol. 30, no. 10, pp. 1549–1559, 2011.

[65] O. Muter and V. Bartkevics, "Advanced analytical techniques based on high-resolution mass spectrometry for the detection of micropollutants and their toxicity in aquatic environments," *Current Opinion in Environmental Science & Health*, vol. 18, pp. 1–6, 2020.

[66] M. Lorenzo, J. Campo, and Y. Picó, "Analytical challenges to determine emerging persistent organic pollutants in aquatic ecosystems," *TrAC Trends in Analytical Chemistry*, vol. 103, pp. 137–155, 2018.

[67] T. H. Boles and M. J. M. Wells, "Analysis of amphetamine and methamphetamine as emerging pollutants in wastewater and wastewater-impacted streams," *Journal of Chromatography A*, vol. 1217, no. 16, pp. 2561–2568, 2010.

[68] S. F. Ahmed, M. Mofijur, S. Nuzhat et al., "Recent developments in physical, biological, chemical, and hybrid treatment techniques for removing emerging contaminants from wastewater," *Journal of Hazardous Materials*, vol. 416, Article ID 125912, 2021.

[69] I. A. Kawa, A. Masood, Q. Fatima et al., "Endocrine disrupting chemical bisphenol A and its potential effects on female health," *Diabetes & Metabolic Syndrome: Clinical Research & Reviews*, vol. 15, no. 3, pp. 803–811, 2021.

[70] M. Faheem and R. K. Bhandari, "Detrimental effects of bisphenol compounds on physiology and reproduction in fish: a literature review," *Environmental Toxicology and Pharmacology*, vol. 81, Article ID 103497, 2021.

[71] J. S. Siracusa, L. Yin, E. Measel, S. Liang, and X. Yu, "Effects of bisphenol A and its analogs on reproductive health: a mini review," *Reproductive Toxicology*, vol. 79, pp. 96–123, 2018.

[72] R. K. Bhandari, S. L. Deem, D. K. Holliday et al., "Effects of the environmental estrogenic contaminants bisphenol A and 17α-ethinyl estradiol on sexual development and adult behaviors in aquatic wildlife species," *General and Comparative Endocrinology*, vol. 214, pp. 195–219, 2015.

[73] T. B. Hayes, L. L. Anderson, V. R. Beasley et al., "Demasculinization and feminization of male gonads by atrazine: consistent effects across vertebrate classes," *The Journal of*

Steroid Biochemistry and Molecular Biology, vol. 127, no. 1-2, pp. 64–73, 2011.

[74] H. He, Y. Liu, S. You, J. Liu, H. Xiao, and Z. Tu, "A review on recent treatment technology for herbicide atrazine in contaminated environment," *International Journal of Environmental Research and Public Health*, vol. 16, no. 24, p. 5129, 2019.

[75] T. Mackuľak, S. Černanský, M. Fehér, L. Birošová, and M. Gál, "Pharmaceuticals, drugs, and resistant microorganisms-environmental impact on population health," *Current Opinion in Environmental Science & Health*, vol. 9, pp. 40–48, 2019.

[76] L. Meng, X. Li, X. Wang, K. Ma, G. Liu, and J. Zhang, "Amoxicillin effects on functional microbial community and spread of antibiotic resistance genes in amoxicillin manufacture wastewater treatment system," *Journal of Environmental Sciences*, vol. 61, pp. 110–117, 2017.

[77] K. K. Sodhi, M. Kumar, and D. K. Singh, "Insight into the amoxicillin resistance, ecotoxicity, and remediation strategies," *Journal of Water Process Engineering*, vol. 39, Article ID 101858, 2021.

[78] H. Montaseri and P. B. C. Forbes, "Analytical techniques for the determination of acetaminophen: a review," *TrAC Trends in Analytical Chemistry*, vol. 108, pp. 122–134, 2018.

[79] M. Parolini, "Toxicity of the non-steroidal anti-inflammatory drugs (NSAIDs) acetylsalicylic acid, paracetamol, diclofenac, ibuprofen and naproxen towards freshwater invertebrates: a review," *Science of the Total Environment*, vol. 740, Article ID 140043, 2020.

[80] Ministère de l'environnement, L'état de l'environnement du maroc, 2015, 187.

[81] M. Benjelloun, Y. Miyah, G. Akdemir Evrendilek, F. Zerrouq, and S. Lairini, "Recent advances in adsorption kinetic models: their application to dye types," *Arabian Journal of Chemistry*, vol. 14, no. 4, Article ID 103031, 2021.

[82] A. Azzouz, L. P. Colón, B. Souhail, and E. Ballesteros, "A multi-residue method for GC-MS determination of selected endocrine disrupting chemicals in fish and seafood from European and North African markets," *Environmental Research*, vol. 178, Article ID 108727, 2019.

[83] S. Chafi, A. Azzouz, and E. Ballesteros, "Occurrence and distribution of endocrine disrupting chemicals and pharmaceuticals in the river bouregreg (Rabat, Morocco)," *Chemosphere*, vol. 287, Article ID 132202, 2022.

[84] F. M. Mpatani, R. Han, A. A. Aryee, A. N. Kani, Z. Li, and L. Qu, "Adsorption performance of modified agricultural waste materials for removal of emerging micro-contaminant bisphenol A: a comprehensive review," *Science of the Total Environment*, vol. 780, Article ID 146629, 2021.

[85] J. Wang and X. Guo, "Adsorption isotherm models: classification, physical meaning, application and solving method," *Chemosphere*, vol. 258, Article ID 127279, 2020.

[86] M. Zbair, K. Ainassaari, A. Drif et al., "Toward new benchmark adsorbents: preparation and characterization of activated carbon from argan nut shell for bisphenol A removal," *Environmental Science and Pollution Research*, vol. 25, no. 2, pp. 1869–1882, 2018.

[87] A. B. Hernández-Abreu, S. Álvarez-Torrellas, V. I. Águeda et al., "Enhanced removal of the endocrine disruptor compound bisphenol A by adsorption onto green-carbon materials. Effect of real effluents on the adsorption process," *Journal of Environmental Management*, vol. 266, 2020.

[88] S. I. Rathnayake, Y. Xi, R. L. Frost, and G. A. Ayoko, "Environmental applications of inorganic-organic clays for recalcitrant organic pollutants removal: bisphenol A," *Journal of Colloid and Interface Science*, vol. 470, pp. 183–195, 2016.

[89] Y. Wang, X. Wei, Y. Qi, and H. Huang, "Efficient removal of bisphenol-A from water and wastewater by Fe_2O_3-modified graphene oxide," *Chemosphere*, vol. 263, Article ID 127563, 2021.

[90] J. H. Lee and S. Y. Kwak, "Branched polyethyleniminepolyethylene glycol-β-cyclodextrin polymers for efficient removal of bisphenol A and copper from wastewater," *Journal of Applied Polymer Science*, vol. 137, no. 12, Article ID 48475, 2020.

[91] M. A. Ahsan, M. T. Islam, C. Hernandez et al., "Adsorptive removal of sulfamethoxazole and bisphenol A from contaminated water using functionalized carbonaceous material derived from tea leaves," *Journal of Environmental Chemical Engineering*, vol. 6, no. 4, pp. 4215–4225, 2018.

[92] I. Akpinar, R. J. Drout, T. Islamoglu, S. Kato, J. Lyu, and O. K. Farha, "Exploiting π-π interactions to design an efficient sorbent for atrazine removal from water," *ACS Applied Materials & Interfaces*, vol. 11, no. 6, pp. 6097–6103, 2019.

[93] J. M. Park and S. H. Jhung, "Polyaniline-derived carbons: remarkable adsorbents to remove atrazine and diuron herbicides from water," *Journal of Hazardous Materials*, vol. 396, Article ID 122624, 2020.

[94] A. Mandal and N. Singh, "Kinetic and isotherm error optimization studies for adsorption of atrazine and imidacloprid on bark of eucalyptus tereticornis L." *Journal of Environmental Science and Health, Part B*, vol. 51, no. 3, pp. 192–203, 2016.

[95] F. Suo, X. You, Y. Ma, and Y. Li, "Rapid removal of triazine pesticides by P doped biochar and the adsorption mechanism," *Chemosphere*, vol. 235, pp. 918–925, 2019.

[96] M. Belhachemi and S. Djelaila, "Removal of amoxicillin antibiotic from aqueous solutions by date pits activated carbons," *Environmental Processes*, vol. 4, no. 3, pp. 549–561, 2017.

[97] I. Es-saidi, A. Oulguidoum, C. El Bekkali, H. Bouyarmane, A. Laghzizil, and J.-M. Nunzi, "Characterization and valorization of natural phosphate in removing of heavy metals and toxic organic species from water," *Journal of African Earth Sciences*, vol. 173, Article ID 104022, 2021.

[98] D. Balarak, F. Mostafapour, E. Bazrafshan, and T. A. Saleh, "Studies on the adsorption of amoxicillin on multi-wall carbon nanotubes," *Water Science and Technology*, vol. 75, no. 7, pp. 1599–1606, 2017.

[99] Z. Shang, Z. Hu, L. Huang, Z. Guo, H. Liu, and C. Zhang, "Removal of amoxicillin from aqueous solution by zinc acetate modified activated carbon derived from reed," *Powder Technology*, vol. 368, pp. 178–189, 2020.

[100] J. Imanipoor, A. Ghafelebashi, M. Mohammadi, M. Dinari, and M. R. Ehsani, "Fast and effective adsorption of amoxicillin from aqueous solutions by L-methionine modified montmorillonite K10," *Colloids and Surfaces A: Physicochemical and Engineering Aspects*, vol. 611, Article ID 125792, 2021.

[101] M. Chauhan, V. K. Saini, and S. Suthar, "Ti-pillared montmorillonite clay for adsorptive removal of amoxicillin, imipramine, diclofenac-sodium, and paracetamol from water," *Journal of Hazardous Materials*, vol. 399, Article ID 122832, 2020.

[102] N. Benyekkou, M. R. Ghezzar, F. Abdelmalek, and A. Addou, "Elimination of paracetamol from water by a spent coffee grounds biomaterial," *Environmental Nanotechnology, Monitoring & Management*, vol. 14, Article ID 100396, 2020.

[103] F. E. Titchou, H. Zazou, H. Afanga, J. El Gaayda, R. A. Akbour, and M. Hamdani, "Removal of persistent organic pollutants (POPs) from water and wastewater by adsorption and electrocoagulation process," *Groundwater for Sustainable Development*, vol. 13, Article ID 100575, 2021.

[104] X. Hou, X. Huang, F. Jia, Z. Ai, J. Zhao, and L. Zhang, "Hydroxylamine promoted goethite surface Fenton degradation of organic pollutants," *Environmental Science & Technology*, vol. 51, no. 9, pp. 5118–5126, 2017.

[105] Q. Li, H. Kong, P. Li, J. Shao, and Y. He, "Photo-fenton degradation of amoxicillin via magnetic TiO_2-graphene oxide-Fe_3O_4 composite with a submerged magnetic separation membrane photocatalytic reactor (SMSMPR)," *Journal of Hazardous Materials*, vol. 373, pp. 437–446, 2019.

[106] F. Zaviska, P. Drogui, G. Mercier, and J.-F. Blais, "Advanced oxidation processes for waters and wastewaters treatment: application to degradation of refractory pollutants. Procédés d'oxydation avancée dans le traitement des eaux et des effluents industriels: application à la dégradation des polluants réfr," *Revue Des Sciences de l'Eau*, vol. 22, 2009.

[107] Y. Xu, F. Ge, M. Xie et al., "Fabrication of magnetic $BaFe_{12}O_{19}/Ag_3PO_4$ composites with an in situ photo-Fenton-like reaction for enhancing reactive oxygen species under visible light irradiation," *Catalysis Science & Technology*, vol. 9, no. 10, pp. 2563–2570, 2019.

[108] Q. C. Do, D.-G. Kim, and S.-O. Ko, "Nonsacrificial template synthesis of magnetic-based yolk-shell nanostructures for the removal of acetaminophen in fenton-like systems," *ACS Applied Materials & Interfaces*, vol. 9, no. 34, pp. 28508–28518, 2017.

[109] I. Altin, X. Ma, V. Boffa, E. Bacaksız, and G. Magnacca, "Hydrothermal preparation of B-TiO_2-graphene oxide ternary nanocomposite, characterization and photocatalytic degradation of bisphenol A under simulated solar irradiation," *Materials Science in Semiconductor Processing*, vol. 123, Article ID 105591, 2021.

[110] Z. Shen, H. Zhou, Z. Pan et al., "Degradation of atrazine by Bi_2MoO_6 activated peroxymonosulfate under visible light irradiation," *Journal of Hazardous Materials*, vol. 400, Article ID 123187, 2020.

[111] B. Gao, J. Wang, M. Dou, C. Xu, and X. Huang, "Enhanced photocatalytic removal of amoxicillin with Ag/TiO_2/mesoporous g-C_3N_4 under visible light: property and mechanistic studies," *Environmental Science and Pollution Research*, vol. 27, 2019.

[112] O. F. S. Khasawneh, P. Palaniandy, P. Palaniandy, M. Ahmadipour, H. Mohammadi, and M. R. Bin Hamdan, "Removal of acetaminophen using Fe_2O_3-TiO_2 nanocomposites by photocatalysis under simulated solar irradiation: optimization study," *Journal of Environmental Chemical Engineering*, vol. 9, no. 1, Article ID 104921, 2021.

[113] Y. Huang, T. Yang, M. Liang et al., "Ni-Fe layered double hydroxides catalized ozonation of synthetic wastewater containing bisphenol A and municipal secondary effluent," *Chemosphere*, vol. 235, pp. 143–152, 2019.

[114] Y. Liu, S. Wang, L. Shi, W. Lu, and P. Li, "Enhanced degradation of atrazine by microbubble ozonation," *Environmental Science: Water Research & Technology*, vol. 6, no. 6, pp. 1681–1687, 2020.

[115] O. A. Alsager, M. N. Alnajrani, H. A. Abuelizz, and I. A. Aldaghmani, "Removal of antibiotics from water and waste milk by ozonation: kinetics, byproducts, and antimicrobial activity," *Ecotoxicology and Environmental Safety*, vol. 158, pp. 114–122, 2018.

[116] A. Mashayekh-Salehi, G. Moussavi, and K. Yaghmaeian, "Preparation, characterization and catalytic activity of a novel mesoporous nanocrystalline MgO nanoparticle for ozonation of acetaminophen as an emerging water contaminant," *Chemical Engineering Journal*, vol. 310, pp. 157–169, 2017.

[117] N. Ambauen, J. Muff, F. Tscheikner-Gratl, T. T. Trinh, C. Hallé, and T. Meyn, "Application of electrochemical oxidation in cold climate regions-effect of temperature, pH and anode material on the degradation of bisphenol A and the formation of disinfection by-products," *Journal of Environmental Chemical Engineering*, vol. 8, no. 5, Article ID 104183, 2020.

[118] S. Komtchou, A. Dirany, P. Drogui, D. Robert, and P. Lafrance, "Removal of atrazine and its by-products from water using electrochemical advanced oxidation processes," *Water Research*, vol. 125, pp. 91–103, 2017.

[119] X. Bian, Y. Xia, T. Zhan et al., "Electrochemical removal of amoxicillin using a Cu doped PbO_2 electrode: electrode characterization, operational parameters optimization and degradation mechanism," *Chemosphere*, vol. 233, pp. 762–770, 2019.

[120] S. Periyasamy and M. Muthuchamy, "Electrochemical oxidation of paracetamol in water by graphite anode: effect of pH, electrolyte concentration and current density," *Journal of Environmental Chemical Engineering*, vol. 6, no. 6, pp. 7358–7367, 2018.

[121] D. Ma, H. Yi, C. Lai et al., "Critical review of advanced oxidation processes in organic wastewater treatment," *Chemosphere*, vol. 275, Article ID 130104, 2021.

[122] R. Elkacmi and M. Bennajah, "Advanced oxidation technologies for the treatment and detoxification of olive mill wastewater: a general review," *Journal of Water Reuse and Desalination*, vol. 9, no. 4, pp. 463–505, 2019.

[123] M. Ouhammou, M. Bouchdoug, A. Jaouad, R. Ouaabou, B. Nabil, and M. Mahrouz, "Textile wastewater discoloration by fenton oxidation process," *Moroccan Journal of Chemistry*, vol. 7, pp. 516–527, 2019.

[124] I. El Mrabet, M. Benzina, H. Valdés, and H. Zaitan, "Treatment of landfill leachates from Fez city (Morocco) using a sequence of aerobic and fenton processes," *Scientific African*, vol. 8, Article ID e00434, 2020.

[125] I. E. Mrabet, M. Kachabi, M. Nawdali et al., "Treatment of landfill leachate from Fez city (Morocco) using fenton and photo-fenton processes," *IOP Conference Series: Earth and Environmental Science*, vol. 161, Article ID 012025, 2018.

[126] M. S. Yahya, N. Beqqal, A. Guessous, M. R. Arhoutane, and K. El Kacemi, "Degradation and mineralization of moxifloxacin antibiotic in aqueous medium by electro-Fenton process: kinetic assessment and oxidation products," *Cogent Chemistry*, vol. 3, no. 1, Article ID 1290021, 2017.

[127] L. Rachidi, G. Kaichouh, M. Khachani et al., "Optimization and modeling of the electro-fenton process for treatment of sertraline hydrochloride: mineralization efficiency, energy cost and biodegradability enhancement," *Chemical Data Collections*, vol. 35, Article ID 100764, 2021.

[128] H. K. Paumo, S. Dalhatou, L. M. Katata-Seru et al., "TiO_2 assisted photocatalysts for degradation of emerging organic pollutants in water and wastewater," *Journal of Molecular Liquids*, vol. 331, Article ID 115458, 2021.

[129] D. Zhu and Q. Zhou, "Action and mechanism of semiconductor photocatalysis on degradation of organic pollutants in water treatment: a review," *Environmental*

Nanotechnology, Monitoring & Management, vol. 12, Article ID 100255, 2019.

[130] S. Ahmed, F. Saleem, A. Khan et al., "Emerging pollutants and their removal using visible-light responsive photocatalysis–a comprehensive review," *Journal of Environmental Chemical Engineering*, vol. 9, 2021.

[131] M. Antonopoulou, C. Kosma, T. Albanis, and I. Konstantinou, "An overview of homogeneous and heterogeneous photocatalysis applications for the removal of pharmaceutical compounds from real or synthetic hospital wastewaters under lab or pilot scale," *Science of the Total Environment*, vol. 765, Article ID 144163, 2021.

[132] R. Saher, M. A. Hanif, A. Mansha et al., "Sunlight-driven photocatalytic degradation of rhodamine B dye by Ag/$FeWO_4$/g-C_3N_4 composites," *International Journal of Environmental Science and Technology*, vol. 18, no. 4, pp. 927–938, 2021.

[133] Shahab-ud-Din, M. Z. Ahmad, K. Qureshi, and I. A. Bhatti, M. Zahid, J. Nisar, M. Iqbal, and M. Abbas, Hydrothermal synthesis of molybdenum trioxide, characterization and photocatalytic activity," *Materials Research Bulletin*, vol. 100, pp. 120–130, 2018.

[134] A. Tabasum, M. Alghuthaymi, U. Y. Qazi et al., "Uv-accelerated photocatalytic degradation of pesticide over magnetite and cobalt ferrite decorated graphene oxide composite," *Plants*, vol. 10, pp. 1–18, 2021.

[135] A. Tabasum, I. A. Bhatti, N. Nadeem et al., "Degradation of acetamiprid using graphene-oxide-based metal (Mn and Ni) ferrites as fenton-like photocatalysts," *Water Science and Technology*, vol. 81, no. 1, pp. 178–189, 2020.

[136] K. Qureshi, M. Z. Ahmad, I. A. Bhatti, M. Zahid, J. Nisar, and M. Iqbal, "Graphene oxide decorated $ZnWO_4$ architecture synthesis, characterization and photocatalytic activity evaluation," *Journal of Molecular Liquids*, vol. 285, pp. 778–789, 2019.

[137] C. E. Bekkali, H. Bouyarmane, M. E. Karbane et al., "Zinc oxide-hydroxyapatite nanocomposite photocatalysts for the degradation of ciprofloxacin and ofloxacin antibiotics," *Colloids and Surfaces A: Physicochemical and Engineering Aspects*, vol. 539, pp. 364–370, 2018.

[138] S. Benjedim, J. Castelo-Quibén, E. Bailón-García et al., "Activated carbon-based coloured titania nanoparticles with high visible radiation absorption and excellent photoactivity in the degradation of emerging drugs of wastewater," *Carbon*, vol. 178, pp. 753–766, 2021.

[139] N. Bougdour, R. Tiskatine, I. Bakas, and A. Assabbane, "Photocatalytic degradation of industrial textile wastewater using S_2O_{82}/Fe^{2+} process," *Materials Today: Proceedings*, vol. 22, pp. 69–72, 2020.

[140] A. Gogoi, P. Mazumder, V. K. Tyagi, G. G. Tushara Chaminda, A. K. An, and M. Kumar, "Occurrence and fate of emerging contaminants in water environment: a review," *Groundwater for Sustainable Development*, vol. 6, pp. 169–180, 2018.

[141] S. Korpe and P. V. Rao, "Application of advanced oxidation processes and cavitation techniques for treatment of tannery wastewater-a review," *Journal of Environmental Chemical Engineering*, vol. 9, no. 3, Article ID 105234, 2021.

[142] S. Park and S. Oh, "Activated sludge-degrading analgesic drug acetaminophen: acclimation, microbial community dynamics, degradation characteristics, and bioaugmentation potential," *Water Research*, vol. 182, Article ID 115957, 2020.

[143] R. K. Langbehn, C. Michels, and H. M. Soares, "Antibiotics in wastewater: from its occurrence to the biological removal by environmentally conscious technologies," *Environmental Pollution*, vol. 275, Article ID 116603, 2021.

[144] B. Wang, L. Lu, Y. Zhang, K. Fang, D. An, and H. Li, "Removal of bisphenol A by waste zero-valent iron regulating microbial community in sequencing batch biofilm reactor," *Science of the Total Environment*, vol. 753, Article ID 142073, 2021.

[145] H. N. P. Vo, T. Koottatep, S. K. Chapagain et al., "Removal and monitoring acetaminophen-contaminated hospital wastewater by vertical flow constructed wetland and peroxidase enzymes," *Journal of Environmental Management*, vol. 250, Article ID 109526, 2019.

[146] A. Cydzik-Kwiatkowska, M. Zielińska, K. Bernat, K. Bułkowska, and I. Wojnowska-Baryła, "Insights into mechanisms of bisphenol A biodegradation in aerobic granular sludge," *Bioresource Technology*, vol. 315, Article ID 123806, 2020.

[147] Z. Derakhshan, A. H. Mahvi, M. T. Ghaneian et al., "Simultaneous removal of atrazine and organic matter from wastewater using anaerobic moving bed biofilm reactor: a performance analysis," *Journal of Environmental Management*, vol. 209, pp. 515–524, 2018.

[148] B. Hassanpour, L. D. Geohring, A. R. Klein, S. Giri, L. Aristilde, and T. S. Steenhuis, "Application of denitrifying bioreactors for the removal of atrazine in agricultural drainage water," *Journal of Environmental Management*, vol. 239, pp. 48–56, 2019.

[149] R. V. Busto, J. Roberts, C. Hunter, A. Escudero, K. Helwig, and L. H. G. Coelho, "Mechanistic and ecotoxicological studies of amoxicillin removal through anaerobic degradation systems," *Ecotoxicology and Environmental Safety*, vol. 192, Article ID 110207, 2020.

[150] Y. Han, L. Yang, X. Chen et al., "Removal of veterinary antibiotics from swine wastewater using anaerobic and aerobic biodegradation," *Science of the Total Environment*, vol. 709, Article ID 136094, 2020.

[151] D. Saidulu, B. Gupta, A. K. Gupta, and P. S. Ghosal, "A review on occurrences, eco-toxic effects, and remediation of emerging contaminants from wastewater: special emphasis on biological treatment based hybrid systems," *Journal of Environmental Chemical Engineering*, vol. 9, no. 4, Article ID 105282, 2021.

[152] C. Grandclément, I. Seyssiecq, A. Piram et al., "From the conventional biological wastewater treatment to hybrid processes, the evaluation of organic micropollutant removal: a review," *Water Research*, vol. 111, pp. 297–317, 2017.

[153] L. García, J. C. Leyva-Díaz, E. Díaz, and S. Ordóñez, "A review of the adsorption-biological hybrid processes for the abatement of emerging pollutants: removal efficiencies, physicochemical analysis, and economic evaluation," *Science of the Total Environment*, vol. 780, Article ID 146554, 2021.

[154] Y. Jiang, S. Chowdhury, and R. Balasubramanian, "Efficient removal of bisphenol A and disinfection of waterborne pathogens by boron/nitrogen codoped graphene aerogels via the synergy of adsorption and photocatalysis under visible light," *Journal of Environmental Chemical Engineering*, vol. 8, no. 5, Article ID 104300, 2020.

[155] A. Aldeguer Esquerdo, I. Sentana Gadea, P. J. Varo Galvañ, D. Prats Rico, and D. P. Rico, "Efficacy of atrazine pesticide reduction in aqueous solution using activated carbon, ozone and a combination of both," *Science of the Total Environment*, vol. 764, Article ID 144301, 2021.

[156] R. Guo, X. Xie, and J. Chen, "The degradation of antibiotic amoxicillin in the fenton-activated sludge combined

system," *Environmental Technology*, vol. 36, no. 7, pp. 844–851, 2014.

[157] M. Iborra-clar, E. Ferrer-polonio, I. Alcaina-miranda, and A. Mendoza-roca, "Removal of pharmaceutical compounds commonly-found in wastewater through a hybrid biological and adsorption process," *Journal of Environmental Management*, vol. 263, Article ID 110368, 2020.

[158] Q. Zhang, Z. Zhu, X. Zhao, X. Xiao, X. Zuo, and J. Nan, "Efficient and effective removal of emerging contaminants through the parallel coupling of rapid adsorption and photocatalytic degradation: a case study of fluoroquinolones," *Chemosphere*, vol. 280, Article ID 130770, 2021.

[159] L. Luo, Y. Yang, M. Xiao et al., "A novel biotemplated synthesis of TiO_2/wood charcoal composites for synergistic removal of bisphenol A by adsorption and photocatalytic degradation," *Chemical Engineering Journal*, vol. 262, pp. 1275–1283, 2015.

[160] T. Wang, P. D. Dissanayake, M. Sun et al., "Adsorption and visible-light photocatalytic degradation of organic pollutants by functionalized biochar: role of iodine doping and reactive species," *Environmental Research*, vol. 197, Article ID 111026, 2021.

[161] H. Bouyarmane, C. El Bekkali, J. Labrag et al., "Photocatalytic degradation of emerging antibiotic pollutants in waters by TiO_2/Hydroxyapatite nanocomposite materials," *Surfaces and Interfaces*, vol. 24, Article ID 101155, 2021.

Hindawi
Journal of Chemistry
Volume 2021, Article ID 4660423, 18 pages
https://doi.org/10.1155/2021/4660423

Research Article

Investigation of Fe-Doped Graphitic Carbon Nitride-Silver Tungstate as a Ternary Visible Light Active Photocatalyst

Eid H. Alosaimi,[1] Nadia Azeem,[2] Noor Tahir,[2] Asim Jilani,[3] Muhammad Zahid,[2] Salman. S. Alharthi,[4] Javed Iqbal,[2] Muhammad Yaseen,[5] Zulfiqar Ahmad Rehan,[6] and Imran Shahid[7]

[1]*Department of Chemistry, College of Science, University of Bisha, P.O. Box 511, Bisha 61922, Saudi Arabia*
[2]*Department of Chemistry, University of Agriculture, Faisalabad 38040, Pakistan*
[3]*Center of Nanotechnology, King Abdulaziz University, Jeddah, Saudi Arabia*
[4]*Department of Chemistry, College of Science, Taif University, P.O. Box 11099, Taif 21944, Saudi Arabia*
[5]*Department of Physics, University of Agriculture Faisalabad, Faisalabad, Pakistan*
[6]*Department of Polymer Engineering, National Textile University Faisalabad, Pakistan*
[7]*Environmental Science Centre, Qatar University, Doha, P.O. Box 2713, Qatar*

Correspondence should be addressed to Muhammad Zahid; rmzahid@uaf.edu.pk and Zulfiqar Ahmad Rehan; zarehan@ntu.edu.pk

Received 3 August 2021; Accepted 13 October 2021; Published 15 November 2021

Academic Editor: Marcelino Maneiro

The rapid population growth and economic development have largely contributed to environmental pollution. Various advanced oxidation processes have been used as the most viable solution for the reduction of recalcitrant pollutants and wastewater treatment. Heterogeneous photocatalysis is one of the broadly used technologies for wastewater treatment among all advanced oxidation processes. Graphitic carbon nitride alone or in combination with various other semiconductor metal oxide materials acts as a competent visible light active photocatalyst for the removal of recalcitrant organic pollutants from wastewater. Rational designing of an environment-friendly photocatalyst through a facile synthetic approach encounters various challenges in photocatalytic technologies dealing with semiconductor metal oxides. Doping in g-C_3N_4 and subsequent coupling with metal oxides have shown remarkable enhancement in the photodegradation activity of g-C_3N_4-based nanocomposites owing to the modulation in g-C_3N_4 bandgap structuring and surface area. In the current study, a novel ternary Fe-doped g-C_3N_4/Ag_2WO_4 visible light active photocatalyst was fabricated through an ultrasonic-assisted facile hydrothermal method. Characterization analysis included SEM analysis, FTIR, XRD, XPS, and UV-Visible techniques to elucidate the morphology and chemical structuring of the as-prepared heterostructure. The bandgap energies were assessed using the Tauc plot. The ternary nanocomposite (Fe-CN-AW) showed increased photodegradation efficiency (97%) within 120 minutes, at optimal conditions of pH = 8, catalyst dose = 50 mg/100 ml, an initial RhB concentration of 10 ppm, and oxidant dose 5 mM under sunlight irradiation. The enhanced photodegradation of rhodamine B dye by ternary Fe-CN-AW was credited to multielectron transfer pathways due to insertion of a Fe dopant in graphitic carbon nitride and subsequent coupling with silver tungstate. The data were statistically assessed by the response surface methodology.

1. Introduction

Water constitutes a major part of the planet Earth. Almost 98% of this water is seawater and cannot be used for drinking purposes because of the high salt content. Approximately 2% of water is drinkable [1]. Extensive contamination due to global industrialization, commercialization, and agricultural practices has led to the release of organic pollutants that immensely polluted the freshwater reservoirs. Hence, water pollution has emerged as one of the foremost global

environmental challenges. Wastewater discharged from industries and various human activities has caused perilous environmental impacts. An alarming population is suffering every day due to the unavailability of clean drinking water. This gross negligence from various industrial units for releasing wastewater without any treatment into freshwater streams has posed grave threats to human health [2].

Previously, conventional methods such as activated carbon adsorption, filtration, extraction, oxidation, ultrafiltration, electrolysis, chemical oxidation, and biological treatment were used which usually caused incomplete mineralization of pollutants. The shortcomings of these conventional methods were overcome with progressive research in the development of various advanced oxidation technologies. Advanced oxidation processes (AOPs) were firstly utilized in the early 1980s for water treatment and purification. In wastewater treatment, hydroxyl radicals act as strong oxidizing agents, breaking down complex organic pollutants and converting them into less harmful products [3]. Advanced oxidation processes include ozone, Fenton, heterogeneous photocatalysis, sonolysis, catalytic wet air oxidation, and electrochemical oxidation. Sometimes, these processes can combine to produce strong oxidizing radicals that attack any pollutant in the water without distinction and convert them into nonharmful compounds such as carbon dioxide, water, and inorganic ions. AOPs can make use of different semiconductor photocatalysts such as binary or ternary metal oxides and carbon-based support materials [4].

Heterogeneous photocatalysis based on metal-oxide-based semiconductor materials has been employed widely for the degradation of recalcitrant pollutants. Among these conventional semiconductor materials, a new carbon-based photocatalyst graphitic carbon nitride (g-C_3N_4) is being investigated for the fabrication of heterostructures for enhanced degradation under sunlight irradiation. Graphitic carbon nitride is an excellent visible light active and two-dimensional polymeric compound that is highly stable chemically and thermally and has a tunable bandgap from 1.7 eV to 2.8 eV [5]. The medium bandgap range of g-C_3N_4, its chemical and thermal stability, polymeric structure, and simple synthesis methods make it an excellent visible light active photocatalyst and a good semiconductor material for the conversion of solar energy [6]. But, the catalytic performance of g-C_3N_4 alone is hindered because of some limitations such as fast charge carrier recombination [7]. The limitations due to fast e^-/h^+ recombination of g-C_3N_4-based photocatalysts can be addressed using various strategies including doping and coupling with metal oxides [8]. The photoresponse of g-C_3N_4 can be enhanced through doping various transition metals including Fe, Mn, Cu. Co, Ni, and Mo and coupling with other metal oxides to enhance visible light response [9]. g-C_3N_4 support-based photocatalysts are now frequently used in various applications of heterogeneous photocatalysis because these photocatalysts profoundly satisfy environmental requirements of green photocatalysis and the formation of hybrid structures [10]. Doping of a transition metal in g-C_3N_4 lattices alters the physical and chemical properties and enhances the visible light absorption response for degradation of pollutants by changing the structure and surface area of g-C_3N_4 [11]. Iron (Fe) has proved to be an excellent candidate for doping with graphitic carbon nitride because of its existence in various oxidation states. Insertion of Fe into g-C_3N_4 has shown enhancement in electrochemical conductivity and light absorption ability [12]. Silver tungstate (Ag_2WO_4) is a ternary semiconductor metal oxide having a bandgap between 2.8 eV and 3.1 eV. This ternary metal oxide has been gaining attention because of its better light-harvesting ability and photoluminescence characteristics. Silver tungstate (AW) is functionalized by coupling with other photoactive materials to increase the photoresponse and improve its stability [13].

Hence, it is the necessity of time to synthesise such visible light-reactive ternary systems that are more efficient than those utilized in conventional methods for wastewater remediation. This work was proposed for the investigation of rhodamine B (RhB) dye degradation by ternary Fe-doped g-C_3N_4/Ag_2WO_4 nanocomposite. To the best of our knowledge, this composite has not been studied earlier for the photodegradation of organic pollutants. Iron-doped graphitic carbon nitride was coupled with silver tungstate in which WO_4 has attracted attention due to high chemical and thermal stability and has reasonable electron transfer behavior. g-C_3N_4 and WO_4 have almost similar bandgaps [14]. The degradation of rhodamine B (RhB) dye was analyzed over Fe/g-C_3N_4 (Fe–CN), g-C_3N_4/Ag_2WO_4 (CN-AW), and Fe-doped g-C_3N_4 -Ag_2WO_4/(Fe-CN-AW). The photocatalytic activity of these three catalysts towards RhB degradation was studied under sunlight. The effect of various parameters, for example, pH, oxidant dose, irradiation time, and catalyst dose, was optimized. The interaction of various parameters was studied using the response surface methodology (RSM). The catalysts were characterized by Fourier transform infrared spectroscopy (FTIR), scanning electron microscopy, X-ray diffraction (XRD), XPS, and UV-Vis techniques.

2. Experimental

2.1. Regents and Materials. Melamine ($C_6H_6N_6 > 99\%$) and silver nitrate ($AgNO_3$; 99.9% purity) were purchased from DAEJUNG, sodium tungstate dihydrate ($Na_2WO_4.2H_2O$; 97% purity) and ethanol (C_2H_5OH; 95.6% purity) were purchased from UNI-Chem, ferric chloride hexahydrate ($FeCl_3.6H_2O$; ˃ 99% purity) and hydrogen peroxide (H_2O_2; 35% purity) were purchased from Merck, sodium hydroxide (NaOH; 98–100.5% purity) and hydrochloric acid (HCl; 35% purity) were purchased from Sigma-Aldrich, and rhodamine B ($C_{28}H_{31}ClN_2O_3$; 92% purity) was purchased from PubChem. Analytical-grade chemicals and solvents were used in all experiments without additional purification. During the whole experimental study, distilled water was utilized.

2.2. Synthesis of g-C_3N_4. Synthesis of g-C_3N_4 was carried out in a muffle furnace (AB UMEGA SNOL-3/1100) by condensation of melamine. The 5 g mass of melamine was measured and placed in a ceramic crucible, covered

completely, and then, placed in a muffle furnace. Melamine was heated at 20°C per minute for about 2 hours, and the temperature gradually rose until it reached the final temperature. The terminal temperatures were 500°C, 550°C, and 600°C. Then, crucibles containing the sample were chilled to 25°C temperature, and the product formed was ground by using a pestle and mortar [15].

2.3. Synthesis of CN-AW. To prepare the Ag_2WO_4/g-C_3N_4 composite, sodium tungstate (0.1 mmol/L) and silver nitrate (0.2 mmol) were added to 40 ml deionized H_2O. To the abovementioned mixture, 1 g of previously prepared g-C_3N_4 was added. Then, the whole mixture was sonicated to get a homogenous solution at a temperature of 20°C for about half an hour. This uniform mixture was gradually poured into a 50 ml capacity autoclave having a Teflon-line. After transferring the mixture into the autoclave, it was heated at 180°C for 12 hours in an electric oven. After that, it was filtered and cleaned with distilled H_2O until its pH became neutral. It was dried at 60°C for 5 hours after filtration to obtain the final product, as shown in Figure 1(b) [16].

2.4. Synthesis of Fe-CN. Iron-doped graphitic carbon nitride (Fe–CN) was synthesised by a simple process in which 0.5 M ($FeCl_3$. $6H_2O$) was mixed in 50 ml ethanol. Then, 0.5 g of graphitic carbon nitride was dissolved into the abovementioned solution with constant stirring and stirred magnetically for two hours at room temperature. The suspension obtained after stirring was then centrifuged at 6000 revolutions per minute for fifteen minutes, and distilled water, as well as acetone, was used to wash it several times until it became neutral. Then, it was dried at room temperature, as shown in Figure 1(c) [17].2.5. Hydrothermal Synthesis of Ternary Fe-CN-AW.

A hydrothermal method was used for the synthesis of the ternary iron-doped graphitic carbon nitride/silver tungstate (Fe-CN-AW) nanocomposite. In the first step, 2.5 mmol (0.28 g) of sodium tungstate ($Na_2WO_4.2H_2O$) was dissolved completely in 40 ml distilled water with magnetic stirring. Another solution was made in which 5 mmol (0.29 g) of $AgNO_3$ was added to 20 ml of distilled H_2O. Both solutions were mixed slowly under continuous stirring. The previously prepared Fe-doped graphitic carbon nitride (2 mol %) was ultrasonically dispersed in 30 ml of distilled water and added to solution A dropwise. After that, the whole suspension was stirred magnetically for four hours at 25°C temperature till a uniform solution was obtained. The resultant mixture was transferred into an autoclave reactor lined with Teflon at an elevated temperature of 180°C for about 24 hours. The final product was rinsed three times with ethanol and distilled water. Employing an electric oven, the sample was later dried for about 12 hours at 60°C. Figure 1(d) explains the stepwise synthesis of ternary Fe-CNAW heterojunction.

2.5. Characterization and Equipment. The phase identification, crystalline nature, and crystal structure of Fe–CN, CN-AW, and ternary Fe-doped CN-AW were analyzed by powder XRD (XRD-PANalytical-Xpert pro DY 3805) containing a Ni-β filter and Cu-Kα radiations (1.54059 Å), over a range from 10°to 80° of 2θ values. The identification of various functional groups was recorded using an FTIR spectrophotometer (Agilent Technologies) in the transmission mode, between 650 $cm^{-1}$and 4000 cm^{-1}. A scanning electron microscope (SEM-JEOL/EO Japan JSM-5910) was used for observing the morphology of all samples. The surface chemical states were analyzed using XPS (XPS system Escalab 250, Thermo Scientific Uk). The optical and photocatalytic properties of doped and undoped nanocomposites were analyzed utilizing a double-beam UV-Vis (Cecil CE 7200) spectrophotometer.

2.6. Photocatalytic Degradation Evaluation. The photocatalytic degradation of rhodamine B dye was estimated under UV and sunlight irradiation. Different feasibility experiments were initially performed to check the activity of the ternary photocatalyst. For attaining a stage of adsorption-desorption equilibrium between the catalyst surface and pollutant molecule, the RhB solution was placed for about half an hour in the dark with continuous stirring on an orbital shaker. The adsorption was measured by taking 5 ml solution and taking absorbance. The adsorption rate usually starts decreasing after 30 minutes. The whole setup was then brought under sunlight irradiation, and the photodegradation process was started. Similar experiments were performed under ultraviolet radiation as well. Optimization of various parameters for RhB degradation was performed, including pH (2–9), initial RhB concentration (10–50 ppm), oxidant dose (2–15 mM), catalyst dose (10–100 mg), and time of irradiation (20–120 minutes). A UV-Vis spectrophotometer was used to check absorbance at 554 nm by taking a 10 ml clear RhB solution obtained after separation of the composite through centrifugation. The degradation process was also studied in the absence of light by placing a beaker of dye solution in the dark. The blank experiment performed without a catalyst and light revealed no distinct photocatalytic activity, signifying that the reaction was driven by the photocatalytic process over the photocatalytic process of light. The following formula was used to calculate % degradation:

$$\%\ \text{degradation} = 1 - \frac{A}{Ao} \times 100, \tag{1}$$

where Ao is described as the initial absorbance and A is the calculated final absorbance after a performed reaction in sunlight. A light meter (HS1010 A) and solar power meter (SM206) were used for measuring the brightness and intensity of sunlight. The measured average light intensity was 1200 W/m^2, and the brightness was measured between the range of 88,000 ± 2000 Lux. The degradation reaction was carried out in the afternoon when the sky was bright and clear. The intensity of the UV light was 254 nm, and the experiment was performed in a UV chamber ZM144 (ZAM ZAM Microtechnologies). The catalyst's reusability was examined by recycling ternary composites by washing with distilled water, drying, and then, reusing till five cycles under sunlight, each at their optimum conditions with 10 ppm RhB solution prepared fresh each time.

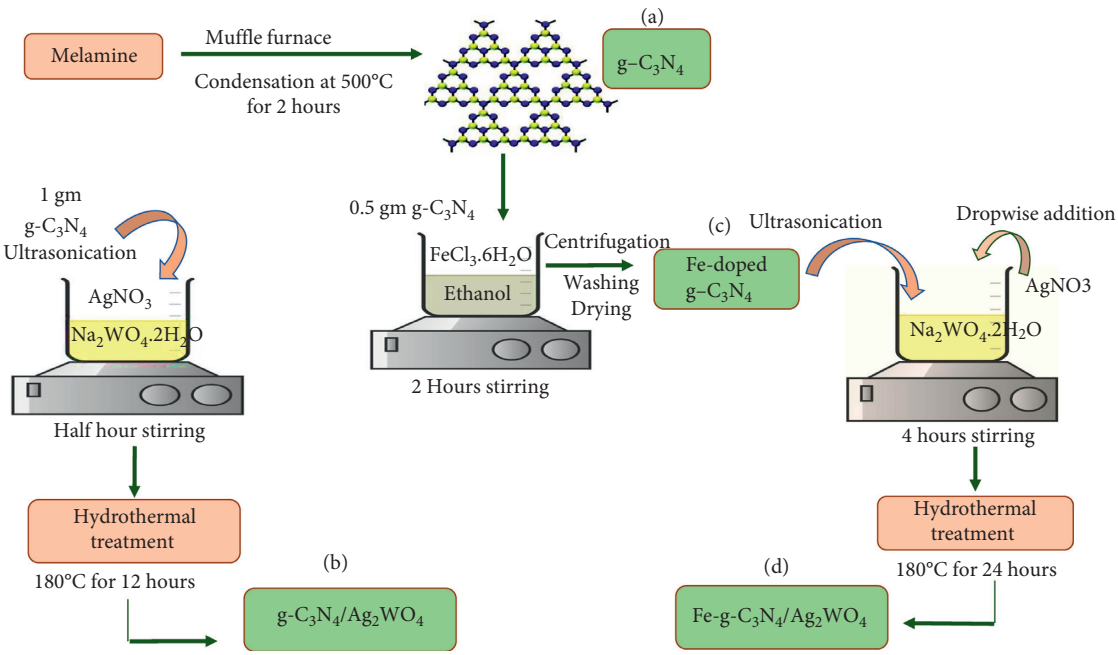

Figure 1: Schematic illustration of (a) g-C_3N_4, (b) g-C_3N_4-Ag_2WO_4, (c) Fe-g-C_3N_4, and (d) Fe-g-C_3N_4/Ag_2WO_4 heterojunctions.

3. Results and Discussion

3.1. FTIR Analysis. The FTIR analysis was recorded between the range of 500 cm^{-1} and 4500 cm^{-1} for the determination of various functional groups present on the surface of the ternary composite. Graphitic carbon nitride was synthesised under varying temperature conditions. FTIR spectra showed all the characteristic transmittance peaks of g-C_3N_4 confirming the synthesis of graphitic carbon nitride, without any prominent change at different temperatures, as shown in Figure 2(f). The broad absorption band of pristine g-C_3N_4 can be seen in all the samples synthesised at various temperatures. The bands beyond 3000 cm^{-1} up to 3300 cm^{-1} are due to N–H bond stretching vibration resulting from partial condensation of amino acids. The series of peaks appearing between 1200 cm^{-1} and 1620 cm^{-1} shows the stretching vibrations of CN heterocycles. At 500°C, two bands were seen at 1598 cm^{-1} and 1395 cm^{-1}. The peaks at 1228 cm^{-1} and 1395 cm^{-1} matched well with g-C_3N_4. At 550°C in the spectrum, N-H stretching vibration was observed by a peak at 3151 cm^{-1} while the vibration bands from 1200 cm^{-1} and 1800 cm^{-1} are related to g-C_3N_4. The spectrum corresponds to 550°C and at 15°C/min has bands in the range from 1300 cm^{-1} to 1828 cm^{-1}, representing vibrations of C-N bonds. The FTIR spectrum of Fe-CN, CN-AW, and Fe-CN-AW was compared and shown in Figures 2(c)–2(e), respectively. In the Fe-CN spectrum, a broad peak appeared at 3078 cm^{-1} which is a distinctive peak of the N-H group. It is due to the vibrational mode of the residual N-H group of graphitic carbon nitride. The vibrational mode of the C-N band was shown by a range of peaks from 1200 cm^{-1} to 1600 cm^{-1}. The peaks appearing at 1234 cm^{-1}, 1385 cm^{-1}, and 1578 cm^{-1} related to the CN heterocycles corresponding to C-NH-C, C-N, and C=N confirm fabrication of graphitic carbon nitride in all samples [18]. A small additional peak at 2145 cm^{-1} indicates the Fe^{3+} dopant's existence in a polymeric network of g-C_3N_4 [19]. A peak near 807 cm^{-1} shows the occurrence of a triazine ring of aromatic nature. The prominent and distinctive g-C_3N_4 bands seem to shift towards lower wavenumbers, and the intensity of FTIR spectra peaks is decreased in the Fe-CN-AW composite. This shift indicates the weakening of C–N and C=N as a result of interaction between g-C_3N_4 and Fe [17]. In the CN-AW composite spectrum, a broad peak was presented at 3153 cm^{-1} which is owing to the N-H band stretching mode [20]. The peak at 2381 cm^{-1} is owed to amide linkages, and carbonyl group presence is represented by a peak at 1600 cm^{-1} [21]. There is a range of peaks from 1200 cm^{-1} to 1600 cm^{-1} similar to the Fe-CN spectrum which is due to the IR active vibrational mode of the C-N bond. Two peaks at 739 cm^{-1} and 630 cm^{-1} show O-W-O and W-O-W groups that are a special feature of tetrahedral tungstates. All the peaks present in pure g-C_3N_4 remain intact in ternary the Fe-g-C_3N_4/Ag_2WO_4 composite.

3.2. XRD Analysis. To determine the various phases and crystal structure of CN, Fe-CN, CN-AW, and Fe-CN-AW, XRD characterization was performed from 2θ values 10° to 80°. The XRD spectra reveal peaks at 27.7° which are in agreement with the actual XRD peaks of g-C_3N_4 (JCPDS-87-1526) [22]. The diffraction peak at 27.7° indexed to the (002) plane is a characteristic of g-C_3N_4, showing stacking of aromatic systems between g-C_3N_4 layers [23]. The XRD pattern of Fe–CN exhibited no significant difference from CN except for a slight shift and gradual decrease in the peak

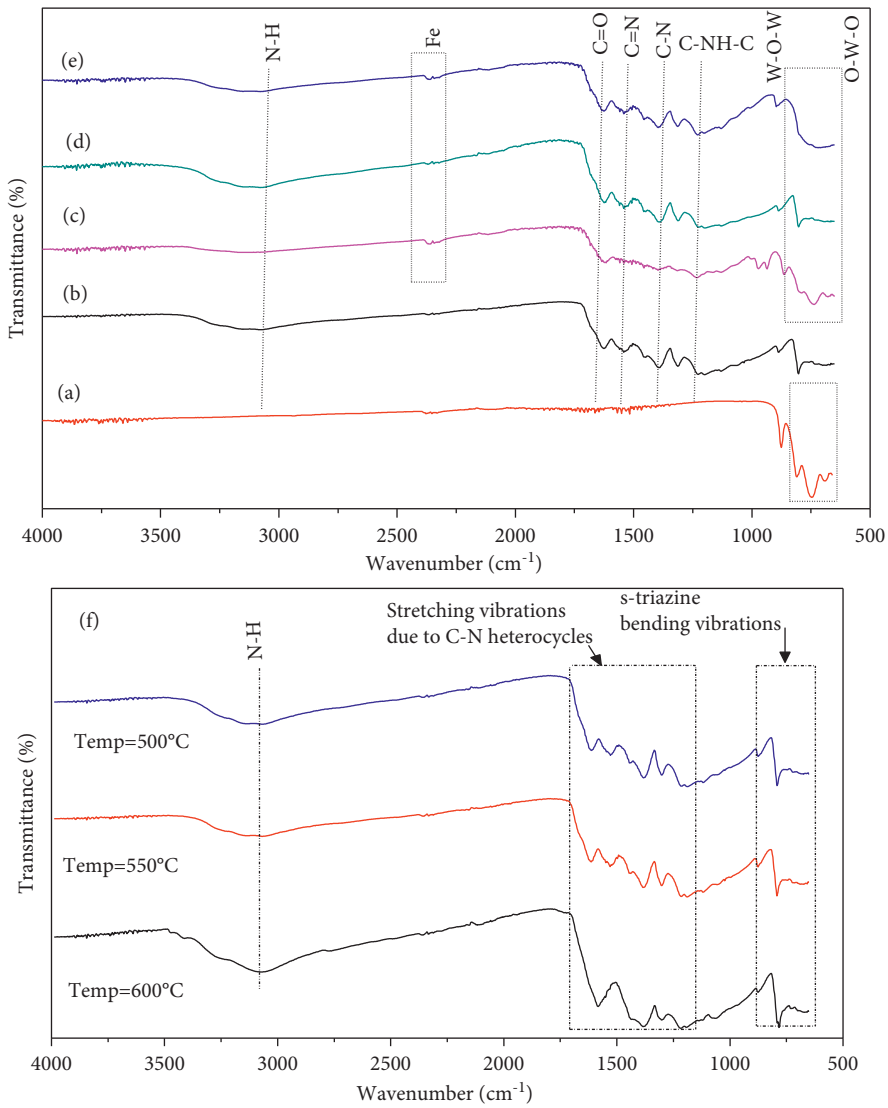

Figure 2: FTIR spectra of (a) AW, (b) g-C_3N_4, (c) Fe–CN, (d) CN-AW, (e) Fe-CN-AW, and (f) g-C_3N_4 at various annealing temperatures.

intensity of the (002) facet in Fe-CN, AW-CN, and Fe-CN-AW. The incorporation of an iron dopant in CN did not change the g-C_3N_4 crystal structure, as no peak of Fe was identified in the samples [19]. The diffraction peaks of g-C_3N_4 remain intact which shows that the doping of iron does not change the peaks of g-C_3N_4 but the intensity of the peaks in the final composite is reduced, confirming effective insertion of the dopant [24]. The XRD data displayed well-defined diffraction peaks consistent with planes (301), (002), (231), (400), (402), (233), (460), and (462), observed at 2θ values 28.4°, 30.58°, 31.67°, 32.88°, 45.4°, 54.9°, 56.9, and 58.04°, respectively, as shown in Figure 3, and are coherent with the corresponding planes of Ag_2WO_4 (JCPDS# 34–0061) [13]. All the characteristic peaks of g-C_3N_4 and Ag_2WO_4 are present in the Fe-doped ternary composite but with lesser intensities than the undoped CN-AW and Fe-CN composites. However, the strong intensity of diffraction peaks in both the composites suggests the successful synthesis and crystalline nature of composites [25]. There is also a very slight shift of the peak at a diffraction angle of $2\theta = 45.3°$, corresponding to a plane (402) towards higher diffraction angles, indicating the insertion of Fe into the host composite lattice. X-ray diffraction is an effective analysis technique to determine the size of nanocrystallites in bulk nanocrystalline materials. The average crystallite size of Fe-doped CN-AW, undoped CN-AW, and Fe-CN catalysts was assessed using the Debye–Scherrer formula.

$$D = \frac{K\lambda}{\beta \cos\theta}, \tag{2}$$

where K is the Scherrer constant (0.94), β explains the full width at half maximum (FWHM) of each diffraction peak, θ is the angle of diffraction, λ is the radiation wavelength, and D is the average crystallite size in nm. The average crystallite size of Fe-CN, CN-AW, and Fe-CN-AW was calculated to be

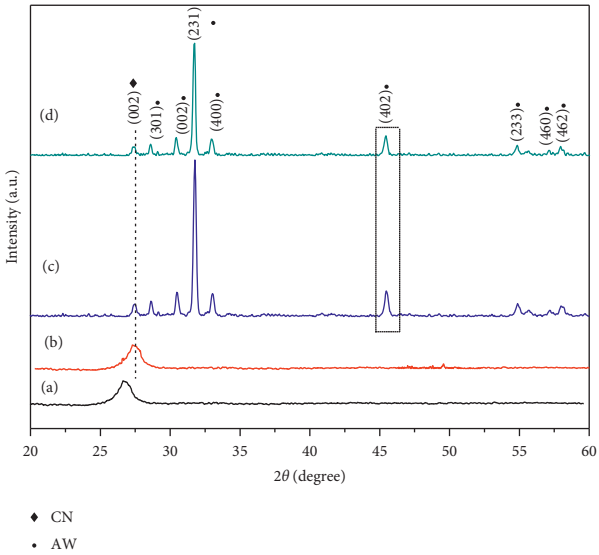

Figure 3: XRD spectra of (a) CN, (b) Fe-CN, (c) CN-AW, and (d) Fe-CN-AW.

19.78 nm, 14.29 nm, and 13.34 nm, respectively. The decreased crystallite size indicates the presence of oxygen vacancies as a result of Fe doping which hinders the further growth of nanoparticles [26]. The defects caused by Fe doping reduce recombination chances of charge carriers and enhance photocatalytic activity [27].

3.3. Scanning Electron Microscopy (SEM) Analysis. The SEM analysis was used to study the morphology of Fe-g-C_3N_4, AW-CN, and Fe-CN-AW nanocomposites at different resolutions. Figures (4(a) and 4(b)) show the morphology of Fe-CN, revealing uniform and smooth sheets of g-C_3N_4 and aggregation of particles as an outcome of Fe doping on g-C_3N_4 sheets. In Figures (4(c) and 4(d)), it can be seen that Ag_2WO_4 is dispersed irregularly in the form of small spherical particles on the surface of g-C_3N_4 sheets. The coupling of AW and g-C_3N_4 reveals that the coupling has not affected the morphology of AW spheres. Instead, the g-C_3N_4 aggregates got attached to the surface of silver tungstate. These particles have smooth particle size distribution when present in the form of nonagglomerated particles. The g-C_3N_4 serves as a support on which Ag_2WO_4 particles are embedded. Figures 4(e) and 4(f) signify the coupling between Fe-CN and AW in the ternary composite. These SEM images illustrate those agglomerates of Fe-CN were successfully anchored over AW. In the presence of Fe, the agglomeration and stacking of particles were enhanced as compared to simple AW-CN. Similar results of doping and coupling were also reported in previous studies [28].

3.4. XPS Analysis. The surface chemical composition and chemical binding states of all the photocatalytic samples were analyzed using XPS analysis. The elemental composition of the Fe-CN-AW nanocomposite examined through an XPS survey scan reveals the presence of peaks at Ag3d (368.3 eV), W (37.51 eV), O1s (530.2 eV), C1s (284.07 eV), Fe (710.8 eV), and N1s (396.21 eV), as shown in Figure 5(a). The C1s peak position indexed at 285.2 eV in all three samples indicates the presence of adventitious residual carbon and is ascribed to the tertiary carbon N=C-N_2 in the Fe-g-C_3N_4 lattice. The N1s peak present at 396.21 eV is credited to the triazine rings of g-C_3N_4 and the uncondensed terminal amino groups [20]. The W4$f_{7/2}$ and W 4$f_{5/2}$ peaks at 35.44 eV and 37.5 eV, respectively, in the W4f spectrum of Ag_2WO_4 are ascribed to WO_4^{2-}. The Ag 3d spectra show two characteristic peaks at 372.1 eV and 368.3 eV which are typically allotted to Ag 3$d_{3/2}$ and Ag3$d_{5/2}$, respectively. The peaks of Ag3d and W4f XPS spectra moved towards the higher binding energies in the Fe-CN-AW. The Fe 2$p_{3/2}$ at a binding energy of 710.8 eV is ascribed to Fe^{3+} ions. The binding energy of 710.8 eV lies inside the binding energy range of the Fe^{3+} valence state (710–711.8 eV). The Fe 2$p_{1/2}$ showed a characteristic peak of Fe^{3+} at 731.54 eV [19]. The atomic percentage of O1s, N1s, C1s, Ag3p3, Ag3d, W4f, and Fe2p3 in Fe-CN-AW is 30.3%, 22.2%, 13.3%, 13.2%, 10.1%, 7.1%, and 4.3%, respectively, while the atomic percentage of O1s, N1s, C1s, Ag3p3, Ag3d, and W4f in undoped counterpart is 18.9%, 19.4%, 24.3%, 4.6%, 16.0%, 12.8%, and 8.6 atomic percentages, respectively, as shown in Figure 5(b).

In XPS spectra, the O1s peak found at a binding energy of 528.18 eV is ascribed to the chemisorbed water molecules on the surface of the sample. Furthermore, oxygen functional groups were investigated through O1s spectra, as shown in Figure 5(c). The peaks were found around 530.2 ± .05 eV, 531.6 ± .06, and 533.5 ± .04 eV and attributed to the metallic contribution of oxygen ($O_{Metallic}$), carbonyl (C=O), and carboxyl (OH), respectively [29, 30]. However, their contributions varied with the addition of dopants. Therefore, Fe-CN showed a total contribution of $O_{Metallic}$ around 74.85%, while C=O and OH were around 20.93 and 4.23 atomic percentage. The C=O was noticed at around 41.32% and 27.49% for CN-AW and Fe-CN-AW, respectively. Moreover, the contribution of OH was maximum for Fe-CN-AW and was around 22.59%. This increment of OH is also favorable to enhance the photocatalytic activity of g-C_3N_4-based materials [31].

3.5. Optical Analysis. To further understand the optical properties of the prepared nanocomposites, an evaluation of optical response was carried out by taking UV-Vis spectra and then determining the bandgap energies of nanocomposites Fe-CN, CN-AW, and Fe-CN-AW in the range of 200–800 nm. Using the Tauc plot, the absorption edge of the ternary Fe-CN-AW nanocomposite was found in the visible range (2.56 eV), as shown in Figure 6. The Fe-CN-AW exhibited a better light absorption range as related to other composites. Fe doping has shown enhancement in photodegradation upon improved prospect of charge carrier production upon light irradiation, eventually increasing photodegradation. The following formula was used to assess the catalyst's bandgap energies [13]:

$$(\alpha h\nu)^2 = B(h\nu - Eg). \quad (3)$$

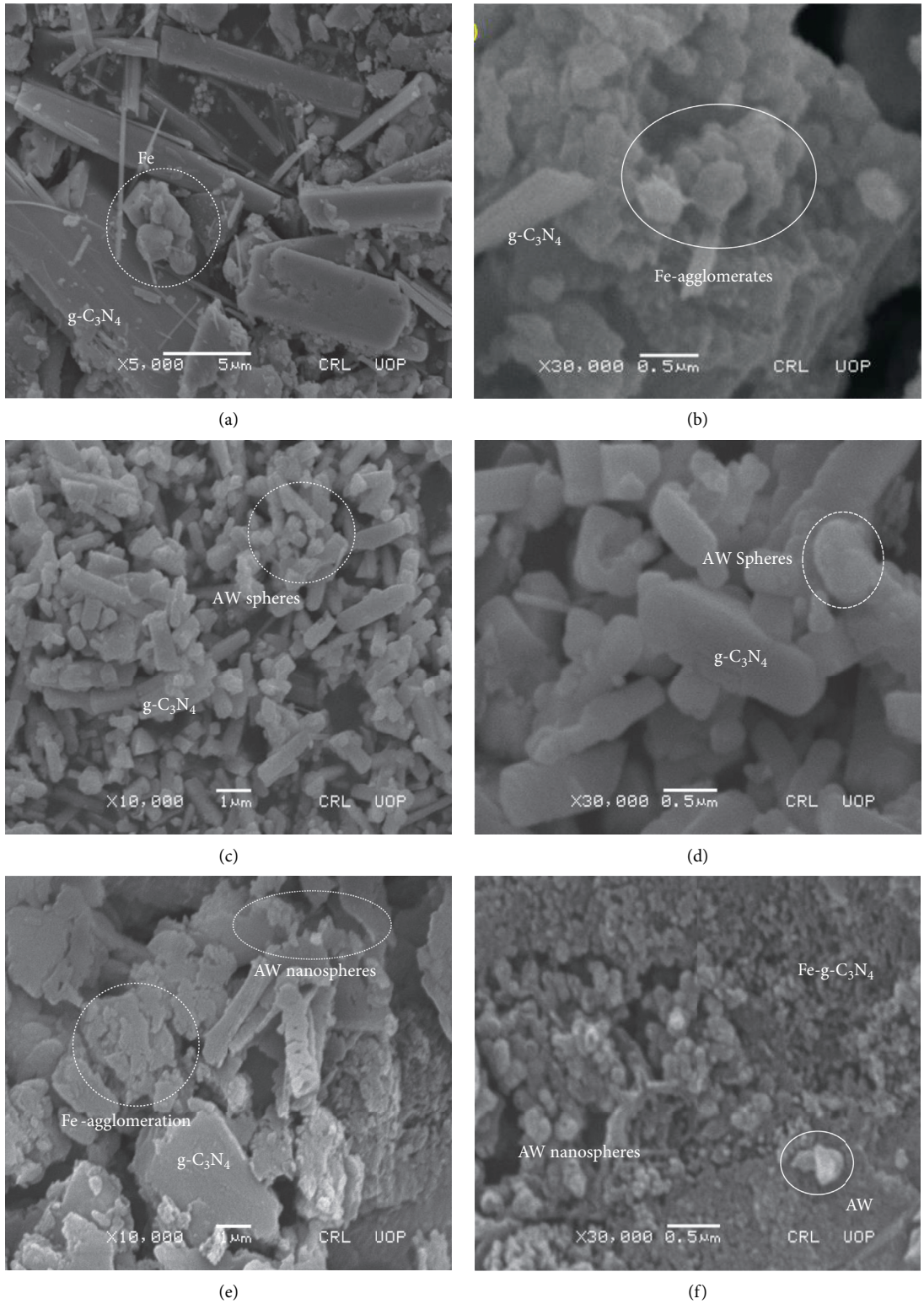

Figure 4: SEM analysis of (a and b) Fe-CN, (c and d) CN-AW, and (e and f) Fe-CN-AW.

In this equation, energy $(E) = h\nu$, at $(\alpha h\nu = 0)$, where $(\alpha h\nu)^2$ is plotted versus energy (eV). At $h\nu$ value, energy is calculated and then extrapolated to $\alpha = 0$. The light frequency, absorption coefficient, and proportionality constant are explained by (α, B, and ν), respectively. The studies reveal that iron doping has strengthened the light absorption response of the ternary photocatalyst in the visible region. The estimated band gap energies were 2.56 eV, 2.8 eV, and 3.3 eV for Fe-CN/AW, Fe-CN, and CN-AW, respectively. The presence of g-C_3N_4 as support

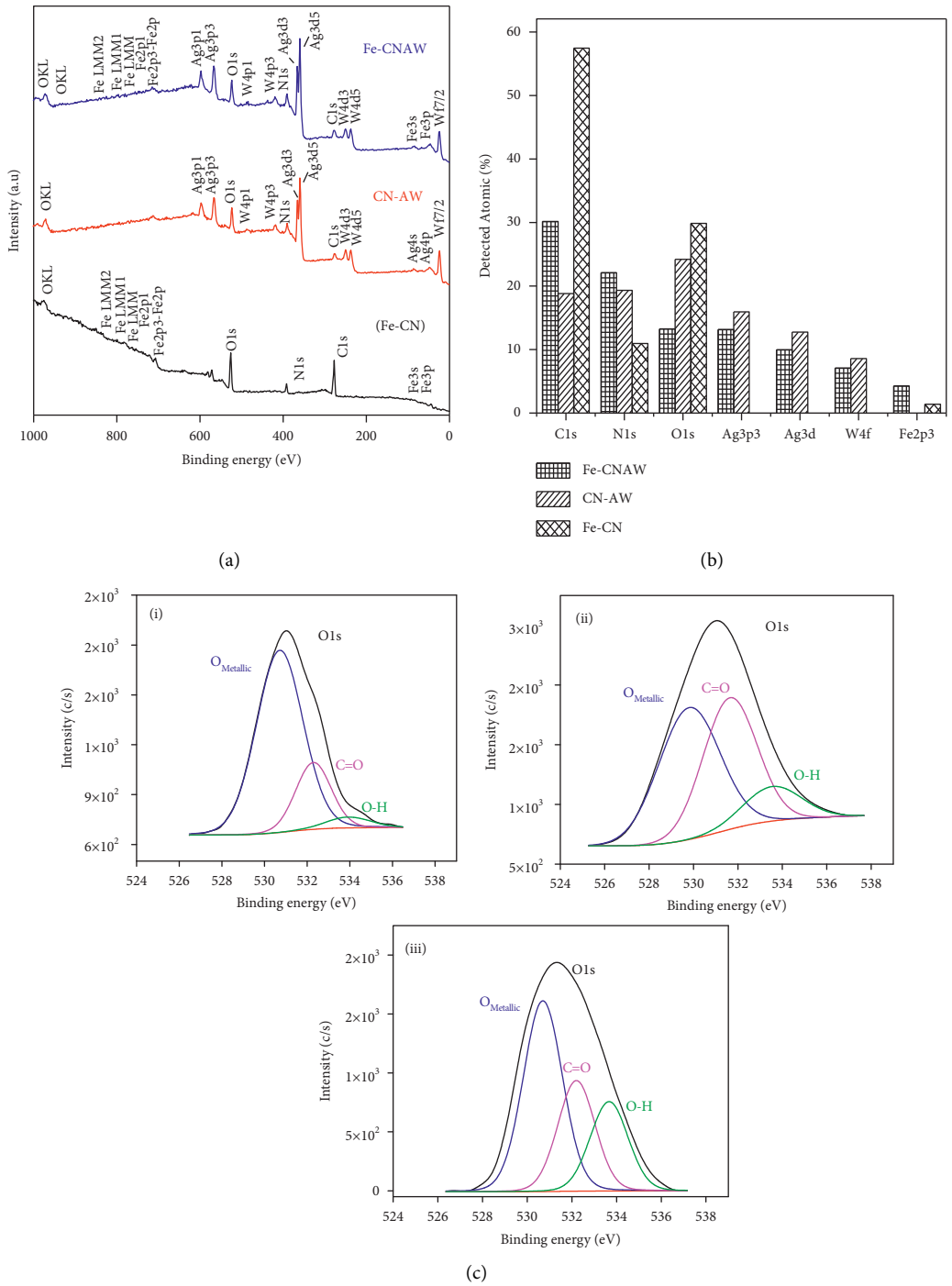

Figure 5: XPS (a) survey spectrum and (b) atomic percentage of various elements in Fe–CN, CN-AW, and Fe-CN-AW; (c) O1s functional groups for (i) Fe–CN, (ii) CN-AW, and (iii) Fe-CN-AW.

narrowed the bandgap of the ternary composite, suggesting efficient separation of charge carriers [23].

4. Operating Parameters Affecting the Photocatalytic Process

The photodegradation process of recalcitrant dyes from the adsorption of molecules of the dye on the photocatalyst's surface to their degradation by reactive radical species is affected by numerous operative parameters. These include pH of the aqueous solution, initial concentration of dyes (IDC), catalyst dose, and intensity of irradiating light sources. These parameters will be discussed in detail as they directly affect the photodegradation of dyes in wastewaters.

4.1. Effect of pH. The photoefficiency of any photocatalytic system is determined by the crucial factor of the pH of

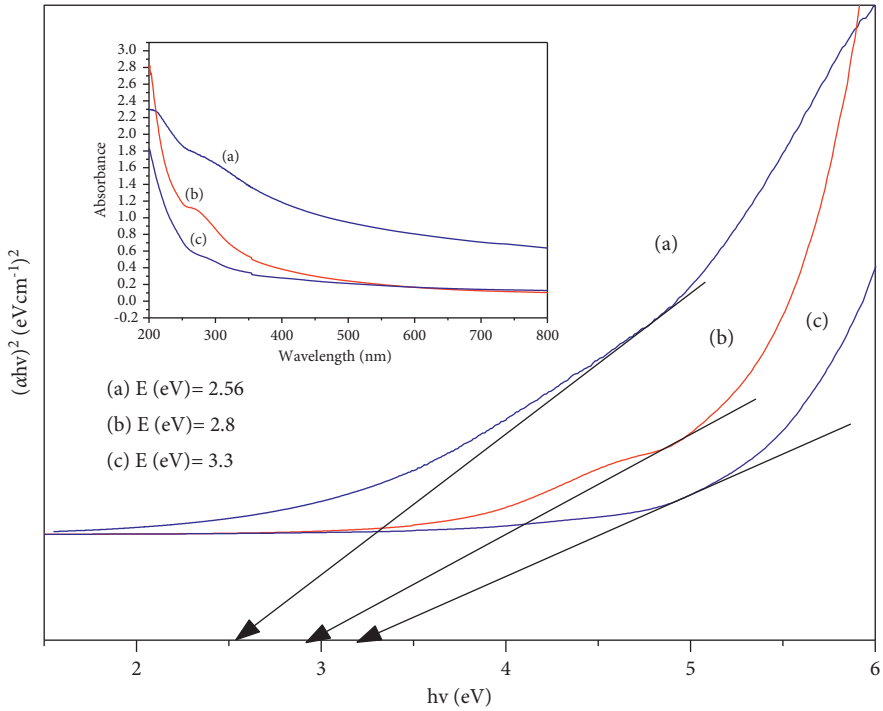

Figure 6: Bandgap energy estimation of (a) Fe-CN/AW, (b) Fe-CN, and (c) CN-AW by the Tauc plot method.

aqueous solutions. The pH of a solution affects not only the photocatalytic degradation process but also the rate at which the dye decolorizes the positive hole (h^+) species formed at lower pH values which act as the key oxidation species, while hydroxyl radicals are the key species at higher or neutral pH values for the degradation process. The surface charge characteristics are determined according to their respective point of zero charges (pH_{PZC}). Acid-base characteristics of photocatalysts significantly impact their degradation efficiencies. At pH < pH_{PZC}, the surface of the catalyst is positively charged, and hence, it develops an electrostatic attraction for anions and repulsion for cations. Contrary to this, at pH > pH_{PZC}, the surface becomes negatively charged and develops an attraction for cations and repulsion for anions [32]. The pH effect on RhB photodegradation was observed by varying pH values. The remaining factors were kept constant in which the catalyst dose was 50 mg/100 mL for doped and 70 mg/100 ml for Fe-CN and CN-AW. IDC was kept at 10 ppm for all composites, and time of irradiation was two hours. Being a cationic dye, upon dissociation in water, RhB is positively charged. The pHPZC of Fe-CN-AW was determined at a pH value of 6.2. The catalyst surface is positively charged at pH values lesser than pHPZC and, hence, repels positively charged RhB molecules. Active sites on the surface of the composite become weaker in an acidic medium, producing fewer hydroxyl radicals, leading to a decline in overall degradation, while active sites existing on the surface exhibited improved production of hydroxyl radicals in the basic medium. Henceforth, at pH values higher than 6.2, the nanocomposite surface becomes negatively charged, attracting positively charged RhB molecules electrostatically, increasing the adhesion property of pollutant molecules on the composite surface [33]. Therefore, in visible light irradiation, nearly 97% degradation by ternary Fe-CN-AW in two hours was observed in a basic medium at an optimum pH of 8, as shown in Figure 7(a). CN-AW and Fe-CN at pH 7 showed nearly 95% and 90% degradation, respectively.

4.2. Effect of Catalyst Concentration. The effectiveness of the photocatalyst for the degradation process is determined by its concentration in the dye solution. To comprehend the relation between catalyst dose and RhB photodegradation, removal of the 10 ppm RhB solution was studied between the range 10 and100 mg/100 ml, while all other parameters such as pH = 8 for Fe-CN-AW and pH = 7 for CN-AW and Fe-CN, catalyst dosage 50 mg/100 ml for doped ternary and 70 mg/100 ml for CN-AW and Fe-CN, and irradiation time 120 minutes remained as such. As the photocatalyst dose was augmented from 10 mg to 50 mg, an intensification in RhB degradation was observed, as shown in Figure 7(b). Fe-CN-AW showed optimum degradation at 50 mg/100 ml, whereas CN-AW and Fe-CN showed maximum degradation at 70 mg/100 ml. This increased degradation is credited to increased active sites on the surface of the catalyst, which then leads to more production of hydroxyl radicals, which increases the process of degradation. However, above the optimum catalyst loading limit for each catalyst, the percentage degradation starts decreasing. This is because of the interference of light by the suspension. The additional amount of catalyst causes aggregation of catalyst particles

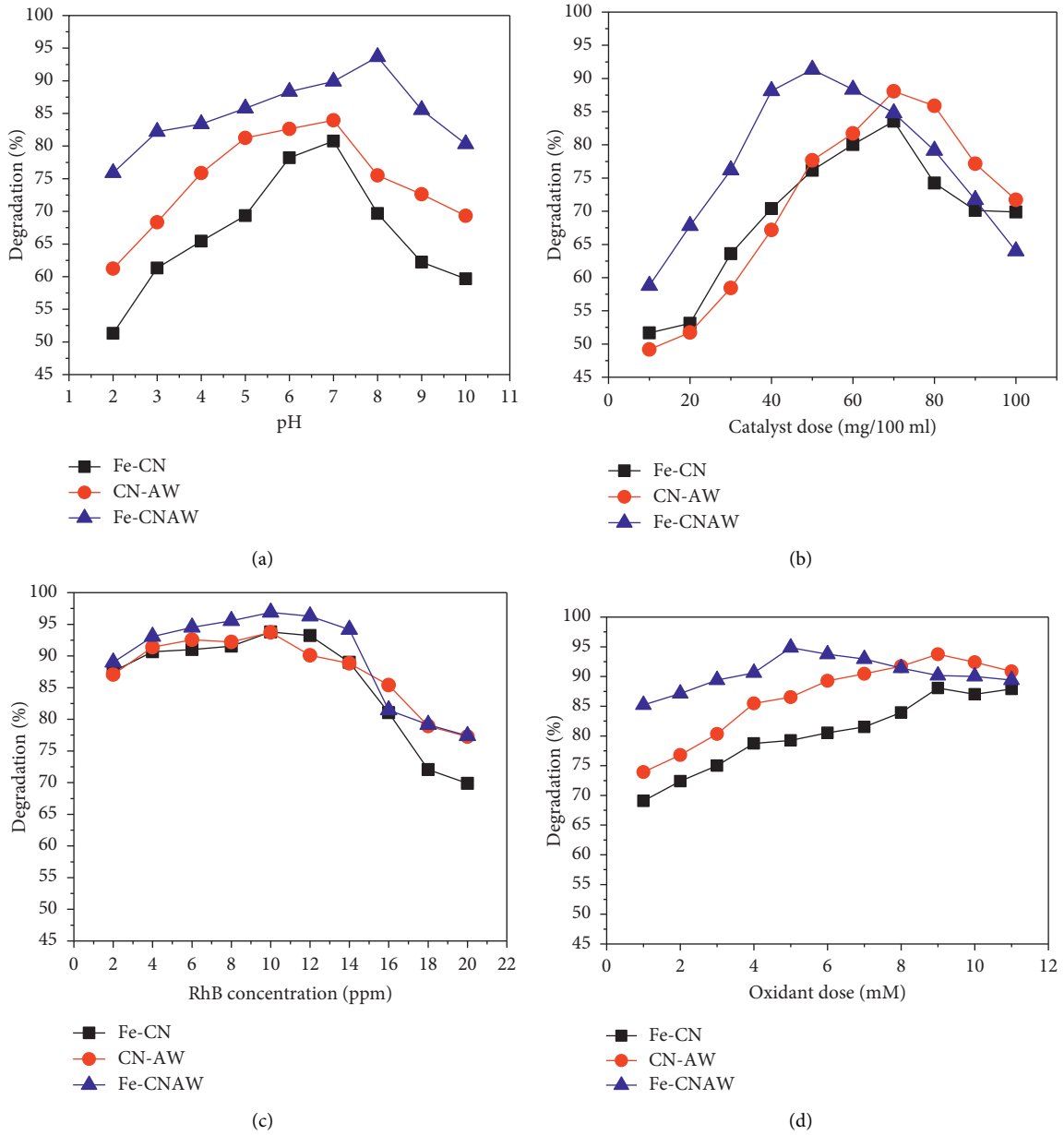

Figure 7: Optimization of reaction parameters using Fe-CN, CN-AW, and Fe-CN-AW: (a) pH, (b) photocatalyst dose, (c) RhB Initial concentration, and (d) oxidant dose.

and inhibits the light irradiation and subsequent absorption of photons by the catalyst surface, reducing the hydroxyl production and ultimately reducing degradation [34].

4.3. Effect of Initial Dye Concentration. In the degradation process, the total amount of dye adsorbed on the surface of the photocatalyst plays a key role, not the dye molecules present in the bulk solution. The initial dye concentration is a critical factor for determining the complete adsorption capacity of dye molecules. The degradation efficiency starts decreasing as the concentration of dye is increased, while the amount of photocatalyst used is kept constant. The degradation started decreasing after the concentration of dye was increased, as shown in Figure 7(c). All samples showed maximum degradation at a concentration of 10 ppm, at their optimal values of pH and catalyst dose. The catalyst Fe-CN-AW showed a degradation of 80% up to 14 ppm, after which it started declining. Owing to an increase in the number of dye molecules, more molecules get attached to the photocatalyst surface, resulting in lesser photons reaching the nanocomposite surface [35]. This eventually results in a decline in hydroxyl ion generation and, subsequently, the decolorization process. Previously, reports have revealed

that the dye degradation rate declined as the dye concentration increased. This is because of the reduction in the path length of photons entering the dye solution as the number of dye molecules increases [33].

4.4. Effect of Oxidant Dose. In the process of photodegradation, oxidants (H_2O_2) have an important role because they hinder the recombination of (e^-–h^+) pairs by capturing the electron. Furthermore, OH radicals are generated from the oxidant by the Ag^{+2} and Fe^{2+} ion interaction. Rhodamine B dye is oxidized completely in the presence of an oxidant (H_2O_2) and a catalyst. In sunlight, the degradation of RhB dye was enhanced by its adsorption on the catalyst surface due to high tendencies of formation of oxidizing species. By the coupling of semiconductors with g-C_3N_4 photocatalysts, degradation is also enhanced. The adsorption ability of g-C_3N_4 is enhanced in the presence of an oxidant. At pH = 7, catalyst dose = 70 mg/100 ml, and oxidant dose = 9 mM, the degradation percentage was 88% for Fe/g-C_3N_4, as represented in Figure 7(d). In the case of the Ag_2WO_4/g-C_3N_4 composite at pH = 7, catalyst concentration = 70 mg, and oxidant dose = 9 Mm, maximum degradation occurs which is 93%, while in the case of Fe-CN-AW at pH = 8, catalyst concentration = 50 mg/100 ml, and oxidant dose = 5 mM, the degradation was equal to 97%.

4.5. Effect of Time. Light energy is a primary source for starting any photocatalytic process because it provides the maximum energy. It is, therefore, necessary to ascertain light irradiation conditions for a substantial impact on the photodegradation process. The trend of RhB degradation in solar light with time over Fe-CN-AW, CN-AW, and Fe-CN is shown in Figure 8(a), which shows increased degradation with increasing time. The dye solutions having all these catalysts in their optimal doses and other fixed reaction conditions for each catalyst were exposed to sunlight for around 2 hours. The percentage degradation of the treated dye solution was observed by taking a plot of percent degradation versus time. The solution color disappeared exactly after 40 minutes of exposure to light, and degradation was complete after around 120 minutes of light irradiation using the new ternary Fe-CN-AW, but intensity decline was slow with CN-AW and Fe-CN. The disappearance of solution color signifies that color-imparting chromophores are disintegrating slowly with time. Furthermore, kinetic models were fitted to these data in which first-order kinetic was fitted well.

4.6. Kinetics of Photodegradation Reaction. The first-order kinetic model was applied for RhB photodegradation by the ternary nanocomposite as explained in equation (3).

First-order kinetics:

$$\ln \frac{\mathrm{Co}}{\mathrm{Ct}} = k_1 t. \quad (4)$$

Figure 8(b) displays the linear association among ln (Co/Ct) versus time of reaction; here, Co and C explain the initial and final concentrations. This shows that RhB degradation by the ternary Fe-CN-AW, CN-AW, and Fe–CN follows first-order kinetics. The plot of ln (Co/C) with time is linear. The linear regression slope is equal to the first-order rate constant (k). The higher k values of Fe-CN-AW than binary CN-AW and Fe–CN directs that decolorization by Fe-CN-AW under sunlight is more than that by CN-AW. The R^2 values for first-order reaction for Fe-CN-AW, CN-AW, and Fe-CN-AW suggest that ternary hybrids follow first-order reaction efficiently and doping has accelerated degradation in the presence of sunlight. This explains that Fe-CN-AW exhibits more photoefficiency than other composites. An assessment of correlation coefficients for first-order kinetics is shown in Table 1.

5. Statistical Analysis

The photocatalytic degradation procedure was mostly determined by the widely employed technique RSM which studies the optimization of parameters. In RSM, mathematics is combined with statistics for empirical representation. The purpose of RSM is to optimize photocatalyst response for different parameters to degrade RhB degradation. It works efficiently for experimental studies. It also reduced the noise and expenses of analytical procedures. It minimizes the expenditure of expensive analysis techniques. In the present work, the Fe-CN-AW ternary composite was synthesised by a hydrothermal technique and utilized for RhB degradation. For example, various parameters such as catalyst dose, pH, oxidant dose, and time were optimized by RSM, and absorbance was noted by using a UV-Vis spectrophotometer.

In RSM, for statistical analysis of dye degradation, a central composite design (CCD) was used. According to the CCD, 30 experiments were conducted for the study of the photo-Fenton procedure. Each experimental trial has specific coRhBinations of four elements, e.g., pH, oxidant dose, catalyst dose, and irradiation time. After each experimental trial, percent degradation was calculated and put into a table. Some experimental trials have the same coordination of factors to have the idea of experimental error. Analysis of variance (ANOVA) was used to evaluate the effectiveness of the regression model, as shown in Table 2.

The photodegradation of RhB was optimized using the central composite design (CCD) of the response surface methodology. Among all RSM designs, the CCD method shows high predictability of responses and is the most efficient method for optimizing several variables. The CCD is used for determining the relationship among independent variables and their responses [36].

Based on the results from batch studies, four effective parameters for the degradation of RhB by Fe-CN-AW and their possible interactions were identified using RSM. The pH (2–9), photocatalyst dose (10–80 mg), oxidant dose (2–12 mM), and time (20–180) in minutes were designated as independent variables, and the effect of their interactions was determined using the CCD. The statistical software Design Expert 7 was used for the optimization of parameters. A total of 30 experiments were obtained randomly for

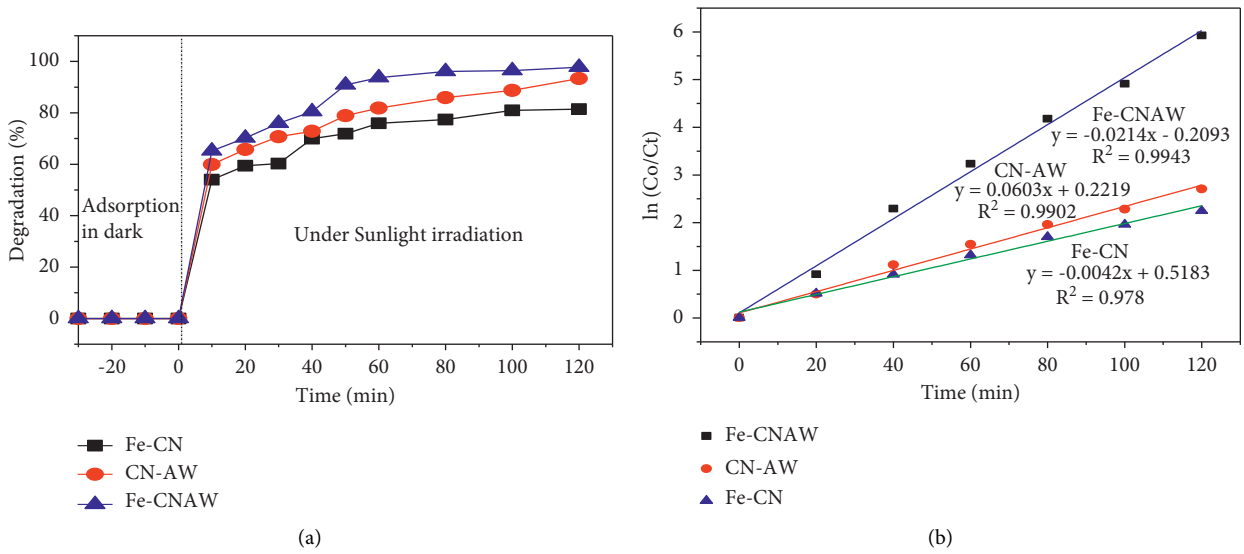

Figure 8: (a) RhB degradation by all catalysts as a function of time under sunlight and (b) first-order kinetic model fitting.

Table 1: Correlation coefficients (R^2) and kinetic parameters for RhB (Co = 10 ppm) degradation.

Nanocomposites	Optimized reaction conditions			First-order kinetics	
	pH	Catalyst load (mg/ml)	IDC (ppm)	$k1$ (min^1)	R^2
Fe-CN-AW	8	50	10	0.0214	0.9943
CN-AW	7	70	10	0.0603	0.9902
Fe–CN	7	70	10	0.004	0.978

studying the optimized parameters and for maximizing RhB photodegradation. The ANOVA (analysis of variance) was used to analyze the effect of all independent variables on the degradation of dye. The response variable (% degradation) was fitted with the quadratic model for corelating with the experimental variables. The predicted and experimental values are tabulated in Table 2. To understand the association of three variables, a second-order polynomial equation was employed. The quadratic regression model for the degradation of MB is represented by equation (3).

$$\begin{aligned} y &= \beta_0 + \beta_1 X_1 + \beta_2 X_2 + \beta_3 X_3 + \beta_4 X_4 + \beta_{12} X_1 X_2 + \beta_{13} X_1 \beta X_3 \\ &\quad + \beta_{14} X_1 \beta X_4 + \beta_{11} X_1^2 + \beta_{22} X_2^2 + \beta_{33} X_3^2 + \beta_{44} X_4^2, \\ Y &= +88.67 + 7.3 * A + 7.1 * B - 2.83 * C + 6.9 * D + 0.38 * A * B + 1.50 * A * C \\ &\quad + 1.38 * A * D + 0.000 * B * C - 3.12 * B * D + 0.50 * C * D \\ &\quad - 6.65 * A^2 - 1.65 * B^2 - 3.77 C^2 - 2.27 * D^2. \end{aligned} \tag{5}$$

The 3D response was studied for the interactive relationship between the four parameters on dye degradation. For the determination of maximum degradation, 3D surfaces were plotted and taken into consideration. From this, interaction among two independent variables was established, keeping the other variables constant. For the degradation of dye, pH is an efficient parameter. The maximum degradation of RhB dye over Fe-CN-AW was observed at pH = 8 and catalyst dosage = 50 mg in 100 ml of dye solution. Figure 9(a) reveals an enhancement in degradation efficiency by increasing the Fe-CN-AW dose up to an optimal value at pH value = 8. These interactions show the effect of pH on the surface charge properties of the Fe-CN-AW ternary composite, consequently affecting the adsorption of RhB molecules on the surface of the catalyst. Meanwhile, the reaction amongst holes (h^+), present on the surface of Fe-CN-AW, and hydroxide ions, leads to the generation of OH radicals, being the chief reactive species to initiate degradation. Therefore, a basic environment supports more hydroxyl radical production and reduction in recombination between e-/h + pairs. Moreover, the electrostatic interactions between negatively charged Fe-CN-AW and positively charged RhB dye molecules increase in the basic medium. In an acidic medium or at higher pH values above 9, the repulsion

Table 2: ANOVA table for degradation of RhB by Fe-g-C_3N_4-Ag_2WO_4

Source	Sum of squares	Df	Mean square	F value	p value prob > F	
Model	5555.55	14	396.83	62.49	<0.0001*	
A-pH	1290.67	1	1290.67	203.25	<0.0001*	
B-catalyst dose	1232.67	1	1232.67	194.12	<0.0001*	
C-oxidant dose	192.67	1	192.67	30.34	<0.0001*	
D-time	1148.17	1	1148.17	180.81	<0.0001*	
AB	2.25	1	2.25	0.35	0.5605	
AC	36.00	1	36.00	5.67	0.0310	
AD	30.25	1	30.25	4.76	0.0454	Significant
BC	0.000	1	0.000	0.000	1.0000	
BD	156.25	1	156.25	24.61	0.0002	
CD	4.00	1	4.00	0.63	0.4398	
A^2	1211.44	1	1211.44	190.78	<0.0001*	
B^2	74.30	1	74.30	11.70	0.0038	
C^2	390.01	1	390.01	61.42	<0.0001*	
D^2	141.44	1	141.44	22.27	0.0003	
Residual	95.25	15	6.35			
Lack of fit	81.92	10	8.19	3.07	0.1136	Not significant$
Pure error	13.33	5	2.67			
Cor total	5650.80	29				

SD	2.52	R-squared	0.9831
Mean	77.20	Adj R-squared	0.9674
C.V.	3.26	Pred R-squared	0.9131
Press	491.04	Adeq precision	27.897

*Significant model terms. $Nonsignificant lack of fit is good. We want the model to fit.

between hydroxide ions and the negatively charged composite causes agglomeration and hinders the formation of hydroxyl radicals, leading to a decrease in degradation efficiency [37]. At higher catalyst dose values above optimum value, the agglomeration of Fe-CN-AW particles leads to reduced surface area for irradiation under sunlight, reducing dye removal efficiency.

Figure 9(b) shows contours and 3D plots of the interaction between oxidant dose and pH. Maximum degradation was observed at an oxidant dose of 5 mM at an optimum pH value of 8. Oxidant (H_2O_2) inhibits the recombination of e^- and h^+ pairs. The response was observed to increase by changing the pH of the solution between values of 6 and 8. An increase in oxidant dose has led to a decline in degradation due to the recombination of hydroxyl radicals and decline in the absorption of light due to saturation. Henceforth, at an oxidant dosage of 5 mM and pH = 8, maximum degradation was observed. Figure 9(c)) shows the relationship between pH and time by a 3D contour plot. Degradation increased as the pH and time were increased until an optimum condition was achieved. This shows that pH and time are crucial factors for enhancing the overall catalytic activity. The increase in RhB degradation by Fe-CN-AW was studied until the optimum values. After that, it begins to decrease. The reason behind it was as time increased, the reaction between the catalyst and dye molecules enhanced, which enhanced the degradation. Figure 9(d) shows the relationship between catalyst dose and oxidant dose. The 3D plots show that increasing the Fe-CN-AW dose from 10 mg/100 ml improved the degradation greatly to an optimum dose of 50 mg/100 ml and an oxidant dose of 5 mM, where it showed a maximum degradation. As the amount of catalyst is increased, the number of active sites for the dye molecules to get adsorbed also increases; eventually, degradation is increased. However, a further increase in catalyst dose resulted in slower degradation rate due to the agglomeration of particles, thus obstructing the light penetration in the solution. The presence of an oxidant prevents e^-/h^+ pairs from recombining. The improved RhB degradation is attributed to the possible reaction of Fe ions with oxidant species producing molecular oxygen species and more hydroxyl radicals leading to enhanced photocatalytic degradation [28].

From Figure 9(e), the interaction between Fe-CN-AW dosage and time is evident. It was seen that as the catalyst dose and time increased up to the optimized values, degradation also enhanced, showing a positive effect of catalyst amount and time. As the time duration of sunlight irradiation was increased from 1 hour to 2 hours and catalyst dose up to 50 mg/100 ml, the degradation increased. A further increase in dose above 50 mg at 2 hours of irradiation shows a steady decline in degradation due to the blocking of the active sites.

6. Scavenger Study and the Proposed Mechanism

To investigate the role of key scavengers for RhB degradation by ternary Fe-CN-AW under sunlight, the following conditions of experimental reaction were used: pH = 8, catalyst loading = 50 mg/100 ml, IDC = 10 ppm, H_2O_2 concentration = 5 mM, and irradiation time 120 minutes. DMSO, EDTA, $K_2Cr_2O_7$, and ascorbic acid were employed as scavenging agents for hydroxyl radicals, holes, electrons, and

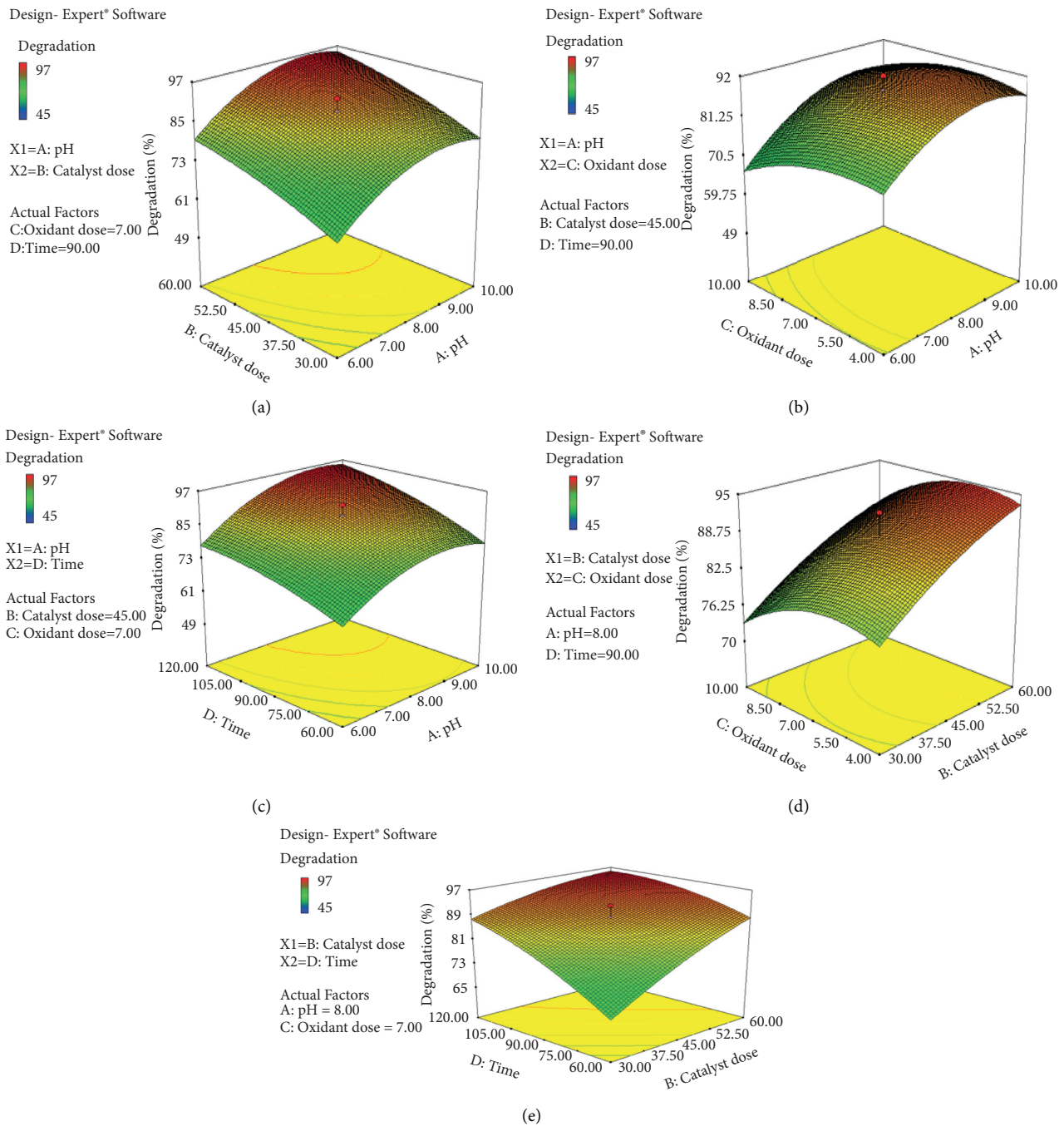

Figure 9: Response surface methodology showing the interaction of various reaction parameters. Interaction between (a) catalyst dose and pH, (b) oxidant dose and pH, (c) time and pH, (d) catalyst dose and oxidant dose, and (e) time and catalyst dosage.

superoxide radical (O_2^{-2}), respectively. The concentration of all these scavengers was kept at 5 mM during the experiments executed under sunlight. The active radical was immediately scavenged by the appropriate scavenger while the rest of the radicals carried out the dye degradation. The evaluation of the activities of the investigated scavenging agents is shown in Figure 10(a). The results indicate that the maximum reduction in catalytic activity was observed by the addition of EDTA, ascorbic acid, and then, DMSO and the least by the addition of $K_2Cr_2O_7$. Figure 10(a) shows the decrease in degradation from 97% to 32%, 47%, 54%, and 89%, respectively. Accordingly, h^+, $\bullet O^{2-}$, and $^{\bullet}OH$ are produced and involved in the photocatalytic reaction, while electrons play a minor role. On this basis, the proposed mechanism of Fe-CN-AW is as suggested in Figure 11.

Under visible light irradiation, both the Fe-CN and Ag_2WO_4 can be excited and produce light-induced es^- and h^+. Photoinduced es^- in the conduction band (CB) of silver tungstate is easily transferred to the Fe-CN valence band (VB). This is probably because of electrostatic interactions

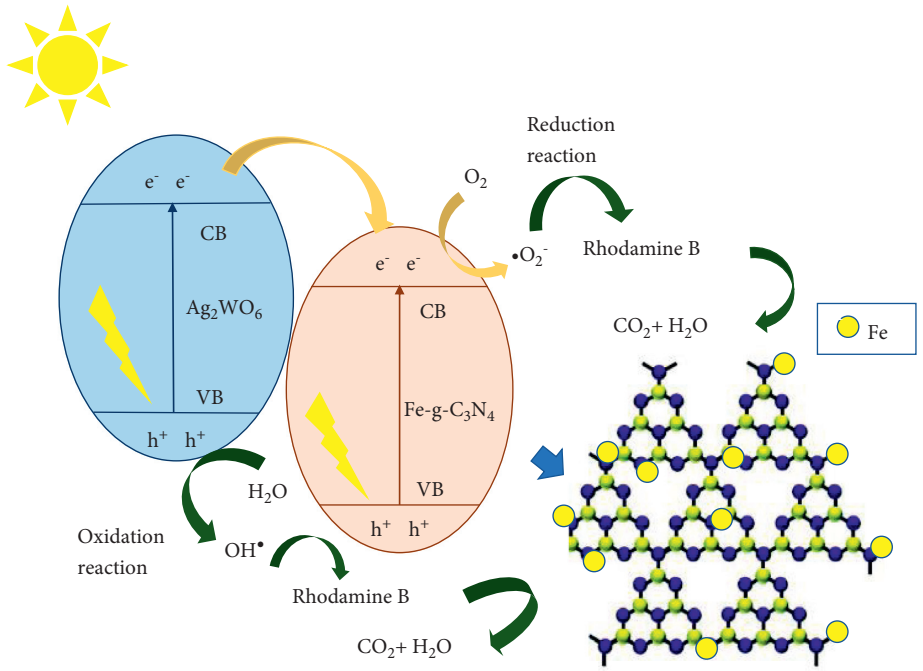

Figure 10: Proposed mechanism of rhodamine B dye degradation using ternary Fe-CN-AW.

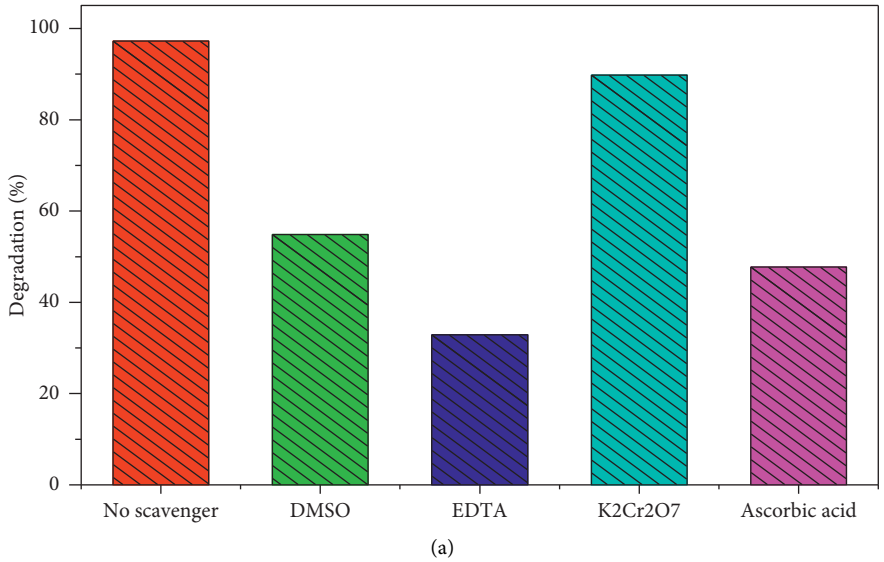

(a)

Figure 11: Continued.

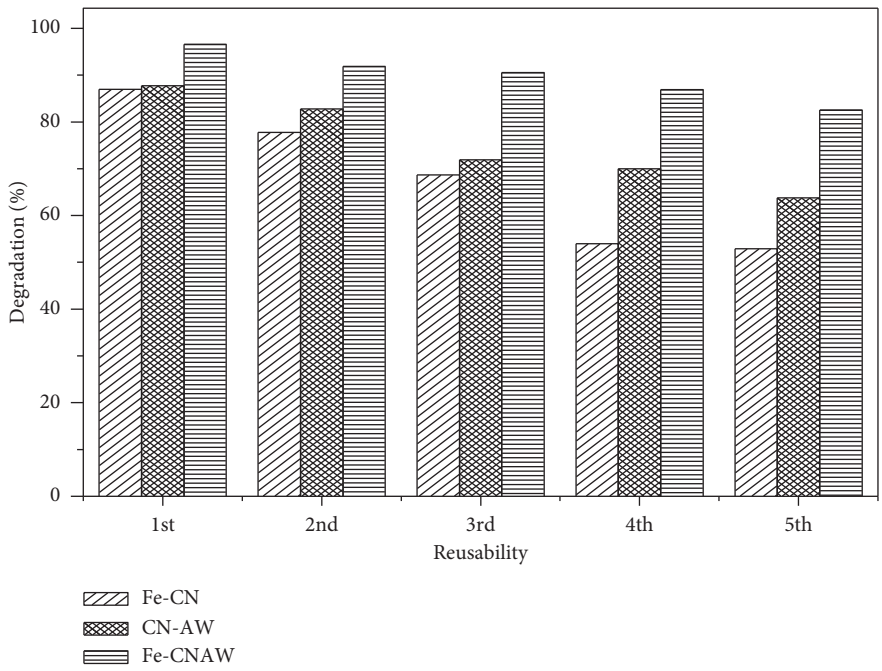

(b)

Figure 11: (a) Experiment on the role of several radical scavengers and (b) reusability experiment by Fe-CN, CN-AW, and Fe-CN-AW nanocomposites.

Table 3: Comparison of the degradation performance of metal/nonmetal doped g-C_3N_4-based ternary photocatalysts.

Sr. no.	Photocatalysts	Fabrication methods	Target pollutants	Light source	Degradation time (min)	Photocatalytic activity (%)	References
1.	P-g–C_3N_4–ag_2WO_4	Thermal polymerization method	Indomethacin	Visible light	60	91	[11]
2.	Ag-g-C_3n_4/$FeWO_4$	Hydrothermal	Rhodamine B	Visible light	120	98	[28]
3.	P–S-g-C_3N_4/ Ag_2CO_3	Ion-exchange deposition method	2,4-Dinitrophenol	Visible light	360	99	[38]
4.	O-g-C_3N_4/$ZnIn_2S_4$	Hydrothermal method	2,4-Dinitrophenol	Visible light	180	92	[39]
5.	P–S-g-C_3N_4/ Ag_2VO_3	Ion-exchange deposition method	Phenol	Visible light	360	99	[40]
6.	Co/Fe-g-C_3N_4/ MOFs	Hydrothermal method	Rhodamine B	UV/Vis	30	99	[12]
7.	Fe– C_3N_4/Ag_2CO_3	Hydrothermal method	Rhodamine B	Visible light	180 minutes	97	This work

among electrons in the CB of Ag_2WO_4 and VB holes of Fe-CN, ultimately decreasing the charge carrier's recombination within the Fe-CN and Ag_2WO_4 heterojunction. The e^- in the CB of Fe–CN becomes trapped by the oxygen present on the surface of the composite, forming $\bullet O^{2-}$. Moreover, holes accumulated in the CB of Ag_2WO_4 react with water molecules, producing hydroxyl radicals. The generated •OH and $\bullet O^{2-}$ radicals then participate in the degradation process. These characteristic features of the doped ternary heterostructure lead to the enhancement of photocatalytic degradation instead of individual and binary components. The catalyst Fe-CN-AW showed 97% degradation under sunlight. A comparison of doped graphitic carbon nitride-based ternary composites is shown in Table 3.

7. Reusability

Keeping optimal conditions specified for all three catalysts, stability of all photocatalysts was confirmed by utilizing catalysts continually in 5 consecutive runs for ensuring field application. The catalysts were separated through centrifugation from the treated RhB solution, and distilled water was used for rinsing thrice. Then, samples were dried at 70°C utilizing an electric oven. All catalysts were weighed after each catalytic recycle and inspected for their efficiency of RhB removal. Reusability trials were conducted at optimized conditions for each catalyst in a time duration of two hours for all composites. No considerable catalytic activity loss was detected even after 5 experimental runs, with a minimal

reduction after the fifth run, as shown in Figure 10(b). Experimental results showed that the Fe-CN-AW ternary heterojunction has high mechanical stability and reusability.

8. Conclusions

The Fe-CN-AW is a novel ternary heterojunction that shows a remarkable result for organic dye degradation. A simple hydrothermal method was employed for the fabrication of the iron-doped ternary photocatalyst. The ternary nanocomposite exhibited exceptional rhodamine B degradation, underneath solar light irradiation. The Fe-CN-AW showed 97% RhB degradation in two hours. The improved photocatalytic efficiency was accredited to the construction of a ternary heterojunction formed because of Fe doping and coupling of graphitic carbon nitride and silver tungstate. The prominent characteristics of all components were present in the ternary heterojunction, with doping further suppressing the recombination of electrons and holes. The catalysts are very stable and show a minimal reduction in efficiency even after five repeated experiments.

Data Availability

The data used to support the findings of this study are included within the article; additional information/data will be made available upon request.

Conflicts of Interest

The authors declare no conflicts of interest.

Acknowledgments

The authors thank Taif University for the generous financial support by the Taif University Researchers Supporting Project, no. (TURSP-2020/90), Taif University, Taif, Saudi Arabia.

References

[1] E. M. Pala, "Ultrastructural deformities in the scales of *Cyprinus carpio* inhabiting two government-sponsored fish farms in north-east India contaminated by municipal wastes and other pollutants," *Microscopy and Microanalysis*, vol. 24, no. 6, pp. 729–733, 2018.

[2] R. Das, "Application photocatalysis for treatment of industrial waste water-a short review," *OALib*, vol. 1, no. 5, pp. 1–17, 2014.

[3] Y. Deng and R. Zhao, "Advanced oxidation processes (AOPs) in wastewater treatment," *Current Pollution Reports*, vol. 1, no. 3, pp. 167–176, 2015.

[4] M. O. Barbosa, N. F. F. Moreira, A. R. Ribeiro, M. F. R. Pereira, and A. M. T. Silva, "Occurrence and removal of organic micropollutants: an overview of the watch list of EU Decision 2015/495," *Water Research*, vol. 94, pp. 257–279, 2016.

[5] J. Fu, "g-C3N4-based heterostructured photocatalysts," *Advanced Energy Materials*, vol. 8, no. 3, pp. 170–503, 2018.

[6] K. C. Devarayapalli, S. V. Prabhakar Vattikuti, T. V. Madhukar Sreekanth, P. Chidanandha Nagajyothi, and J. Shim, "Pyrolysis synthesized g-C 3 N 4/Nb 2 O 5 nanocomposite for enhanced photocatalytic activity under white LED light irradiation," *Chemistry*, vol. 4, no. 45, pp. 13250–13258, 2019.

[7] A. Habibi-Yangjeh and M. Mousavi, "Deposition of CuWO 4 nanoparticles over g-C 3 N 4/Fe 3 O 4 nanocomposite: novel magnetic photocatalysts with drastically enhanced performance under visible-light," *Advanced Powder Technology*, vol. 29, no. 6, pp. 1379–1392, 2018.

[8] S. V. P. Vattikuti, B. P. Reddy, C. Byon, and J. Shim, "Carbon/CuO nanosphere-anchored g-C3N4 nanosheets as ternary electrode material for supercapacitors," *Journal of Solid State Chemistry*, vol. 262, pp. 106–111, 2018.

[9] K. C. Devarayapalli, K. Lee, N. D. Nam, S. V. P. Vattikuti, and J. Shim, "Microwave synthesized nano-photosensitizer of CdS QD/MoO3-OV/g-C3N4 heterojunction catalyst for hydrogen evolution under full-spectrum light," *Ceramics International*, vol. 46, no. 18, pp. 28467–28480, 2020.

[10] S. V. P. Vattikuti, P. A. K. Reddy, J. Shim, and C. Byon, "Visible-light-driven photocatalytic activity of SnO2-ZnO quantum dots anchored on g-C3N4 nanosheets for photocatalytic pollutant degradation and H2 production," *ACS Omega*, vol. 3, no. 7, pp. 7587–7602, 2018.

[11] J. Huang, "Ultrathin Ag2WO4-coated P-doped g-C3N4 nanosheets with remarkable photocatalytic performance for indomethacin degradation," *Journal of Hazardous Materials*, vol. 392, p. 122355, 2020.

[12] P. Liu, "Co/Fe co-doped porous graphite carbon derived from metal organic framework for microelectrolysis-Fenton catalytic degradation of Rhodamine B," *Journal of Environmental Chemical Engineering*, vol. 9, no. 5, Article ID 105924, 2021.

[13] S. Kumar, "Visible light-assisted photodegradation by silver tungstate-modified magnetite nanocomposite material for enhanced mineralization of organic water contaminants," *Applied Nanoscience*, vol. 10, pp. 1–15, 2019.

[14] J. Chen, "Fabrication of hierarchical sheet-on-sheet WO3/g-C3N4 composites with enhanced photocatalytic activity," *Journal of Alloys and Compounds*, vol. 777, pp. 325–334, 2019.

[15] P. Praus, "Graphitic carbon nitride: synthesis, characterization and photocatalytic decomposition of nitrous oxide," *Materials Chemistry and Physics*, vol. 193, pp. 438–446, 2017.

[16] K. Dai, "A facile fabrication of plasmonic g-C3N4/Ag2WO4/Ag ternary heterojunction visible-light photocatalyst," *Materials Chemistry and Physics*, vol. 177, pp. 529–537, 2016.

[17] S. Tonda, "Fe-doped and-mediated graphitic carbon nitride nanosheets for enhanced photocatalytic performance under natural sunlight," *Journal of Materials Chemistry*, vol. 2, no. 19, pp. 6772–6780, 2014.

[18] T. Li, "Mechanisms for highly efficient mineralization of bisphenol A by heterostructured Ag2WO4/Ag3PO4 under simulated solar light," *ACS Sustainable Chemistry & Engineering*, vol. 7, no. 4, pp. 4177–4185, 2019.

[19] P. Raizada, A. A. P. Khan, and P. Singh, "Construction of carbon nanotube mediated Fe doped graphitic carbon nitride and Ag3VO4 based Z-scheme heterojunction for H2O2 assisted 2, 4 dimethyl phenol photodegradation," *Separation and Purification Technology*, vol. 247, p. 116957, 2020.

[20] B. Zhu, "Fabrication and photocatalytic activity enhanced mechanism of direct Z-scheme g-C3N4/Ag2WO4 photocatalyst," *Applied Surface Science*, vol. 391, pp. 175–183, 2017.

[21] S. Honary, "Green synthesis of silver nanoparticles induced by the fungus Penicillium citrinum," *Tropical Journal of Pharmaceutical Research*, vol. 12, no. 1, pp. 7–11, 2013.

[22] K. Devarayapalli, "Mesostructured g-C3N4 nanosheets interconnected with V2O5 nanobelts as electrode for

coin-cell-type-asymmetric supercapacitor device," *Materials Today Energy*, vol. 21, p. 100699, 2021.

[23] M. U. Rahman, "Solar driven photocatalytic degradation potential of novel graphitic carbon nitride based nano zero-valent iron doped bismuth ferrite ternary composite," *Optical Materials*, vol. 120, p. 111408, 2021.

[24] X. Wang, "Recyclable nanoscale zero valent iron doped g-C3N4/MoS2 for efficient photocatalysis of RhB and Cr (VI) driven by visible light," *ACS Sustainable Chemistry & Engineering*, vol. 4, no. 7, pp. 4055–4063, 2016.

[25] N. Nadeem, "Degradation of reactive dye using heterogeneous photo-Fenton catalysts: ZnFe2O4 and GO-ZnFe2O4 composite," *Materials Research Express*, vol. 7, no. 1, p. 015519, 2020.

[26] N. Tahir, "Fabrication of visible light active Mn-doped Bi2WO6-GO/MoS2 heterostructure for enhanced photocatalytic degradation of methylene blue," *Environmental Science and Pollution Research*, pp. 1–16, 2021.

[27] C. V. Reddy, "Mn-doped ZrO2 nanoparticles prepared by a template-free method for electrochemical energy storage and abatement of dye degradation," *Ceramics International*, vol. 45, no. 12, pp. 15298–15306, 2019.

[28] R. Saher, "Sunlight-driven photocatalytic degradation of rhodamine B dye by Ag/FeW 4/gC3N4 composites," *International journal of Environmental Science and Technology*, vol. 18, no. 4, pp. 927–938, 2021.

[29] J. F. Moulder, *Handbook of X-Ray Photoelectron Spectroscopy*, pp. 230–232, Perkin-Elmer Corporation, Waltham, MA, UA, 1995.

[30] B. Yu, "Functionalized graphene oxide/phosphoramide oligomer hybrids flame retardant prepared via in situ polymerization for improving the fire safety of polypropylene," *RSC Advances*, vol. 4, no. 60, pp. 31782–31794, 2014.

[31] P. Li, "Carboxyl groups on g-C3N4 for boosting the photocatalytic U (VI) reduction in the presence of carbonates," *Chemical Engineering Journal*, vol. 414, pp. 12–88, 2021.

[32] R. Ahmad, "Photocatalytic systems as an advanced environmental remediation: recent developments, limitations and new avenues for applications," *Journal of Environmental Chemical Engineering*, vol. 4, no. 4, pp. 4143–4164, 2016.

[33] A. Rafiq, "Photocatalytic degradation of dyes using semiconductor photocatalysts to clean industrial water pollution," *Journal of Industrial and Engineering Chemistry*, vol. 97, 2021.

[34] M. Abdellah, "Photocatalytic decolorization of methylene blue using TiO2/UV system enhanced by air sparging," *Alexandria engineering journal*, vol. 57, no. 4, pp. 3727–3735, 2018.

[35] N. Nadeem, "Improved photocatalytic degradation of dye using coal fly ash-based zinc ferrite (CFA/ZnFe2O4) composite," *International journal of Environmental Science and Technology*, pp. 1–16, 2021.

[36] I. D. Tunç, "Growth of ZnO nanowires on carbon fibers for photocatalytic degradation of methylene blue aqueous solutions: an investigation on the optimization of processing parameters through response surface methodology/central composite design," *Ceramics International*, vol. 46, no. 6, pp. 7459–7474, 2020.

[37] S. Mortazavian, A. Saber, and D. E. James, "Optimization of photocatalytic degradation of Acid Blue 113 and Acid Red 88 textile dyes in a UV-C/TiO2 suspension system: application of response surface methodology (RSM)," *Catalysts*, vol. 9, no. 4, pp. 300–360, 2019.

[38] P. Raizada, "Visible light assisted photodegradation of 2, 4-dinitrophenol using Ag2CO3 loaded phosphorus and sulphur co-doped graphitic carbon nitride nanosheets in simulated wastewater," *Arabian Journal of Chemistry*, vol. 13, no. 1, pp. 3196–3209, 2020.

[39] A. Uddin, "Hydrothermal synthesis of 3D/2D heterojunctions of ZnIn2S4/oxygen doped g-C3N4 nanosheet for visible light driven photocatalysis of 2, 4-dichlorophenoxyacetic acid degradation," *Journal of Alloys and Compounds*, vol. 845, p. 156206, 2020.

[40] P. Raizada, "Fabrication of Ag3VO4 decorated phosphorus and sulphur co-doped graphitic carbon nitride as a high-dispersed photocatalyst for phenol mineralization and *E. coli* disinfection," *Separation and Purification Technology*, vol. 212, pp. 887–900, 2019.